EXPERIMENTAL AND NUMERICAL STUDIES OF BUBBLE DEVELOPMENT PROCESS IN ROTATIONAL FOAM MOLDING

EXPERIMENTAL AND NUMERICAL STUDIES OF BUBBLE DEVELOPMENT PROCESS IN ROTATIONAL FOAM MOLDING

By

MARYAM EMAMI, B.Sc., M.Sc. (CHEM. ENG.)

A Thesis Submitted to the School of Graduate Studies

in Partial Fulfillment of the Requirements

for the Degree Doctor of Philosophy

McMaster University

Dedicated to the loving memory of my mother and father,

Zohreh Hojati & Mostafa Emami

DOCTOR OF PHILOSOPHY (2013) McMaster University

Chemical Engineering Hamilton, Ontario

TITLE: Experimental and Numerical Studies of Bubble Development Process in Rotational Foam Molding

AUTHOR: Maryam Emami, B.Sc., M.Sc. (Chemical Engineering)

SUPERVISORs: Professor John Vlachopoulos, Professor Michael R. Thompson

NUMBER OF PAGES: xiii, 134

ABSTRACT

Commercial interests in polymeric foams continue to increase due to their unique physical characters and the new emerging applications for foamed materials. This thesis investigates the foam development process under non-pressurized conditions as applicable to rotational molding to elucidate the underlying mechanisms in the bubble transformation process and provide an accurate basis for predicting the morphological structure and macroscopic properties of the foamed materials. It was found that the foaming mechanism is comprised of four distinct stages: two stages of bubble nucleation, primary and secondary nucleation, followed by bubble growth and bubble coalescence/shrinkage. During the primary nucleation stage, the interstitial regions of the sintered plastic powder as well as the agglomerated blowing agent particles acted as nucleation sites for the blowing gas. Subsequently, secondary nucleation formed a new generation of bubbles within the polymer melt. Following the nucleated bubbles during the foaming process revealed that primary nucleation was the controlling stage in determining the final cellular structure. Growth and coalescence mechanisms were dynamically active and competed during both heating and cooling cycles. The developing bubble structure during the foaming was evaluated by several parameters, including bubble density and bubble size. In order to demonstrate the combined effect of the bubble growth and coalescence, a new parameter, total bubble projected area, was introduced. Through actual rotational foam molding experiments, it was found that the whole foaming process in respect to thickness variation can be best described by this parameter and it provides a true picture of the foam development process.

Statistical analysis of the evolving cellular structure revealed that the rate of nucleation is influenced by the rheology of the polymer materials. The visualization experiments showed that lower viscosity and melt elasticity of the gas-laden matrix allowed a greater number of bubbles to survive and grow larger than the critical nucleus. Furthermore, theoretical predictions obtained from the Kagan model for viscous systems simulated experimentally observed trend for the impact of viscosity on the nucleation rate rather

well and suggested that higher viscosity could impede the number of nuclei generated in the foaming system.

The influence of the rheological properties on the bubble growth mechanism was also investigated. Morphological analysis was used to determine the rheological processing window in terms of shear viscosity, elastic modulus, melt strength and strain-hardening, intended for the production of foams with greater foam expansion, increased bubble density and reduced bubble size. A bubble growth model and simulation scheme was also developed to describe the bubble growth phenomena that occurred in non-pressurized foaming systems. It was verified that the viscous bubble growth model was capable of depicting the growth behaviors of bubbles under various processing conditions.

Furthermore, an evaluation of the effect of scale of production on rotational foam molding process with respect to rheological impact was conducted and experimental observations from microscopic, lab- and pilot-scale foam systems were used for investigation. A systematic comparison of the expansion behavior of polyethylene foams indicated that the size of the foam system does not affect the principles of the foaming process. It was demonstrated that the observed trend of the impact of rheology in microscopic studies can be practically extended to higher scales foaming systems and it can provide guidelines for the selection of the polymer materials for customized foam applications.

ACKNOWLEDGMENTS

I would like to express my gratitude to my supervisors, Dr. John Vlachopoulos and Dr. Michael Thompson for the boundless freedom they gave me to explore new ideas in the course of this project, for their constant support and for giving me numerous opportunities for scientific advancement and personal improvement.

I am grateful to my Ph.D. committee members, Dr. Raja Ghosh and Dr. Samir Chidiac, for their valuable advice, their support and encouragement, which are greatly appreciated.

Financial support provided for this work by the following organizations is gratefully acknowledged: Total Petrochemical Co. (Feluy, Belgium), NSERC of Canada, Ontario Government, School of Graduate Studies and Chemical Engineering Department of McMaster University.

I am sincerely grateful to Mr. Eric Mazires (Total Research & Technology, Feluy) for many helpful discussions and all the opportunities he provided me to attend special events and conferences and meet people from the industry, to Dr. Shaffiq Jaffer (Total American Services, Inc.) for his advice and suggestions during the course of this project, and Polymer Processing Research Centre at Queen's University of Belfast, UK for providing the opportunity to perform pilot-scale rotational molding experiments.

Thanks to all people in CAPPA-D group and in particular, Elizabeth Takacs, for her help and collaboration, but most importantly for her friendship and support throughout the years.

I would like to thank the people in Chemical Engineering Department, Kathy Goodram, Lynn Falkiner, Cathie Roberts, and Nanci Cole for welcoming and providing a friendly environment, also Paul Gatt and Dan Wright for their exceptional and unique role in technical support.

I would like to thank my husband, Maziyar Yousefizad, my beloved son, Adrian, and my siblings, Najmeh, Hamideh, and Mohammad for the constant support and their deep and sincere love.

TABLE OF CONTENTS

LIST OF TABLES

LIST OF FIFURES

Chapter 1

Introduction and General Literature Review

Foams, as engineering materials, are now used in all industrial sectors and represent an extraordinary class of materials. Foaming in polymers involves unique scientific mechanisms and processing techniques, distinctive morphology transformations, and structure formations. Plastic foaming technology has been developing for many decades; likewise, polymeric foams have evolved from scientific concepts to lab research, pilot line samples, and commercialization, since the 1930s. Continuous advancements of foaming technology have greatly spurred commercial applications of plastics foams. They are intended for packaging, thermal and electrical insulation, buoyancy, and structural applications and their extraordinary character comes from their diverse functionalities such as stiffness, strength, impact resistance, dielectric and thermal resistance, and permeability, which can be customized to obtain properties ranging beyond the limits of all other classes of engineering materials.

Plastic foams have been produced by a variety of processes, however, regardless of the methods, the foaming mechanism always involves a series of kinematic events initiated

within polymer/blowing agent mixtures which include dissolution of blowing agents, gas phase separation and hardening of cellular structures. Extensive experimental and theoretical investigations have been conducted to elucidate the plastic foaming behaviors and further develop foaming technologies. Rotational foam molding technology has been proven to be very effective in reducing material consumption without compromising structural properties and it can be used to combat the low mechanical, insulative and shock mitigation properties due to the hollow structure present in many rotationally molded products [1].

Many studies have addressed the technology of rotational foam molding [2,3]; however, a great challenge in engineering rotomolded foams is to address the fundamental concepts of this unique non-pressurized foaming process. In this thesis, a systematic investigation of the foaming process in rotational molding at a microscopic level will be presented to clarify the fundamental mechanisms involved in the process and provide an improved explanation for the developed morphological structure. Furthermore, a detailed experimental examination and theoretical study of the influence of polymer matrix rheology on bubble dynamics during different stages of non-pressurized foaming and the resultant foam structure will be reported.

1.1 Rotational Foam Molding

Processing of plastic foam involves some general principles and concepts that apply to foams made of various materials and produced by different molding technologies. Most plastic foams are fabricated by an expansion process, which consists of the expansion of a gaseous phase dispersed within the polymer matrix. The gaseous phase may be generated from either a physical blowing agent or a chemical blowing agent [4,5,6]. Physical blowing agent can provide gas for the expansion of polymers by the change of physical state, which may involve volatilization of a liquid or release of a pressurized gas at a specified temperature and pressure [7]. Chemical blowing agents are substances that decompose at a certain processing temperature and evolve blowing gases such as N_2 and/or CO_2. Commonly, solid organic and inorganic substances (such as

azodicarbonamide and sodium bicarbonate) are used as chemical blowing agent. Specifically, chemical blowing agents are divided by their enthalpy of reaction into two groups including exothermic and endothermic foaming agents. The chemical reaction that generates the gas can either absorb energy (endothermic) or release energy (exothermic). The employment of physical blowing agents in the foaming process requires elevated mold pressures. In non-pressurized foaming systems such as rotational foam molding, chemical blowing agents have been the most common method for generating cellular structure [4,5,6].

In the rotational foam molding process, the polymer matrix has to form a continuous melt phase to reduce the adverse effect of incoherent polymer melt on the bubble morphology of the cellular structure and minimize losses of the liberated blowing gas to the atmosphere [2,3]. Polymer powder particles, when in contact with each other at elevated temperatures, tend to decrease their total surface area by coalescence. This process is an inherent phenomena associated with rotational molding which is called sintering and is usually accompanied by a decrease in the total volume of the particulate bed. The sintering process proceeds in two stages, first by developing interfaces and bridges between adjacent particles, followed by a stage in which the density increases by elimination of the inter-particle cavities [8,9]. The driving force for the sintering is surface tension and the main factor opposing this mechanism is the resistance to flow, expressed by viscosity [10]. Polymer sintering is of particular interest in rotational molding. It is considered as the controlling mechanism for the process, since it has a profound influence on properties of the final part such as presence of bubbles, thickness uniformity and part quality and controls a major part of heating time in the molding cycle [11].

In order to develop a foam structure with high bubble density and narrow bubble size distribution in rotational molding, the sintering step should be completed before the onset of bubble nucleation and growth [2,12]. Blowing agent should be uniformly dispersed in the matrix and when in solid form, wetted by the molten polymer. The gases released in

the polymer melt above the decomposition temperature of the blowing agent initiate the foaming expansion process, which generally comprises of three fundamental steps: bubble nucleation, bubble growth, bubble stabilization.

1.2 Foaming Process

1.2.1 Bubble Nucleation

Foam expansion process begins with bubble nucleation. In this thesis, the term, "bubble nucleation" is used generically to denote any process that leads autogenously to the formation of a bubble in the polymer matrix. The bubble nucleation step occurs simultaneously with the decomposition of the blowing agent particles. Considering the polymer melt has been saturated with the blowing agent, the already saturated system becomes supersaturated as the gas solubility reduces with increased temperature. Consequently, the polymer-gas solution tends to form tiny bubbles in order to restore a low-energy stable state [13,14,15]. The classical nucleation theory (CN theory) [16,17] classifies bubble nucleation into two types: homogeneous nucleation and heterogeneous nucleation. CN theory states that a bubble that has a radius greater than the critical radius (R_{cr}) tends to grow spontaneously while the one that has a radius smaller than R_{cr} collapses. In addition to CN theory, another stream of thought postulated that pre-existing cavities or microvoids, which serve as seeds for bubble formation, exist in the supersaturated solution [18,19]. In light of these different views, three types of cell nucleation can be defined.

Classical Homogeneous Nucleation

The classical homogeneous nucleation involves nucleation in the liquid bulk of a uniform polymer-gas solution. There are no pre-existing gas cavities present prior to the material system becoming supersaturated. Han et al. [20] and Lee [21] reported nucleation rates during typical plastic foaming processes that were much higher than those calculated

using the CN theory. Therefore, it is widely believed that this mechanism is not the route through which bubbles form in plastic foams.

Classical Heterogeneous Nucleation

This type of nucleation suggests that supersaturation will result in the formation of a bubble at a heterogeneous nucleating site (e.g., nucleating agents or impurities). Similar to the homogeneous case, this form of nucleation suggests that the system initially contains no gas cavities, either in the bulk or on the surfaces of heterogeneous nucleating sites. Wilt [22] showed that heterogeneous nucleation at a smooth planar surface or a surface with conical or spherical projections will not occur in an H_2O-CO_2 solution because the required level of supersaturation is very high. A similar conclusion can be applied to plastic foaming because of the higher liquid-gas interfacial tension. However, the study indicated that it is theoretically possible for classical heterogeneous nucleation to occur in a conical cavity for an H_2O-CO_2 solution [22]. For plastic foaming of a PMMA-CO_2 system, Geol also showed that this type of nucleation activity could occur at a reasonably high rate theoretically, which qualitatively agreed with experimental observations [15]. Nevertheless, in all previous investigations of bubble nucleation during plastic foaming, the experimental data was not in good quantitative agreement with theoretical predictions without the use of fitting parameters. Therefore, whether the classical nucleation theory can explain the real mechanisms behind bubble nucleation is still controversial.

Pseudo-Classical Nucleation

This form of nucleation includes homogeneous and heterogeneous nucleation from metastable micro-bubbles or micro-voids in the solution bulk, as well as pre-existing gas cavities at the surface of the processing equipment or at the surface of suspended particles. When the polymer-gas system is perturbed to a supersaturated state, the radius of curvature of each meniscus is still less than R_{cr} as determined by CN theory. Therefore,

there exists a finite free energy barrier to activate the expansion of the pre-existing gas cavities [21], which will finally be overcome as the degree of supersaturation increases during the continuous temperature increase. As a result, the pre-existing cavities will grow spontaneously.

Classical Nucleation Theory (CN Theory)

Gibbs [16] was the pioneer of the CN theory studies, proclaiming the concept of critical radius for bubble nucleation. Using classical thermodynamics, various researchers have derived the free energy barrier for homogeneous nucleation [23,22,24,25] and those for heterogeneous nucleation on different types of surfaces [22,26,27].

Free Energy Barrier for Homogeneous Nucleation

When the system is on the verge of bubble nucleation, the free energy change entailed by the homogeneous formation of a bubble (ΔG_{hom}) can be expressed as [27,13]:

$$\Delta G_{hom} = \gamma_{lg} A_{lg} - (P_{bub} - P_{sys}) V_{bub} \qquad \text{Eq. 1-1}$$

where P_{bub} is the pressure inside the bubble; P_{sys} is the surrounding system pressure; V_{bub} is the bubble volume; γ_{lg} and A_{lg} are the interfacial energy and the surface area at the liquid-gas interface, respectively. Figure 1.1 depicts the variation of energy (ΔG_{hom}) with bubble radius (R_{bub}), and in this figure R_{cr} represents the critical radius. Since the free energy change required to homogeneously form a critical bubble is maximum, the corresponding state is an unstable equilibrium one. In other words, the nuclei smaller than R_{cr} tend to collapse, while those larger than R_{cr} tend to grow. A bubble is thus considered to have nucleated when its radius is larger than R_{cr}. The free energy change entailed by forming a critical bubble is defined to be the free energy barrier for bubble nucleation. By taking the derivative of ΔG_{hom} with respect to the R_{bub} and setting it to zero, it turned out that R_{cr} is expressed as:

$$R_{cr} = \frac{2\gamma_{lg}}{P_{bub,cr} - P_{sys}} \quad \text{Eq. 1-2}$$

where $P_{bub,cr}$ is the pressure inside a critical bubble. Combining Eq. 1-1 and Eq. 1-2, the free energy barrier for homogeneous nucleation (ΔG^*_{hom}) is:

$$\Delta G^*_{hom} = \frac{16\pi\gamma^3_{lg}}{3(P_{bub,cr} - P_{sys})^2} \quad \text{Eq. 1-3}$$

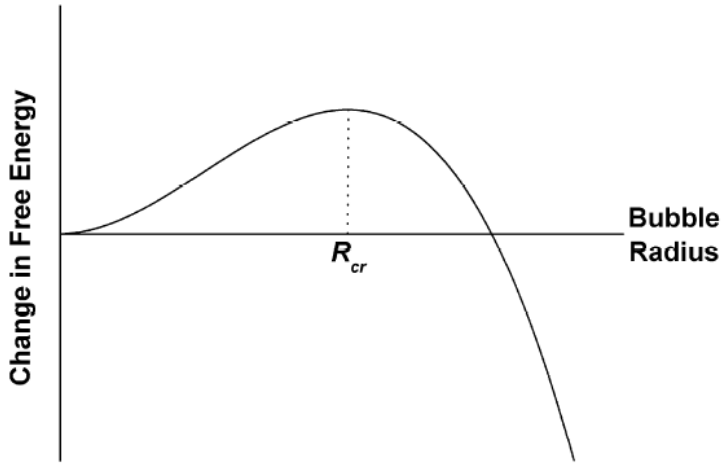

Figure 1-1: Free energy change to nucleate a bubble homogeneously.

Free Energy Barrier for Heterogeneous Nucleation

Similarly, when the system is on the verge of bubble nucleation, the free energy change entailed by nucleating a bubble heterogeneously (ΔG_{het}) can be expressed as:

$$\Delta G_{het} = (\gamma_{sg} - \gamma_{sl})A_{sg} + \gamma_{lg}A_{lg} - \left(P_{bub} - P_{sys}\right)V_{bub} \quad \text{Eq. 1-4}$$

where A_{ij} and γ_{ij} are the surface area and the interfacial energy, respectively, of the interface between phase *i* and phase *j*. The subscripts g, l, and s represent the gas, liquid, and solid phases, respectively. Plotting the general relationship between ΔG_{het}t and R_{bub} will result in a graph that is similar to **Error! Reference source not found.**, but with a

lower maximum value. It also turns out that R_{cr} for heterogeneous nucleation is identical to that of homogeneous case. Therefore, the free energy barrier for heterogeneous nucleation (ΔG^*_{het}) is:

$$\Delta G^*_{het} = \frac{16\pi\gamma_{lg}^3 F}{3(P_{bub,cr} - P_{sys})^2} = \Delta G^*_{hom} F \qquad \text{Eq. 1-5}$$

where F is the energy reduction factor for heterogeneous nucleation. Depending on the geometry of the nucleating site, various expressions for F have been reported.

For both homogeneous nucleation and heterogeneous nucleation, classical thermodynamics suggest that the thermodynamic potential at which R_{bub} equals to R_{cr} is a maximum. This state is therefore an unstable equilibrium state, and the polymer-gas solution is metastable. The value of R_{cr} defines the required perturbation, provided by molecular motion or any other external work, required to form a bubble. However, the spontaneous formation of a bubble of size R_{cr} corresponds to a spontaneous decrease in the entropy of the corresponding thermodynamic system. Since such process contradicts the second law of thermodynamics, classical thermodynamics cannot be used to predict when a gas bubble would form spontaneously and take the system out of the metastable state. In this context, it is necessary to consider kinetics when studying bubble nucleation.

1.2.2 Bubble Growth and Stabilization

Bubble growth behavior in polymer melts or other fluids has been an active research topic of many experimental and theoretical studies. Nearly all bubble growth models can be classified into the single bubble growth model and the cell model (i.e., swarm of bubbles growing without interaction).

The Single Bubble Growth Model

The single bubble growth model studies the growth of a single bubble in an infinite sea of liquid. Rayleigh [28], Epstein and Plesset [29], and Scriven [30] were among the earliest

researchers who used it as the base model to conduct theoretical or experimental investigations on bubble growth behavior. The analysis of diffusion-induced bubble growth in viscous liquids with both mass and momentum transfer was pioneered by Barlow and Langois [31]. They used the thin boundary layer approximation, which assumes that the dissolved gas concentration gradient vanishes within a thin shell around the bubble. This is a widely adopted approximation that allows for a considerable degree of simplification in the equations governing mass transfer in a viscous liquid. Furthermore, Barlow and Langois also assumed that an unlimited supply of gas was available, and thereby the uniform concentration far from the bubble surface was always identical to its initial level. During actual plastic foaming, however, the availability of dissolved gas is finite. Hence, the dissolved gas content will eventually be depleted and cannot sustain the growth thereafter. Despite these shortcomings, their work is considered to be a great improvement over previous studies [29], which had considered only the diffusion process in bubble growth and had neglected the hydrodynamic effects.

Street [32] considered the growth of a spherical stationary cavity in a viscoelastic Oldroyd fluid. They extended the work of Barlow [31] to formulate and numerically simulate the bubble growth process for a liquid of an infinite medium under non-isothermal conditions. Their theoretical model accounts for the heat, mass, and momentum transfer processes governing the growth of a vapor bubble in a solution consisting of a viscous liquid and a dissolved blowing agent. In their work, the viscous liquid was assumed to obey a non- Newtonian (power law) fluid model. They identified that the most important parameters controlling the growth rate are the diffusivity and the concentration of blowing agent, the viscosity level of the melt, and the extent to which the liquid is shear thinning.

Han and Yoo [33] carried out an experimental investigation and a theoretical study to elucidate the oscillatory behavior of a gas bubble in a viscoelastic liquid. The rheological property of the fluid was modeled by the Zaremba-DeWitt model. They took into account both the hydrodynamic and diffusion effects. Using a third order polynomial

approximation for the gas concentration profile around the bubble, the finite difference method was employed to solve the governing equations. Their study showed that gas diffusivity has a profound influence on the occurrence of oscillatory behavior. Furthermore, they indicated that while the melt elasticity enhances the oscillatory behavior of bubble growth, the viscosity suppresses it.

Venerus *et al*. [34] formulated a rigorous model to describe bubble growth in a non-linear viscoelastic fluid. The convective and diffusive mass transport as well as surface tension and inertial effects had been taken into account in their study. They found that the influence of non-linear fluid rheology on bubble growth dynamics is relatively minor when compared to fluid elasticity. Using the developed model, they evaluated various approximations being used by previous investigations and indicated that the thin boundary layer approximation has a very limited range of applicability.

The aforementioned fundamental investigations on bubble growth have led to an increased understanding of the phenomena. However, during plastic foaming, bubbles grow simultaneously and they are expanding in close proximity to one another with a limited supply of gas. In this context, the practical application of the single bubble growth model in the plastic foaming industry was very limited.

The Cell Model

In order to address the problematic approximations in the single bubble growth model, Amon and Denson [35] introduced the well-known cell model, which suggested that a large amount of gas bubbles grow in close proximity to each other in a polymer-gas solution. This model represented a significant advancement in the field of bubble growth simulation. It described the actual foaming situation more realistically by dividing the polymer-gas solution into spherical unit bubbles consisting of equal and limited amounts of dissolved gas. Assuming the polymer melt and the gas in the bubble had behaved like Newtonian fluid and an ideal gas, respectively, they applied the cell model to simulate the bubble growth during plastic foaming. Unlike the single bubble growth model, their

model yielded a finite radius for the growing bubble. Furthermore, they concluded that the surface tension and the initial radius have less effect on bubble growth dynamics than the thermodynamic driving force (i.e., the degree of supersaturation) as well as the mass and momentum transfers. Later, other researchers extended their work to a low-pressure structural foam-molding process by considering the heat transfer, solidification, and flow in the cavity [36,37,38]. The predicted bubble growth profiles were in good qualitative agreement with the experimental measurements of the bulk density of expanding thermoplastic polymeric foam. However, quantitative discrepancies existed between the two. These differences were believed to be related to the omission of melt elasticity and bubble coalescence in the model.

Arefmanesh and Advani also applied the cell model to a low-pressure structural foam molding process and studied the simultaneous growth of a given number of cells in a Newtonian fluid [39]. In their work, they approximated the dissolved gas concentration gradient in the unit cell as a polynomial profile. They further assumed that the cell growth is under an isothermal condition, and that the gas inside each expanding cell behaves like an ideal gas. Later, they extended their earlier research by considering the viscoelastic properties (i.e., based on the Maxwell model) of the fluid [37] and the non-isothermal effects [38]. Effects of various parameters on the bubble growth dynamics were investigated in these studies. The results showed that higher gas diffusivity enhanced the bubble growth rate while higher viscosity retarded it, especially in the initial growing stage.

Ramesh et al. proposed a modified viscoelastic cell model, which accounts for the effect of dissolved gas content and the temperature on rheological and other physical properties [40]. Using the Maxwell model to describe the viscoelastic property of the polymer-gas solution, they simulated the growth of closely spaced spherical bubbles during the foaming process and compared the results with experimental data. The simulation results indicated that the predictions based on the modified cell model were in qualitative agreement with the experimental data while the quantitative agreement was also

satisfactory. The simulation results demonstrated that gas loss to the surrounding, dissolved gas content, and transient cooling effects were the most important factors that governed the bubble growth.

1.3 Rheology and Foams

During the foaming process, the matrix polymer is deformed and displaced as bubbles form and grow. The speed and ease of bubble formation and growth are determined by the melt properties of the matrix polymer. When bubbles expand, the surrounding material is required to stretch, introducing extensional forces in the surrounding melt. Rheological properties of the polymeric matrix and gas-laden polymer melt in polymer foaming have received great attention by researchers due to the important role of polymer matrix response to the mechanisms involved in the foaming process. In rotational foam molding, it has been suggested that localized shear can be very much larger during the foaming process than is normally expected in unfoamed rotational molding and melt viscosity and elasticity affect bubble growth dynamics in the foaming process. Liu *et al.* [2] stated that the zero shear viscosity is one of the most important material parameters in rotational molding of foams, as a low zero shear viscosity will aid the sinterability of the powder and remove trapped air bubbles, which can induce bubble coarsening. They also mentioned, though, that a very low zero shear viscosity may not be beneficial due to an increase in undesired bubble coalescence. However, the proposed expansion rate of 10,000 s^{-1} during the very early stages of bubble growth brings the use of zero shear viscosity as the most important determination of a materials' performance into question [41].

Due to the stretching actions, melt strength of the molten polymer can play a substantial role in controlling the foaming process. Bradley and Phillips [42] stressed the importance of extensional viscosity and strain-hardening in the foaming process in their production of low density foams using high-melt-strength polypropylene. Park and Cheung [43] and Naguib [44] used a long-chain-branching polypropylene, which exhibited significant strain-hardening under extension, and demonstrated much higher bubble density and

expansion ratio during foam extrusion compared to linear polypropylene. Similar conclusions were obtained by Yamaguchi *et al*. [45], who blended a cLLDPE (linear low-density polyethylene with some crosslinks) with an LLDPE to enhance the strain-hardening behavior. Enhanced strain-hardening favored uniform deformation during foaming, and resulted in foams with a uniform bubble size distribution. Recently, Spitael and Macosko [46] and Stange and Münstedt [47] characterized the uniaxial extensional viscosities for a series of linear polypropylenes, long chain branched (LCB)-polypropylenes, and their blends at conditions relevant to foaming, and then attempted to relate those rheological properties to bubble morphology in foamed samples. Besides showing that long chain branching suppresses bubble coalescence, they found that a small amount of LCB- polypropylene (e.g., 10% by weight) in the blend could improve the expansion and reduce the occurrence of bubble opening with linear polypropylenes. Stange and Münstedt attributed the higher volume expansion of LCB- polypropylenes and the blends to their higher strains at rupture and their more uniform deformation during extension compared to linear polypropylenes. Spitael and Macosko did not find any direct correlation between strain-hardening and bubble density or expansion ratio.

1.4 Thesis Objectives

The objectives of this research study are:

- to elucidate the fundamental mechanisms involved in a non-pressurized foaming system such as rotational foam molding and provide an improved explanation for the developed morphological structure during the foaming process.

- to investigate the mechanisms involved in the nucleation of a foam under non-pressurized conditions and the significance of viscosity constraints on bubble nucleation.

- to study the effects the rheology of the polymer matrix on bubble dynamics during different stages of foaming and the resultant foam structure and correlate foamability of

polymer materials with their off-line rheological properties, both experimentally and theoretically.

- to conduct a systematic investigation of the influence of different scales of production on rotational foam molding technology from microscopic to lab- and pilot-scale systems to evaluate of the impact of rheology on the final properties of the foamed material and identify the effect of equipment size on expansion behavior of polymer foams.

1.5 Thesis Outline

This thesis is a "sandwich" style and consists of four chapters corresponding to four papers published or accepted for publication in refereed journals. These are preceded by an introductory chapter and followed by a chapter of general conclusions and an appendix. The papers have been written by the author of this thesis and subsequently approved by the coauthors and modified after receiving the reviewers' comments. The author has conducted all experiments and analysis as well.

Chapter 2 is a paper by M. Emami, E. Takacs, M. R. Thompson, J. Vlachopoulos, and E. Maziers published in *Advances in Polymer Technology*, DOI: 10.1002/adv.21323 (2013). This paper explores the foam development process under atmospheric pressure as applicable to rotational molding, investigating the influence of the processing parameters, and characterizing the morphology of the foamed structure.

Chapter 3 is a paper by M. Emami, M. R. Thompson, and J. Vlachopoulos accepted for publication in *Polymer Engineering and Science* (May 2013). This paper studies the bubble nucleation mechanism involved in the foaming process under non-pressurized conditions and investigates the significance of viscosity constraints on nucleation theoretically and experimentally.

Chapter 4 is a paper by M. Emami, M. R. Thompson, and J. Vlachopoulos accepted for publication in *Polymer Engineering and Science* (August 2013). This paper reports on an experimental examination to correlate foamability of polymer materials in a non-

pressurized foaming system with their off-line rheological properties. A bubble growth model and simulation scheme is also presented to describe the bubble growth phenomenon that occurs in such a foaming process.

Chapter 5 is a paper by M. Emami, J. Vlachopoulos, M. R. Thompson, and E. Maziers that will be submitted to *Advances in Polymer Technology*. This paper presents a systematic investigation to evaluate of the impact of rheology on the final properties of the foamed material at different scales of production and identify the effect of equipment size on expansion behavior of polymer foams.

Chapter 6 provides a summary of contributions and concluding remarks for this thesis as well as recommendations for future work, respectively.

Chapter 7 is an appendix which discusses the details of the mathematical formulations and simulation scheme mentioned for the models demonstrated in Chapters 3 and 4.

1.6 References

[1] E. Archer, E. Harkin-Jones, and M.P. Kearns, "Processing Characteristics and Mechanical Properties of Metallocene Catalyzed Linear Low-Density Polyethylene Foams for Rotational Molding," *Polym. Eng. Sci.*, 44, 638- 647, 2004.

[2] G. Liu, C.B. Park, and J.A. Lefas, "Production of Low-Density LLDPE Foams in Rotational Molding," *Polym. Eng. Sci.*, 38, 1997- 2009, 1998.

[3] M. Emami, E. Takacs, M.R. Thopmson, J. Vlachopoulos, and E. Maziers, "Visual Studies of Model Foam Development for Rotational Molding Processes," *Adv. Polym. Tech.*, 32, E809, 2013.

[4] D. Klempner and K.C. Frisch, *Handbook of Polymeric Foams and Foam Technology*. New York: Oxford University Press, 1991.

[5] L. Xu and R.J. Crawford, "Analysis of the Formation and Removal of Gas Bubbles in Rotationally Moulded Thermoplastic," *J. Mater. Sci.*, 28, 2067-2074, 1993.

[6] C.B. Park and N.P. Suh, "Filamentary Extrusion of Microcellular Polymers Using a Rapid Decompressive Element," *Polym. Eng. Sci.*, 36, 34- 48, 1996.

[7] S.T. Lee, *Foam Extrusion: Principles and Practice*. Lancaster, PA: Technomic Publishing Company, 2000.

[8] C.T. Bellehumeur, M. Kontopoulou, and J. Vlachopoulos, "The Role of Viscoelasticity in Polymer Sintering," *Rheol. Acta*, 37, 270-272, 1998.

[9] Z. Tadmor and C.G. Gogos, *Principles of Polymer Processing*. New York: John Wiley & Sons, 1979.

[10] M. Kontopoulou and J. Vlachopoulos, "Melting and Densification of Thermoplastic Powders," *Polym. Eng. Sci.*, 41, 155-162, 2001.

[11] M.K. Bisaria, E. Takacs, C.T. Bellehumeur , and J. Vlachopoulos, "Anatomy of Rotomolding," *Rotation*, 3, 12-18, 1994.

[12] M. Emami, E. Takacs, and J. Vlachopoulos, "Rotational Foam Molding of Metallocene Catalyzed Polyethylene: CBA Screening and Process Characteristics," *J. Cell. Plast.*, 46, 333-351, 2010.

[13] J. Colton and N. Suh, "The Nucleation of Microcellular Thermoplastic Foam with Additives: Part I: Theoretical Considerations," *Polym. Eng. Sci.*, 27, 485-492, 1987.

[14] J. Colton and N. Suh, "The Nucleation of Microcellular Thermoplastic Foam with Additives: Part II: Experimental Results and Discussion," *Polym. Eng. Sci.*, 27, 493-499, 1987.

[15] S.K. Goel and E.J. Beckman, "Generation of Microcellularpolymeric Foams Using Supercritical Carbon Dioxide. Part I.Effect of Pressure and Temperature on Nucleation," *Polym. Eng. Sci.*, 34, 1137–1147, 1994.

[16] J.W. Gibbs, *The Scientific Papers of J. Willard Gibbs*. Mineola, NY: Dover Publ. Inc., 1961.

[17] J. Zeldovich, "On the Theory of New Phase Formation: Cavitation," *Acta Physicochem. U.S.S.R.*, 18, 1-22, 1943.

[18] E.N. Harvey, W.D. McElroy, and A.H. Whiteley, "On Cavity Formation in Water," *J. Appl. Phys.*, 18, 162-172, 1947.

[19] C.A. Wrad and E. Levart, "Conditions for Stability of Bubble Nuclei in Solid Surfaces Contacting a Liquid-gas Solution," *J. Appl. Phys.*, 56, 491-500, 1984.

[20] J. Han and C. Han, "Bubble Nucleation in Polymeric Liquids. II. Theoretical Considerations," *J. Polym. Sci. B: Polym. Phys.*, 28, 743-761, 1990.

[21] S.T. Lee, "Shear Effects on Thermoplastic Foam Nucleation," *Polym. Eng. Sci.*, 33, 418-422, 1993.

[22] P.M. Wilt, "Nucleation Rates and Bubble Stability in Water-Carbon Dioxide Solutions," *J. Colloid Interf. Sci.*, 112, 530-538, 1986.

[23] C.A. Wrad, A. Balakrishnan, and F.C. Hooper, "On the Thermodynamics of Nucleation in Weak Liquid-Gas Solutions," *J. Basic Eng. ASME*, 92, 695-704, 1970.

[24] Y. Kagan, "The Kinetics of Boiling of a Pure Liquid," *Russ. J. Phys.Chem.*, 34, 42-46, 1960.

[25] J.L. Katz and M. Blander, "Condensation and Boiling: Corrections to Homogeneous Nucleation Theory for Non-ideal Gases," *J. Colloid Interf. Sci.*, 42, 496-502, 1973.

[26] R. Cole, "Boiling Nucleation," *Adv. Heat Transfer*, 10, 86-166, 1974.

[27] M. Blander, "Bubble Nucleation in Liquids," *Adv. Colloid Interface Sci.*, 10, 1-32, 1979.

[28] L. Rayleigh, "On the Pressure Developed in a Liquid During the Collapse of a Spherical Cavity," *Philos. Mag.*, 34, 94-98, 1917.

[29] P.S. Epstein and M.S. Plesset, "The Stability of Gas Bubbles in Liquid-Gas Solutions," *J. Chem. Phys.*, 18, 1505-1509, 1950.

[30] L.E. Scriven, "On the Dynamics of Phase Growth," *Chem. Eng. Sci.*, 10, 1-13, 1959.

[31] E.J. Barlow and W.E. Langlois, "Diffusion of Gas from a Liquid into an Expanding Bubble," *IBM J. Res. Dev.*, 6, 329-337, 1962.

[32] J.R. Street, "The Rheology of Phase Growth in Elastic Liquid," *J. Rheol.*, 1, 103-131, 1968.

[33] C.D. Han and H.J. Yoo, "Studies on Structural Foam Processing: IV. Bubble Growth during Mold Filling," *Polym. Eng. Sci.*, 21, 518-533, 1981.

[34] D.C, Venerus, N. Yala, and B. Bernstein, "Analysis of Diffusion-Induced Bubble Growth in Viscoelastic Liquids," *J. Non-Newton. Fluid*, 75, 55-75, 1998.

[35] M. Amon and C.D. Denson, "A Study of the Dynamics of Foam Growth: Analysis of the Growth of Closely Spaced Spherical Bubbles," *Polym. Eng. SCi.*, 24, 1026-1034, 1984.

[36] M. Amon and C.D. Denson, "A Study of the Dynamics of Foam Growth: Simplified Analysis and Experimental Results for Bulk Density in Structural Foam Molding," *Polym. Eng. Sci.*, 26, 255-267, 1986.

[37] A. Arefmanesh and S.G. Advani, "An Accurate Numerical Solution for Mass Diffusion-Induced Bubble Growth in Viscous Liquids Containing Limited Dissolved Gas," *Int. J. Heat Mass Transfer*, 35, 1711-1722, 1992.

[38] A. Arefmanesh and S.G. Advani, "Nonisothermal Bubble Growth in Polymer Foams," *Polym. Eng. Sci.*, 35, 252-260, 1995.

[39] A. Arefmanesh and S.G. Advani, "Diffusion-Induced Growth of a Gas Bubble in a Viscoelastic Fluid," *Rheol Acta*, 30, 274-283, 1991.

[40] N.S. Ramesh, D.H. Rasmussen, and G.A. Campbell, "Numerical and Experimental Studies of Bubble Growth During the Microcellular Foaming Process," *Polym. Eng. Sci.*, 31, 1657–1664, 1991.

[41] J.L. Throne, "The Foaming Mechanism in Rotational Molding," in *SPE/ANTEC*, 46, 2000, 1304-1308.

[42] M.B. Bradley and E.M. Phillips, "Novel Polypropylenes for Foaming on Conventional Equipment," *Plast. Eng.*, 47, 82-84, 1991.

[43] C.B. Park and L.K. Cheung, "A Study of Cell Nucleation in the Extrusion of Polypropylene Foams," *Polym. Eng. Sci.*, 37, 1-10, 1997.

[44] H.E. Naguib, C.B. Park, U. Panzer, and N. Reichelt, "Strategies for Achieving Ultra-low Density PP Foams," *Polym. Eng. Sci.*, 42, 1481-1492, 2002.

[45] M. Yamaguchi and K I. Suzuki, "Rheological Properties and Foam Processability for Blends of Linear and Crosslinked Polyethylenes," *J. Polym. Sci. Part B. Pol.Phys.*, 39, 2159- 2167, 2001.

[46] P. Spitael and C.W. Macosko, "Strain Hardening in Polypropylenes and Its Role in Extrusion Foaming," *Polym. Eng. Sci.*, 44, 2090-2100, 2004.

[47] J. Stange and H. Münstedt, "Rheological Properties and Foaming Behavior of Polypropylenes with Different Molecular Structures," *J. Rheol.*, 50, 907-923, 2006.

Chapter 2

Visual Studies of Model Foam Development for Rotational Molding Processes

This chapter has been published as:

M. Emami, E. Takacs, M.R. Thompson, J. Vlachopoulos, and E. Maziers, "Visual Studies of Model Foam Development for Rotational Molding Processes" *Adv. Polym. Tech.*, 32, E809-E821, 2013 (DOI: 10.1002/adv.21323). I am the sole contributor to this paper.

Abstract

This work explores the foam development process under atmospheric pressure as applicable to rotational molding, investigating the influence of the processing parameters, and characterizing the morphology of the foamed structure. Detailed understanding of the bubble transformation during foaming of non-pressurized polymer melts provided an accurate basis for predicting the morphological structure and macroscopic properties of foams produced by rotational molding. The experimental results are based on visualization studies using a hot stage microscopy setup. The cellular structure developed during the foaming was analyzed for its bubble density, bubble size and statistical

parameters considering the combined effect of these two factors. It was found during this investigation that the foaming mechanism is comprised of four distinct stages. It included two major stages of bubble nucleation, *primary nucleation* in interstitial regions and *secondary nucleation* in the polymer melt. Statistical analysis of the developing foamed structure revealed that primary nucleation in the interstitial regions was the controlling stage in determining the final cellular structure. Subsequently, the nucleation stages were followed by bubble growth and bubble coalescence/shrinkage. The microscopic observations were complemented by actual rotational foam molding experiments.

2.1 Introduction

Commercial interest in polymeric foams continues to increase since the cellular structure of foamed materials provides unique physical features while reducing the weight and cost of resins in formed parts. Foams have improved insulating properties, impact-resistant characteristics, energy absorbing properties and outstanding stiffness-to-weight ratios [1,2]. In rotational molding, foams exhibiting skin-core morphologies can be used to produce innovative, high-value parts with little specialized equipment required. Foam structures can be used to combat the low mechanical and shock mitigation properties due to the hollow structure present in many rotationally molded products [3].

Processing of plastic foam involves the dispersion of gases within a polymer matrix. The gaseous phase may be generated from either a physical blowing agent or a chemical blowing agent. The employment of physical blowing agents in the foaming process requires elevated mold pressures. In atmospherically governed foaming systems such as rotational foam molding, chemical blowing agents have been the most common method for generating cellular structure. Chemical blowing agents are solid or liquid materials that decompose under certain conditions to liberate gas [4,5,6].

To develop a foam structure in the rotational molding process, the polymer matrix has to form a continuous melt phase to minimize losses of the liberated blowing gas to the

atmosphere and reduce the adverse effect of incoherent polymer melt on the bubble morphology of the foam structure [7,8]. Polymer powder particles tend to decrease their total surface area by fusing together when in contact with each other at elevated temperatures- this is called *sintering*. The driving force for the sintering is surface tension and the main factor opposing this mechanism is the resistance to flow, expressed by viscosity [9]. Polymer sintering is viewed as the fundamental and controlling mechanism for the rotational molding process, because it commands a significant part of the heating time. The sintering process proceeds in two stages, first by developing interfaces between adjacent particles, followed by a stage in which the density increases by elimination of the inter-particle cavities [10,11].

In the rotational foam molding process, the sintering step should be completed before the onset of bubble nucleation and growth in order to produce foams with higher bubble density and more uniform bubble size distribution [7,8]. Blowing agent should be uniformly dispersed in the matrix and when in solid form, wetted by the molten polymer. The gases released in the polymer melt above the decomposition temperature of the blowing agent initiate the foaming expansion process, which generally comprises three fundamental steps: bubble nucleation, bubble growth, bubble coalescence and stabilization. The bubble nucleation step occurs simultaneously with the decomposition of the blowing agent particles and it begins at an initiation site within the polymer melt that has been supersaturated with the blowing gas. Due to the continual supply of gas, the pressure in the nucleated bubbles increases while the pressure of the polymer matrix is maintained at atmospheric pressure during the entire process. This pressure difference is the main driving force for the growth of the bubble nuclei. The rate of bubble growth is limited by the available blowing gas, the rate of gas diffusion within the polymer matrix, and the viscoelastic properties of the polymer melt. As the bubbles grow, adjacent bubbles eventually come into contact with each other. These bubbles share a common wall and the thickness of the wall decreases as the bubbles expand further till they coalesce. Bubble coalescence is thermodynamically favorable because the free energy is lowered by reducing the surface area of the bubbles. However, coalescence generally

results in a coarse cellular structure and a reduction in the bubble population density, both of which could have detrimental effects on the mechanical and thermal properties of molded foams [12,13]. The coalescence of bubbles occurs primarily because of the low melt strength of the molten polymer. The melt strength, by definition, may be considered the degree of resistance to stretching forces during volume expansion. Therefore, the bubble wall stability will increase as melt strength increases [8,14,15].

Many studies have addressed the technology of rotational foam molding; however, few investigations concentrate on the fundamental concepts of this unique foaming process [7,8,14,15]. The aim of this work is to investigate the foaming process at a microscopic level, in order to clarify the fundamental mechanisms involved in rotational foam molding. The study examines the effects of processing conditions and seeks an improved explanation for the developed morphological structure.

2.2 Experimental

2.2.1 Materials

A medium density polyethylene (MDPE) supplied by Total Petrochemicals (Feluy, Belgium) was used for this study. The material was determined to have a density of 0.934 g/cm^{3}and a melt flow index of 8 g/10 min (ASTM D1238, 190˚C/2.16 kg). The polyethylene material had an average particle size of 310μm, according to ASTM D1921. An exothermic chemical blowing agent (CBA), 4,4'-oxy-bis(benzenesulfonylhydrazide), was used for the foaming experiments. Particle size measurements by optical microscopy of the CBA revealed an average dimension of 6 μm for the powder. All the materials were used as-received.

2.2.2 Visualization Procedure

A hot stage optical microscopy setup was used to observe and investigate the foaming mechanism. Dry-blended mixtures of the MDPE and CBA were prepared for the

experiments using varied contents of the blowing agent. Low CBA contents of 0.25% and 0.5% were used in this study in order to minimize error involved in the two-dimensional image analysis of bubble morphology by avoiding excessive bubble overlap in the cellular structure. A sample cup holder, made of glass (D = 2.5cm. H = 1 cm), was loaded with a predetermined amount of the blend and placed in the center of the hot stage. The initial thickness of the powder bed inside the cup was approximately 2 mm. The temperature of the stage was controlled with the aid of a discrete temperature controller. The samples were heated up and once the processing temperature reached the desired level, the stage was cooled. Figure 2.1 shows a temperature-time plot representative of the heating conditions in the hot stage compared to those used in the subsequent rotational molding trials. The temperature of the polymer melt was constantly monitored and recorded by a K-type thermocouple. This setup simulated well the conditions of a full processing cycle for an actual rotational molding unit. The process of foam development was observed through an Olympus optical microscope and recorded with a Panasonic BP-310 digital video camera. Image analysis was performed using SigmaScan Pro 5 (SYSTAT Inc., San Jose, CA, USA) in order to quantify the morphology during different stages of foaming. All the experiments were done under atmospheric pressure and the duration of the experiments was 30 min.

2.2.3 Rotational Foam Molding Procedure

Rotational molding experiments of foams with a monolayer wall structure were performed in a laboratory scale uniaxial rotomolding machine. The machine consisted of an electrically heated oven surrounding a square-shaped Teflon-coated steel mold. The mold was approximately 9.5cm × 9.5cm × 10cm cube shaped. A shot weight of l00g was used in each experiment which produced a uniform part with a wall thickness of 3 mm.

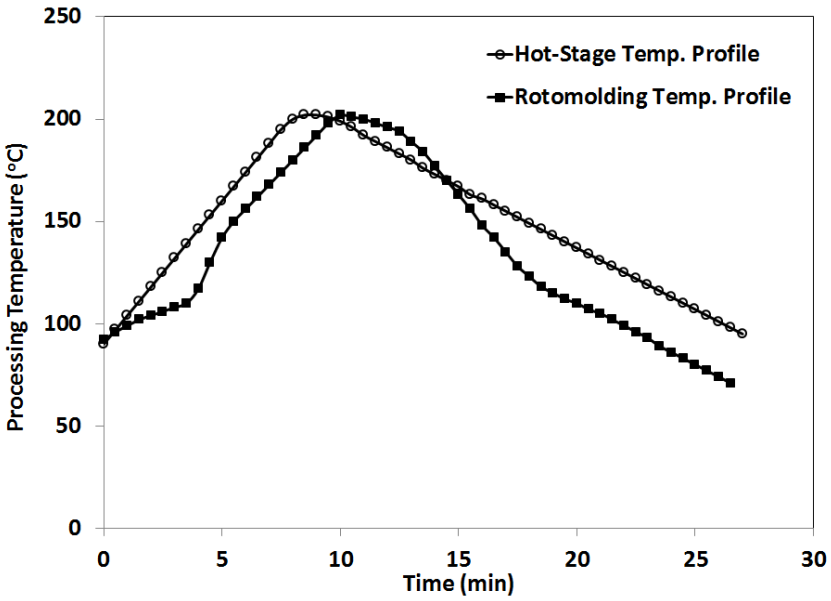

Figure 2-1: Temperature-time plot of the heating conditions in the hot stage and rotational molding trials.

The mold rotation speed was set at 4 RPM. A thermocouple inserted into the center of the mold through a rotating hollow shaft was used to measure and record the in-mold temperature changes during processing. A Panasonic SDR-H80 digital video camera was used to record the ongoing foam development process through the front glass scaled window. Images were analyzed by using SigmaScan Pro 5 (SYSTAT Inc., San Jose, CA, USA) for the foam thickness measurements.

2.2.4 Thermal Characterization

Thermal characteristics of the MDPE and blends of MDPE/CBAs were evaluated by using a TA Instruments Q200 differential scanning calorimeter (DSC) (New Castle, DE, USA). Samples of 5-10 mg of powder were sealed in an aluminum hermetic pan, and subsequently heated from 20 ˚C to 200˚C at a rate of 10˚C/min to analyze the interaction between the polyethylene and the foaming agent during the foaming process. This temperature range and heating rate appropriately corresponded to the conditions used by

the rotomolding process and visualization study, as evident by the previously mentioned temperature profiles of each in Figure 2.1. The sample was then cooled to 20˚C, and a second heating sequence was performed at the same heating rate in order to characterize the post-processing product, namely the final foamed polyethylene. A nitrogen atmosphere was used during the measurements. The DSC experiments were replicated five times to determine their reproducibility, showing results with a maximum deviation between the repeated runs of about 2%.

Thermal stability of the blowing agent was studied by thermogravimetric analysis (TGA Netzsch STA 409) under atmospheric air. Testing was done under non-isothermal conditions over a temperature range from room temperature to 200°C, with a heating rate of 10°C/min.

2.3 Results and Discussion

2.3.1 Thermal Properties and Decomposition Behavior

The decomposition behavior of the pure blowing agent was studied by TGA and DSC analyses and a comparison of the measurements is presented in Figure 2.2. According to TGA data, the blowing agent showed a rapid decrease in sample weight over a narrow range in temperature during heating, with both onset and peak weight loss corresponding to 167^{o}C. The weight loss of 44.7% noted in the thermogram at 167^{o}C corresponded to complete liberation of nitrogen and water vapor by thermal decomposition of the blowing agent. The chemical residuals from the reaction demonstrated thermal stability with no further change in masses noted for the blowing agent from 167^{o}C to 200^{o}C. DSC analysis results of the pure blowing agent were consistent with the TGA measurements despite being conducted under nitrogen rather than air. The DSC thermogram showed a sharp exothermic reaction with a peak temperature of 167.6˚C. The thermal reaction, corresponding to the decomposition behavior of CBA, occurred over a very short period

of time and it was followed by a positive shift in the baseline which is believed is due to the mass reduction and different composition of the by-product materials.

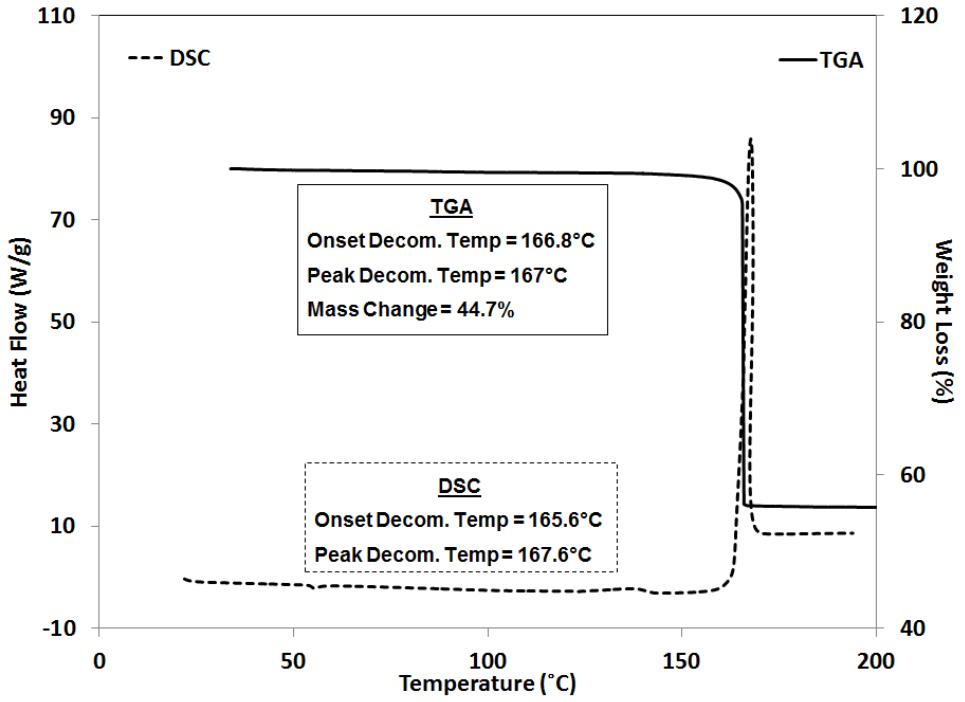

Figure 2-2: Thermal analysis of the pure blowing agent, using TGA and DSC techniques.

Figure 2.3 shows the DSC curves of MDPE and an example of a tested powder mixture comprised of the resin with 0.5% CBA. The onset melting point, peak melting temperature and crystallization temperature of neat MDPE were found to be 115˚C, 122˚C and 108˚C, respectively. The decomposition behavior of the blowing agent in the presence of the resin and the effect of by-products on the thermal properties of the resin were subsequently investigated by testing of the mixture. The first heating cycle of the mixture showed an endothermic peak demonstrating MDPE melting and an exothermic peak corresponding to the CBA decomposition (seen in the expanded window in Figure 2.3). The onset of exothermic peak in this case corresponded to the peak decomposition temperature determined for the pure CBA (167˚C). Even though pure CBA exhibited a very sharp decomposition profile, the reaction in a matrix of polymer covered a broader

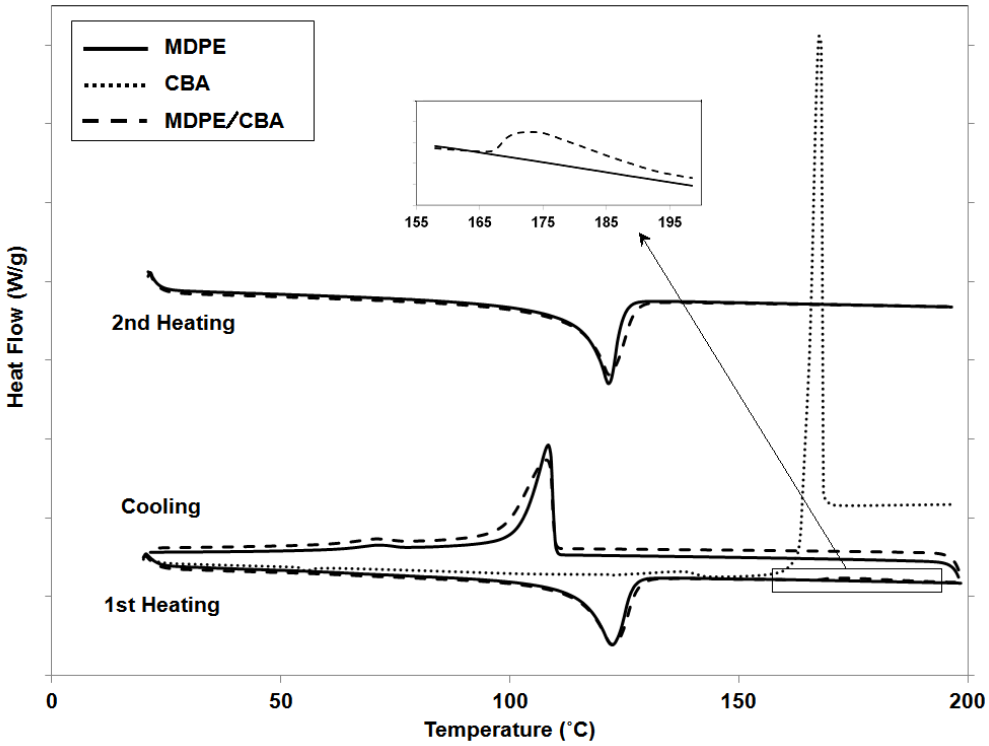

Figure 2-3: Thermal analysis of the resin (MDPE), blowing agent (CBA), and resin-blowing agent mixture (MDPE/CBA using 0.5% CBA), using DSC.

temperature range of approximately 30˚C. A consecutive second heating run yielded a single endothermic peak at 122˚C. It was noted that the onset and peak melting temperatures of the endotherm remained consistent with the first run and that of the neat MDPE resin despite the presence of CBA residuals in this case, though a minor increase in the degree of crystallinity was observed (46% and 50% for pure MDPE and MDPE/CBA blend, respectively). These results revealed the fact that the foamed polyethylene maintained virtually similar thermal properties after foaming in the DSC pan. It was also observed that for the second heating cycle, no additional peaks appeared, indicating that CBA decomposed completely during the first heating run.

The information provided by the DSC and TGA analysis outlined the thermal transitions involved in the foam formation process to be studied. The data was used to determine appropriate processing conditions.

2.3.2 Foaming Process- Visualization Experiments

Foam development was investigated using the mentioned hot stage microscopy setup in the experimental section. The experimental data were used to elucidate the foaming mechanism at ambient pressure covering four major stages: two stages of bubble nucleation, followed by bubble growth, and bubble shrinkage/coalescence. Explicit details of each stage are described in the following sections.

Bubble Nucleation

By approaching the melting point of the polyethylene matrix at 122˚C, adjacent polymer particles became bridged at their contact points and produced a porous three dimensional network, though the individual particles still remained distinctive in shape (Figure 2.4a and 2.4b). At 135˚C, the powder was completely melted (Figure 2.4c). As the processing temperature increased further, sintering proceeded with particles starting to lose their identity by reaching 155˚C and a coherent network of voids was formed as the interstitial air trapped in the melt decreased in size, as shown in Figures 2.4d and 2.4e. The shrinkage of these interstitial voids is a phenomenon controlled by the diffusion of air from the area towards the surrounding melt [16]. Further densification of the sintering polymer was observed until the onset of decomposition for the blowing agent at 163˚C, when the voids began to appear more spherical in shape (as highlighted by the arrows in the expanded view of Figure 2.4f). The interstitial voids at this point were 7-75μm in size (referring to the expanded view of Figure 2.4f). Before CBA decomposition, there was not enough time for the polymer mass to fully densify and for void elimination to be completed, which is due to the high viscosity and low sintering rate of the molten polyethylene at this range of temperature [16]. The interstitial voids remaining from sintering of the MDPE were observed to start to grow from this point, as shown by the morphological transition from images in Figures 2.4g to 2.4h. In this paper, this is referred to as the *primary nucleation* stage.

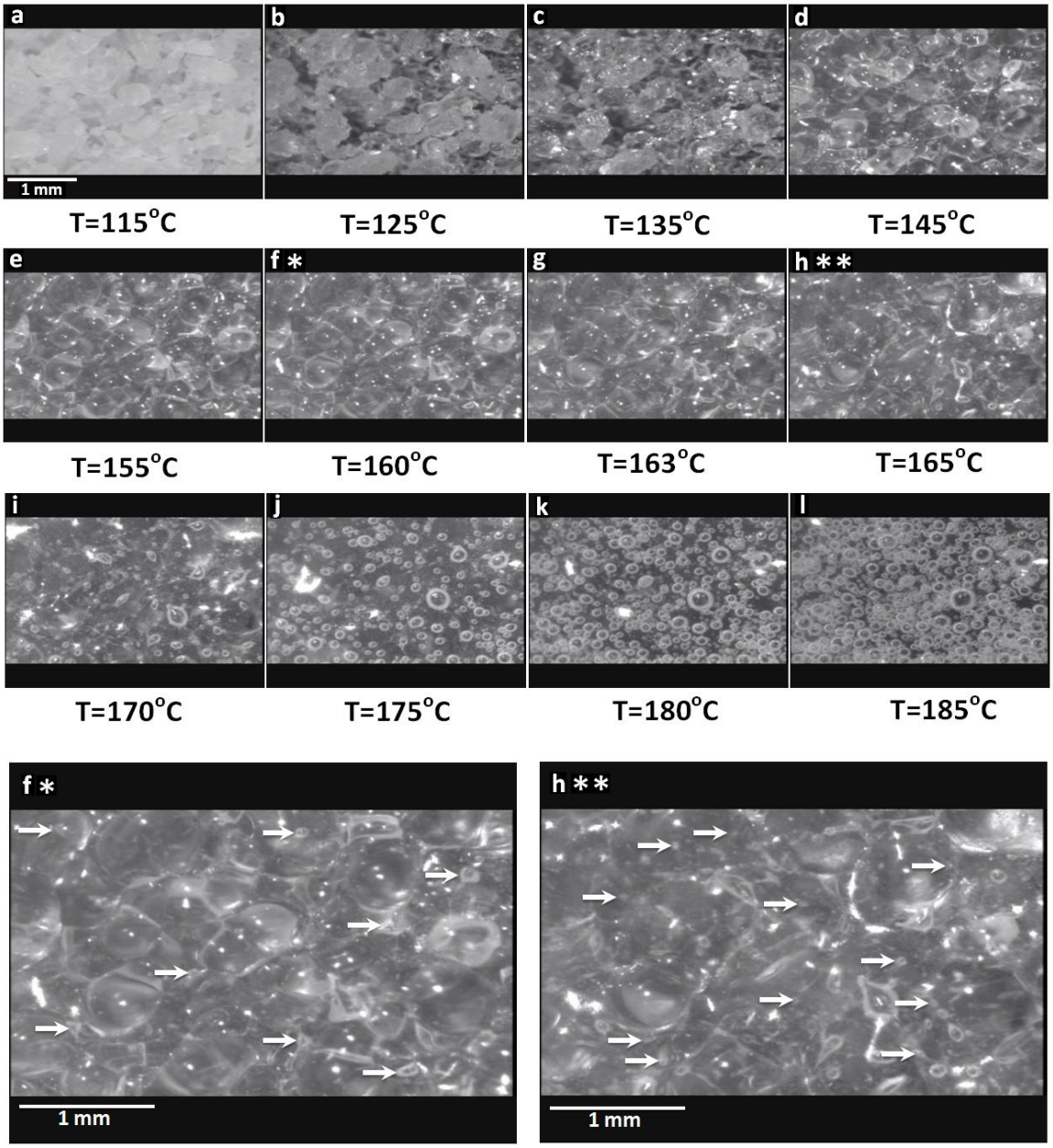

Figure 2-4: Nucleation stage of the foam development process, using 0.5%wt CBA and heating rate of 10-15˚C/min- a) polymer powder, b) bridged polymer particles, c) molten polymer, d & e & f & g) polymer particles sintering and densification, h) primary nucleation, i & j) growth of the first generation of bubbles, k) secondary nucleation, and l) growth of all generated bubbles.

The interstitial regions of the sintered powder were acting as nucleation sites for the diffused gases generated from the decomposing CBA during the primary nucleation stage.

It was also observed during this timeframe that some smaller bubbles, about 30-40µm, were formed at the boundaries of incompletely fused polymer particles, which were believed to correspond with the dimensions of agglomerated CBA particles (highlighted in the expanded view of Figure 2.4h). The shapes of the bubbles formed during the primary nucleation stage were defined by the interstitial voids they grew from and hence tended to be more irregular in shape than traditional bubbles. As the time progressed, the diffused gases from the decomposed CBA particles caused the nucleated bubbles to grow and their shapes became more spherical (Figures 2.4i and 2.4j) as the system sought to reduce its total surface energy [17].

With the passage of time after primary nucleation occurred (a delay of 70 s as the system reached 180^{o}C), a new generation of bubbles formed and then grew within the polymer melt in areas not previously experiencing foaming, as shown in Figures 2.4k and 2.4l. This is being referred to as the *secondary nucleation* stage in this paper. The polymer melt at this stage appeared homogeneous without the discrete outlines of individual particles as witnessed during the onset of the first stage of nucleation. Nucleation of this second series of bubbles occurred over a short period of time (10s) with the resulting foam demonstrating greater uniformity in bubble size, being in the order of 20-30µm, compared to those bubbles initiated by primary nucleation.

In order to investigate the significance of the two stages of nucleation in determining the final cellular structure, individual bubbles were followed during the foam development process. Figure 2.5 shows examples of the analysis done on the morphology for the stages of primary and secondary nucleation in order to determine contributions by the bubbles formed during each to the final cellular structure. It was observed that those bubbles formed by primary nucleation were the most likely to persist during the entire foaming process. Most of the bubbles generated during secondary nucleation disappeared over time and very few remained in the final bubble population. These second-generation

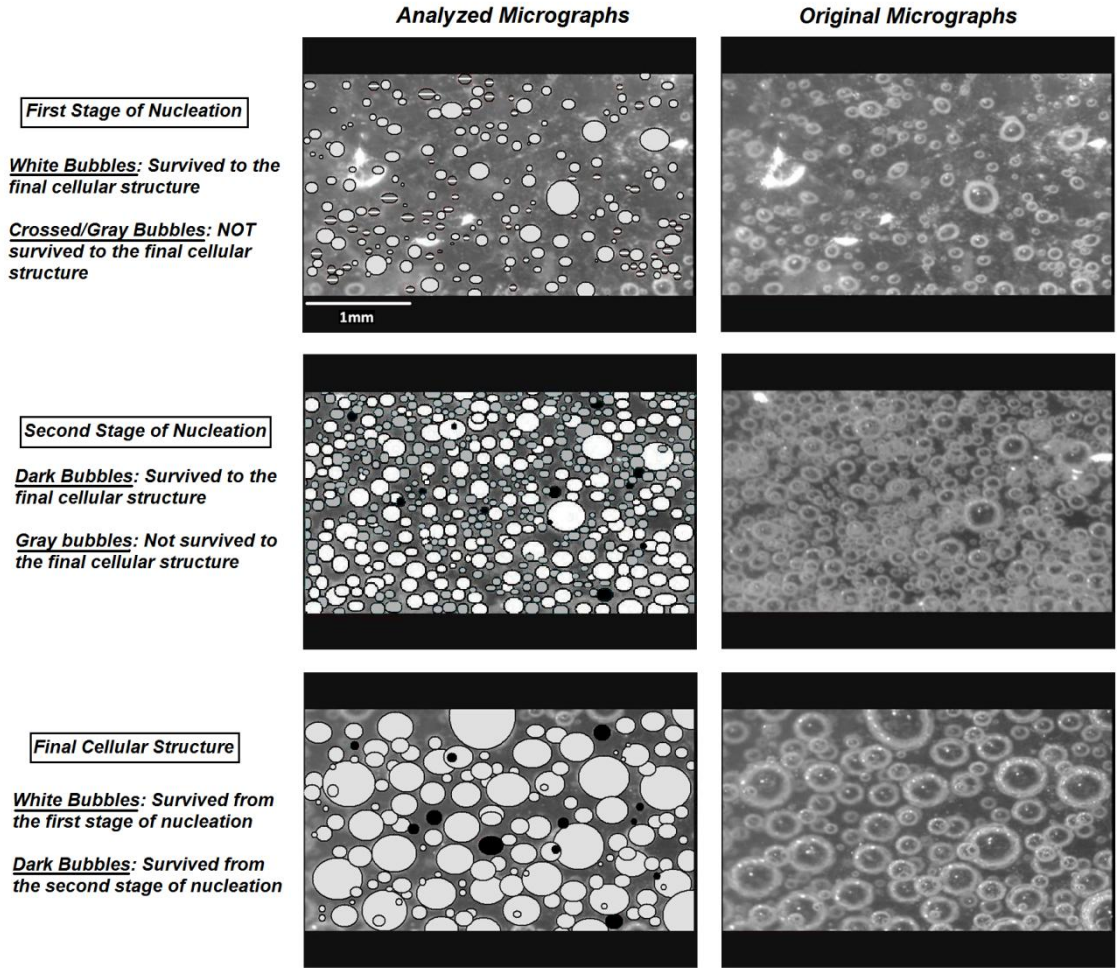

Figure 2-5: Micrographs of first and second generation of nucleated bubbles and final cellular structure, using 0.5% CBA and heating rate of 10-15˚C/min.

bubbles either joined other bubbles through bubble coarsening or collapsed as the gas diffused back into the polymer melt. It was noted that only bubbles nucleated in areas of the melt far from the first generation of bubbles were likely to survive. Figure 2.6 plots the parameter of cell density from this bubble-life analysis indicated in Figure 2.5. On average, the origins of more than 90% of the surviving bubbles corresponded to the primary nucleation stage though only 40% of total bubble nuclei observed in the test were generated during the first stage. Almost 75% of the bubble nuclei generated during the primary stage participated in the final cellular structure, whereas barely 5% of the second

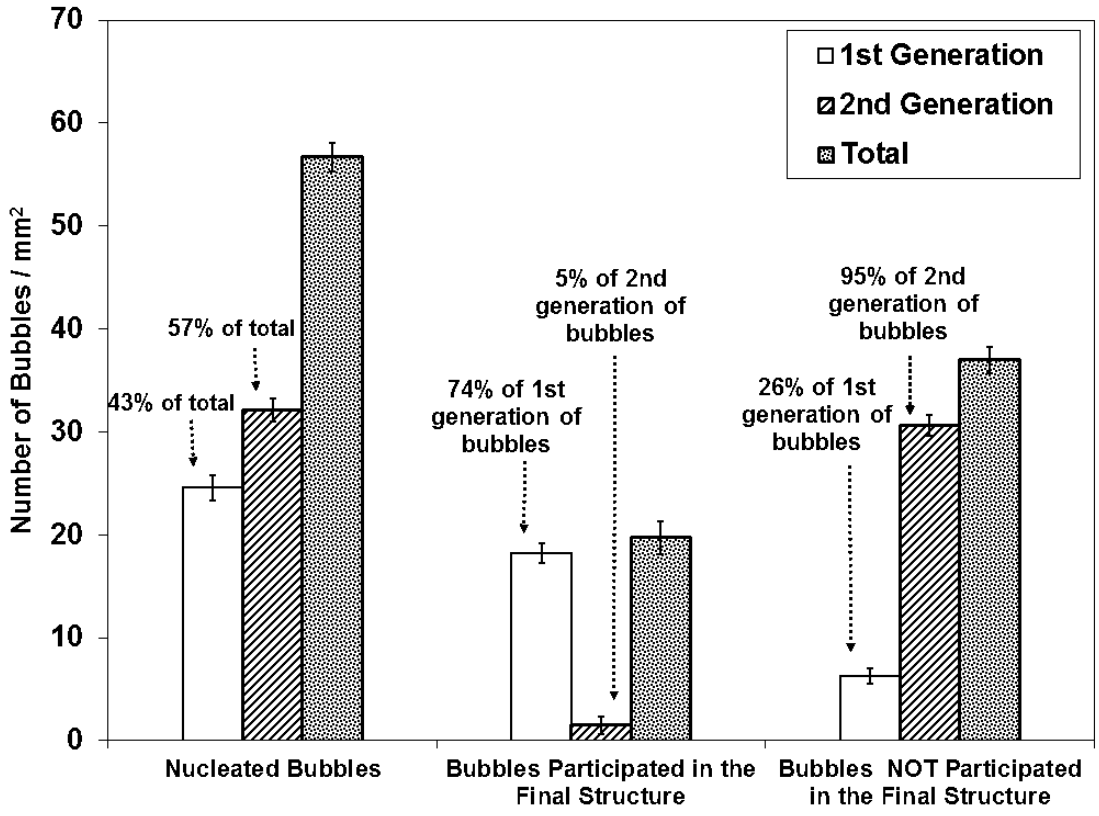

Figure 2-6: Contribution of primary and secondary nucleation in the final cellular structure, using 0.5% CBA and heating rate of 10-15˚C/min.

generation of bubble nuclei survived to the final foam product. This behavior is believed to be associated with the critical nucleated bubble radius theory [18]. According to this theory, there is a minimum size (R^*) for the bubble to be viable which is related to the maximum free energy of the system. Nucleated bubbles are forever in an unstable state with their environment. If the bubble size is less than R^*, the system can lower its free energy by dissolution of the gas into the surrounding polymer, whereas if the bubble size is larger than R^*, the growth of the bubble causes a reduction in the free energy. The data from the analysis suggested that the bubble nuclei formed using the interstitial regions between sintered particles generally exceeded R^* in dimension, while those formed spontaneously within the polymer melt during secondary nucleation were generally below

*R**. It was thought that too much of the dissolved gas from the decomposed CBA had already diffused to the primary nuclei that the secondary nuclei lacked adequate sources of gas to grow unless far isolated.

Bubble Growth and Coalescence/ Shrinkage

Once bubbles were nucleated, growth and coarsening occurred simultaneously with both mechanisms dynamically competing against one another during the span of the foaming process. The size of first generation bubbles grew through gas diffusion as well as by coalescing with adjacent bubbles, mostly from the second generation of bubbles. Most of the secondary nucleated bubbles disappeared through foam coarsening by coalescence, or shrank in size with some of them totally disappearing. A very limited number of second generation bubbles survived to the end of the foaming process, as mentioned above. The bubble growth/coalescence phenomena continued during the cooling cycle until the polymer matrix reached the crystallization point. The size and shape of the bubbles were actively changing as long as the matrix was molten. By reaching the crystallization point at 108˚C, the cellular structure reached a stabilized morphology.

The bubble growth and coalescence phenomena were evaluated by parameters related to the entire processing cycle similar to that done for the nucleation stages. Figures 2.7a and 2.7b show the typical bubble density and bubble size curves at different stages of the process. The profile for bubble density consisted of two characteristic stages (Figure 2.7a). Initially, a rapid increase in the number of bubbles was observed as the system was in transition between the two stages of nucleation (165˚C-180˚C). This was followed by a significant reduction in bubble density representing the early stages of coalescence and gas re-dissolution; the steepness of this decline corresponded to the high levels of activity of coalescence and gas re-dissolution as heat continued to be applied to the polymer. Interestingly, this rapid decline during the heating cycle started immediately after secondary nucleation occurred, though bubble density continued to decline up to the end of the foaming process. The rate of decrease in bubble density was much slower during

the cooling cycle as the system approached the crystallization temperature of the polymer. Comparatively, the nominal size of the bubbles increased during the entire foaming process (Figure 2.7b). The most rapid bubble growth was noted as the bubble density declined during the heating cycle, though bubble growth continued during cooling, albeit at a slower pace. The rate of bubble growth reached its lowest value near the crystallization point of the MDPE. Continuous changes in the bubble density and bubble size indicated that the foam morphology was not stabilized until crystallization occurred.

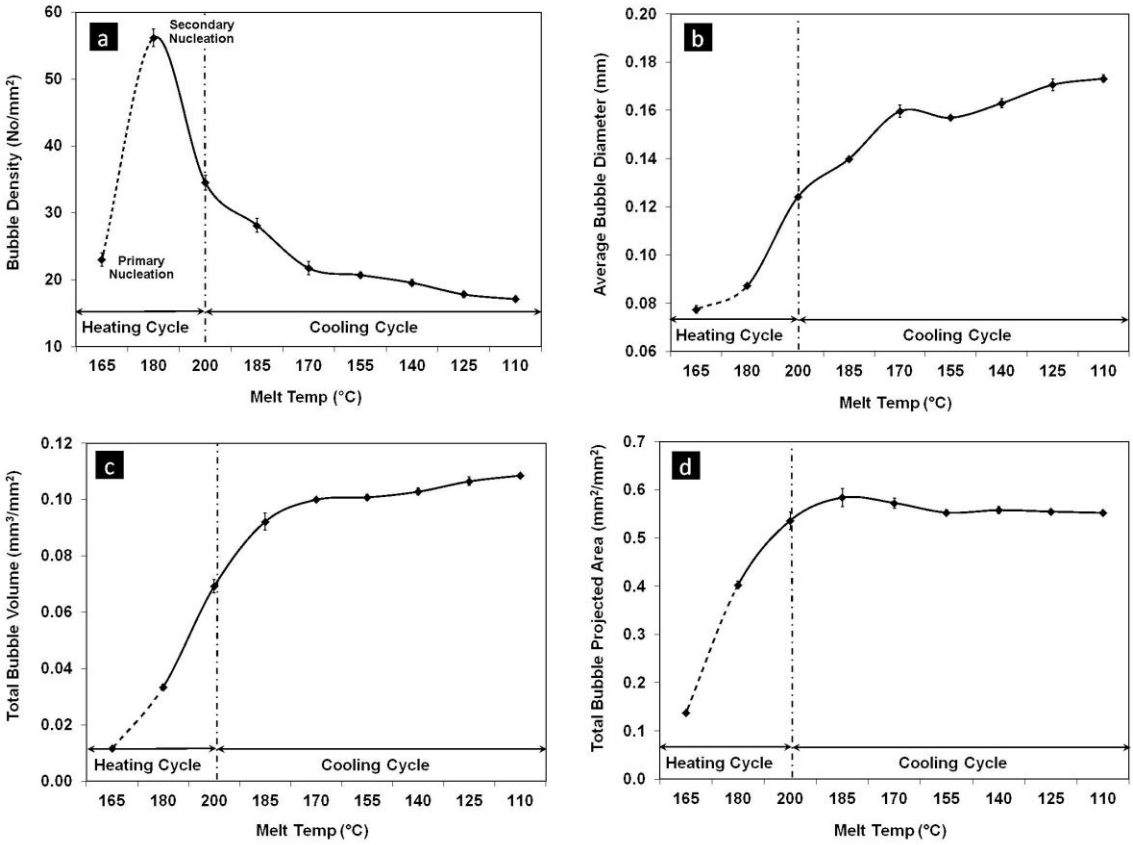

Figure 2-7: Evaluation of different stages of the foaming process using 0.5% CBA, a) Bubble number distribution, b) Bubble size distribution, c) Bubble volume distribution, and d) Bubble projected area distribution. The dashed line between two stages of nucleation has no physical meaning.

It has been shown that it is the combined effect of bubble density and bubble size which defines the final foam properties [7]. These two parameters are effective statistical values

for characterizing the cellular structure of the foam. However, individually they do not carry information regarding two- and three-dimensional variations in the foamed structure and show limited capabilities to capture all phenomena occurring during foam development. In this regard, two cumulative parameters were found to be more informative in this regards, namely total bubble volume and total bubble projected area, which are the cumulative volume and projected area of all the bubbles observed per unit area of the foamed sample, respectively (Figures 2.7c and 2.7d). Total bubble volume represents the total gas phase volume not dissolved within the polymer melt. The total projected area is the cumulative two-dimensional area measurement of the three-dimensional foamed particle, by projecting the bubble shapes on to a plane parallel to the foam wall. It was observed that the total volume of bubbles followed a smoother version of the trend of changes of the size distribution, which generally demonstrates the activity of the bubble growth mechanism. The total volume of bubbles increased over time rapidly until it reached a plateau at around 180˚C during the cooling cycle. From this time forward the system entered into a more-or-less stabilized state. The total projected area of bubbles showed an increasing trend up to a plateau again at 180˚C where a reduction in the total area was observed. The rising and declining trends seen with this parameter are associated with the dominant mechanisms of bubble growth and bubble coalescence/shrinkage of the foaming process, respectively. In the last stages of foaming, the total area of bubbles showed a plateau reflecting foam stability, a steady state condition between these two competing mechanisms. Through actual rotational foam molding experiments, the next section of this paper will further discuss the significance of these two parameters for evaluating the foaming process.

2.3.3 Rotational Foam Molding

The foaming behavior of MDPE/CBA mixtures was studied under actual processing conditions using a uniaxial rotomolding machine to investigate the correlation between the properties of the developing foam product and cellular structure parameters discussed in the previous section. The experiments were conducted with a maximum air

temperature in the chamber of 200°C and a heating rate of 9-12°C/min. As a characteristic parameter, thickness of the foam was monitored and recorded during the foaming experiment.

During the heating cycle, the thickness of the molded part started to expand as the operating temperature reached the onset decomposition temperature of the blowing agent. The thickness expansion continued to the end of the heating cycle, while the foam thickness showed a different behavior during the cooling run. At the early stages of cooling, the foam thickness continued to increase until it reached a maximum of 7.8 mm (thickness of the unformed part was 3mm at this point in comparison). As the experiment continued beyond this point, the foam thickness decreased at a considerable rate and experienced substantial shrinkage with the walls retracting 30% from their maximum thickness. After a certain time, no notable change was observed for the thickness of foam, reaching an asymptotic value (5.5 mm). It is the first time that such an observation has been reported in the open literature. The foam thickness variation during the foaming process is presented in Figure 2.8.

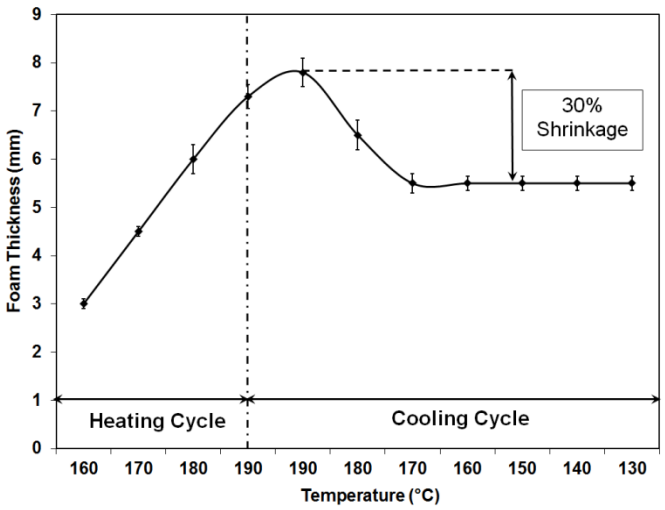

Figure 2-8: Foam thickness during rotational foam molding experiment, using 0.5% CBA and heating rate of 10˚C/min.

Based on the observations of rotational foam molding experiments, the significance of four distributions (number, size, volume and projected area) from the hot stage studied were compared against the monitored thickness changes in the mold. It appeared that the whole foaming process in the rotomolding machine with respect to thickness variation can be best described by the *total bubble projected area* parameter (discussed in the previous section). This parameter and foam thickness followed the same trend of change over the processing time. While bubble size and the total bubble volume parameter can be considered representative measures of the bubble growth mechanism and the bubble number distribution correlates well with bubble coalescence and disappreance, bubble projected area distribution captured the combined effect of these two mechanisms involved and provides a true picture of the actual rotational foam molding process.

2.3.4 Effect of Processing Temperature on the Cellular Structure

Using the hot stage microscopy setup again and a slightly lower value of CBA, 0.25%, the effect of different maximum processing temperatures on the foaming performance and the developing cellular structure was studied. The lower CBA concentration was necessary to completely avoid bubble overlap during foaming and accurately compare these newly introduced statistical parameters for the bubble structure at different processing conditions. Bubble density, bubble size, total projected bubble area and the corresponding temperature profiles for each test condition which stipulated the maximum temperatures reached, are all presented as a function of time in Figure 2.9. Pictures of the melt at different stages of foaming are presented in Figure 2.10 to aid in visualizing the changes.

The bubble density (Figure 2.9a) for all experiments followed similar trends, including a sharp increase in the number of bubbles as the foaming melt transitioned between the two stages of nucleation, before a sudden decrease in the bubble density due to bubble coalescence. It was noted that the number of nucleated bubbles and the rate of nucleation were virtually independent of the processing temperature. However, by decreasing the

maximum processing temperature from 200°C to 180°C, a significant increase in the bubble density at the maximum processing temperature and in the final foamed structure was observed. This behavior can be explained by the higher activity of bubble dissolution and bubble coarsening mechanisms at higher processing temperatures, which indicated that the activity of these two mechanisms was a strong function of melt temperature. Higher gas re-dissolution may be due to the higher solubility of nitrogen in a polyethylene matrix at higher temperatures [19], and lower melt strength and viscoelastic properties of the polymer matrix at said temperatures which can lead to further bubble coalescence.

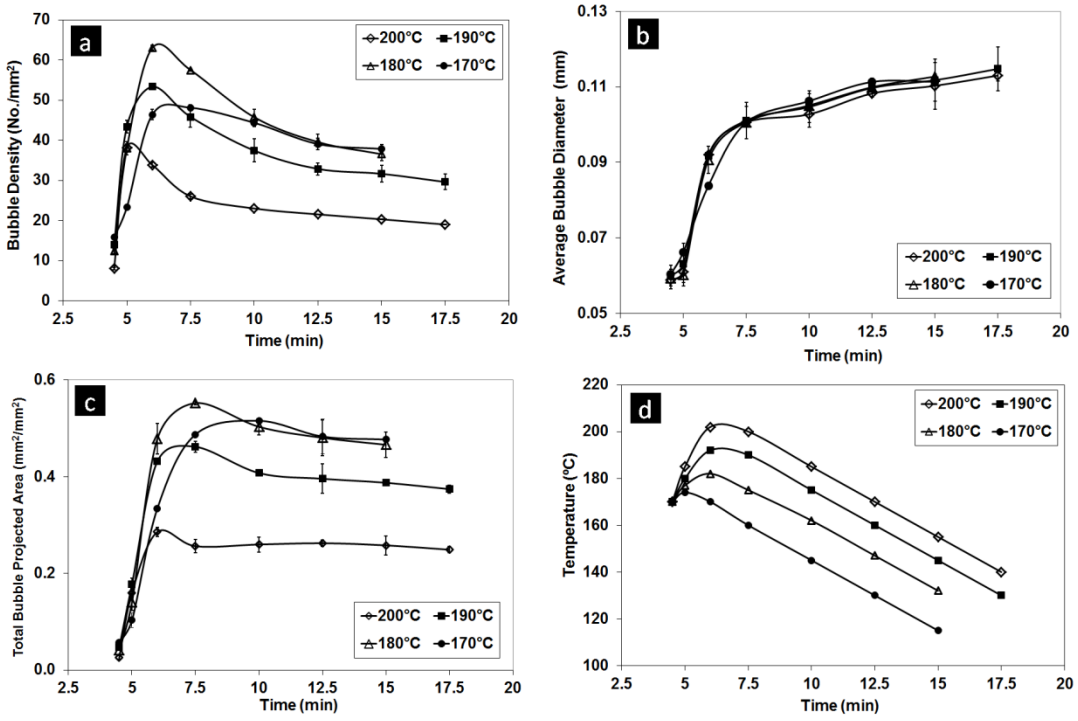

Figure 2-9: Effect of processing temperature using 0.25% CBA, a) Bubble number distribution, b) Bubble size distribution, c) Bubble projected area distribution, and d) Temperature profile.

When 170°C was the maximum processing temperature, the peak number of bubbles seen in the polymer was considerably lower compared to the maximum number of bubbles observed for the maximum temperature of 180°C and 190°C, which was believed to be due to the higher melt strength of the polymer at this lower temperature and the incomplete decomposition of the blowing agent. According to the thermal analysis of the

MDPE/CBA mixture, the decomposition reaction of the blowing agent occurred over a range of 20°C starting at 167°C. Coalescence showed its lowest level of activity at 170°C as the evolved gas could not overcome the high resistance of the polymer matrix to deform. Correspondingly, the final cellular structure of the foam processed at maximum 170°C showed a higher bubble density compared to the other tested temperatures.

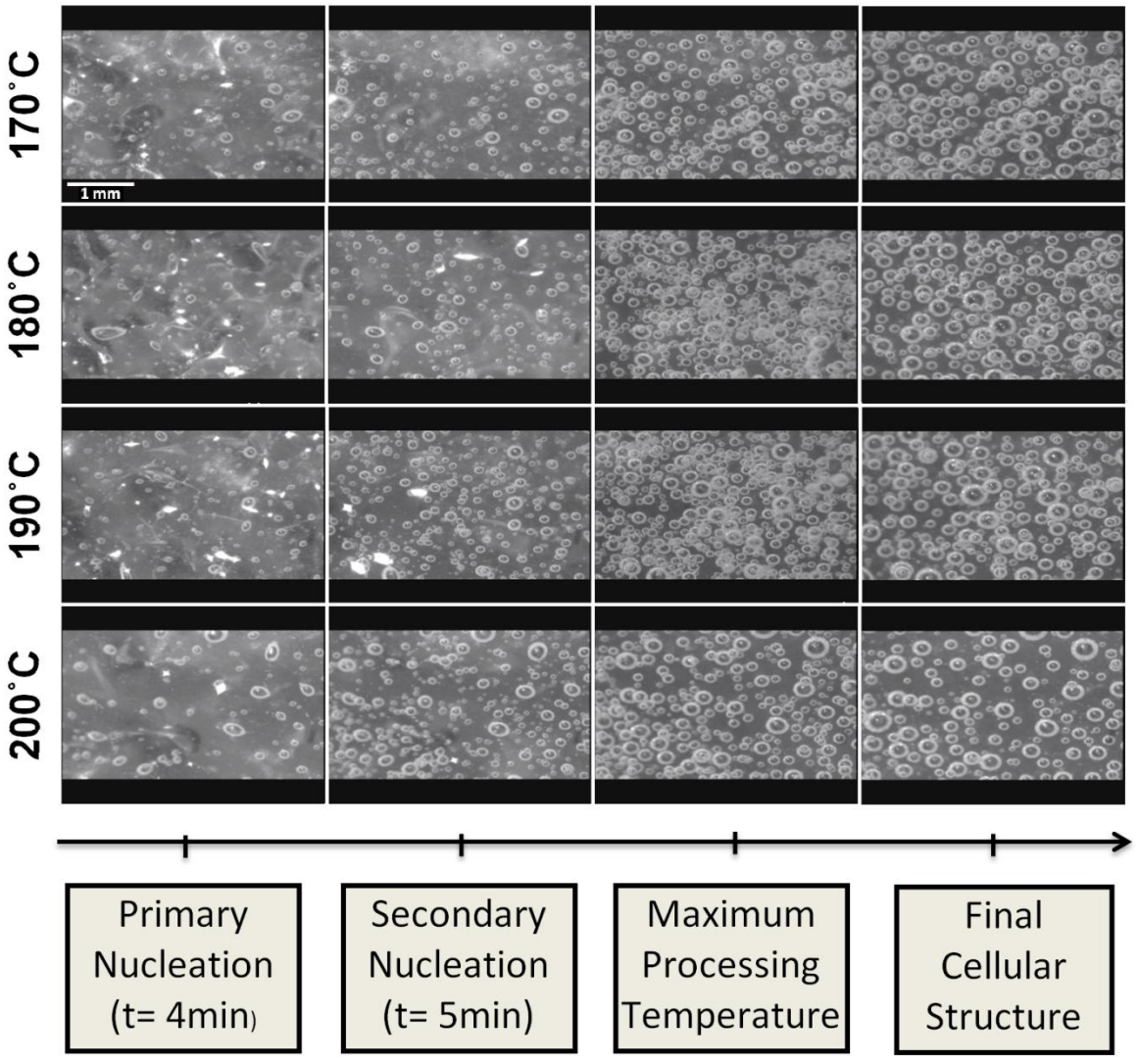

Figure 2-10: Effect of maximum processing temperature on the cellular structure of foams, using 0.25% CBA and heating rate of 10-15˚C/min.

Processing temperature did not show a notable effect on the size of the bubbles during the foaming process. In general, all samples demonstrated increasing bubble size with time, with the highest rate of bubble growth noted between 5min and 7.5 min in Figure 2.9b. The rate of bubble expansion slowed to a negligible value when the temperature approached the crystallization point of the polymer in all runs.

The total bubble projected area parameter, reported in Figure 2.9c, showed a peak reflecting the bubble shrinkage after rapid growth; a phenomenon seen in the rotomolder. The total bubble area at the processing temperature of 170°C experienced a 7.5% reduction from the peak till the end of the process, while this reduction for 180°C, 190°C and 200°C conditions was 15.5%, 19% and 13%, respectively. The effect of processing temperature on the final cellular structure is summarized in Figure 2.11. At the final stage of foaming, foams processed at the lower temperature showed the greater bubble density which can be translated to lower foam density. The processing temperature did not have a considerable effect on the final average size of the bubbles. It can be concluded that due to the control of the coalescence mechanism, processing temperature can be used as an effective tool for controlling the cellular network and hence the physical properties of the molded foam.

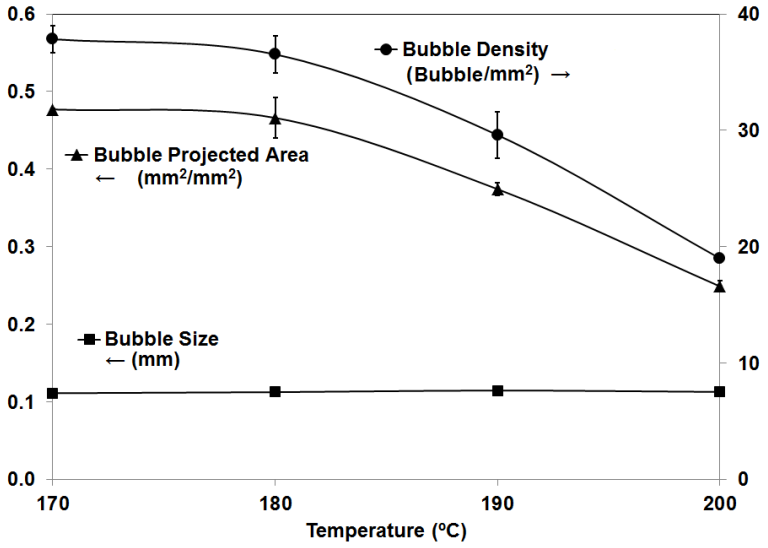

Figure 2-11: Effect of maximum processing temperature on the final cellular structure, using 0.25% CBA.

Increasing pressure inside the mold is a common occurrence in rotational molding. Our microscopic studies simulate the rotational foam molding process under atmospheric pressure. Further studies of the foaming process under elevated pressure can address the effect of processing pressure on the developing cellular structure and could be a subject for future work.

2.4 Conclusions

This work presents visualization studies on foam development under atmospheric pressure and non-isothermal conditions, simulating the rotational foam molding process. The experimental results indicate that the foaming process is comprised of four major stages: two stages of bubble nucleation, primary and secondary nucleation, followed by bubble growth and bubble coalescence/shrinkage. During the primary nucleation stage, the interstitial regions of the sintered plastic powder as well as the agglomerated blowing agent particles acted as nucleation sites for the diffused gases generated from the decomposing CBA. Subsequently, secondary nucleation formed a new generation of bubbles within the polymer melt which resulted in a cellular structure with greater uniformity compared to the bubbles initiated by primary nucleation. Following the nucleated bubbles during the foaming process revealed that primary nucleation in the interstitial regions was the controlling stage in determining the final cellular structure. The majority of the first generation of bubbles endured the entire foaming process, while most of the bubbles generated during secondary nucleation disappeared over time and very few survived to the final bubble population. Growth and coalescence mechanisms were dynamically active and competed during both heating and cooling cycles. The developing bubble structure was evaluated by several statistical parameters. It was shown that bubble size and bubble density represented growth and coalescence/disappearance mechanisms, respectively. In order to demonstrate the combined effect of the bubble growth and coalescence, a new parameter, total bubble projected area, was found most effective. Through actual rotational foam molding experiments, it was found that the

whole foaming process in respect to thickness variation can be best described by this parameter and it provides a true picture of the foam development process.

Experimental studies on the influence of the processing time and temperature showed that these parameters have significant effect on the cellular structure. Processing time and temperature were found to be effective tools for controlling the cellular network and physical properties of the developed foam structure.

2.5 References

[1] J.L. Throne, *Thermoplastic Foams*. Hinckley OH: Sherwood Publishers, 1996.

[2] R.J. Crawford and J.L. Throne, *Rotational Molding Technology*. Norwich, NewYork: William Andrew Publishing, 2002.

[3] E. Archer, E. Harkin-Jones, and M.P. Kearns, "Processing Characteristics and Mechanical Properties of Metallocene Catalyzed Linear Low-Density Polyethylene Foams for Rotational Molding," *Polym. Eng. Sci.*, 44, 638- 647, 2004.

[4] D. Klempner and K.C. Frisch, *Handbook of Polymeric Foams and Foam Technology*. New York: Oxford University Press, 1991.

[5] L. Xu and R.J. Crawford, "Analysis of the Formation and Removal of Gas Bubbles in Rotationally Moulded Thermoplastic," *J. Mater. Sci.*, 28, 2067-2074, 1993.

[6] C.B. Park and N.P. Suh, "Filamentary Extrusion of Microcellular Polymers Using a Rapid Decompressive Element," *Polym. Eng. Sci.*, 36, 34- 48, 1996.

[7] M. Emami, E. Takacs, and J. Vlachopoulos, "Rotational Foam Molding of Metallocene Catalyzed Polyethylene: CBA Screening and Process Characteristics," *J. Cell. Plast.*, 46, 333-351, 2010.

[8] G. Liu, C.B. Park, and J.A. Lefas, "Production of Low-Density LLDPE Foams in Rotational Molding," *Polym. Eng. Sci.*, 38, 1997- 2009, 1998.

[9] M.K. Bisaria, E. Takacs, C.T. Bellehumeur , and J. Vlachopoulos, "Anatomy of Rotomolding," *Rotation*, 3, 12-18, 1994.

[10] C.T. Bellehumeur, M. Kontopoulou, and J. Vlachopoulos, "The Role of Viscoelasticity in Polymer Sintering," *Rheol. Acta*, 37, 270-272, 1998.

[11] Z. Tadmor and C.G. Gogos, *Principles of Polymer Processing*. New York: John Wiley & Sons, 1979.

[12] D.I. Collias and D.G. Baird, "Tensile Toughness of Microcellular Foams of Polystyrene, Styrene-Acrylonitrile Copolymer, and the Effect of Dissolved Gas on the Tensile Toughness of the Same Polymer Matrices and Microcellular Foams.," *Polym. Eng. Sci.*, 35, 1167-1177, 1995.

[13] M. Shimbo, D.F. Baldwin, and N.P. Suh, "The Viscoelastic Behavior of Microcellular Plastics with Varying Cell Size," *Polym. Eng. Sci.*, 35, 1387-1393, 1995.

[14] D. Xu, R. Pop-Iliev, C.B. Park, and R.G. Fenton, "Fundamental Study of CBA-blown Bubble Growth and Collapse Under Atmospheric Pressure," *J. Cell. Plast.*, 41, 519-538, 2005.

[15] R. Pop-Iliev, N. Dong, D. Xu, and C.B. Park, "Visualization of the Foaming Mechanism of Polyethylene Blown by Chemical Blowing Agents Under Ambient Pressure," *Adv. Polym. Tech.*, 26, 213-222, 2007.

[16] M. Kontopoulou and J. Vlachopoulos, "Melting and Densification of Thermoplastic Powders," *Polym. Eng. Sci.*, 41, 155-162, 2001.

[17] A.W. Adamson, *Physical Chemistry of Surfaces*, 5th ed. Chichester: John Wiley & Sons, 1990.

[18] J. Colton and N. Suh, "The Nucleation of Microcellular Thermoplastic Foam with Additives: Part I: Theoretical Considerations," *Polym. Eng. Sci.*, 27, 485-492, 1987.

[19] Y. Sato et al., "Solubilities and Diffusion Coefficients of Carbon Dioxide and Nitrogen in Polypropylene, High-Density Polyethylene, and Polystyrene Under High Pressures and Temperatures," *Fluid Phase Equilibr.*, 162, 261-276, 1999.

Chapter 3

Bubble Nucleation in Non-Pressurized Polymer Foaming Systems

This chapter has been accepted for publication as:

M. Emami, M. R. Thompson, and J. Vlachopoulos "Bubble Nucleation in Non-Pressurized Polymer Foaming Systems" *Polym. Eng. Sci*., May 2013. I am the sole contributor to this paper.

Abstract

The mechanism of bubble nucleation in the foaming process under atmospheric pressure is investigated in the present study. The experimental observations using a plastic-foaming visualization setup revealed two stages of nucleation, primary nucleation in interstitial regions and secondary nucleation in the polymer melt, which followed the sintering and densification of the polymer matrix. Statistical analysis of the evolving cellular structure during the nucleation stage was used to study the significance of rheology on the behavior of polymer materials during the nucleation. The role of viscosity on the nucleation rate was also investigated theoretically by using a modified

form of the classical nucleation theory and it was verified with the experimentally observed data.

3.1 Introduction

Commercial interests in polymeric foams continue to increase due to the new emerging applications for foamed materials and the ability to foam a wider variety of plastic materials. Despite their significant success, continued growth of foamed polymers into new markets depends on the ability to enhance control over the cellular structure. The number and size of the bubbles have a significant effect on the final properties and ultimate applications of plastic foams [1,2]. Large, nonuniform bubbles lead to a deterioration of mechanical properties of the final product, whereas smaller and more uniform bubbles can retain much of the original physical integrity of the material.

One of the critical steps in the production of foamed polymers is bubble nucleation. In plastic foaming, nucleation refers to the process of generating gas bubbles in a polymer melt through a reversible thermodynamic process. Creation of small bubbles always leads to a free energy increase and so they are in an unstable equilibrium with their environment [3]. According to classical nucleation theory (CN theory), there is a critical nucleus which is theoretically in chemical, hydrodynamical, and thermal equilibrium with its surroundings [4]. In particular, nucleated bubbles which grow larger than critical nucleus survive, whereas those smaller collapse. Various mechanisms of nucleation have been proposed in the literature for nucleation of gas bubbles in thermoplastics, including homogeneous, heterogeneous, mixed-mode, shear-induced, and void nucleation theories. Notable work on experimental and theoretical studies of bubble nucleation for thermoplastic polymers using classical nucleation theory has been carried out by Colton and Suh [3,5], Han and Han [6], and Goel and Beckman [7].

Colton and Suh [3,5] were the first to develop a theoretical model based on CN theory to predict the bubble nucleation density in amorphous thermoplastic foams. They chose the

polystyrene-zinc stearate system for their corroborative experimental work and found that their theoretical predictions did not agree well with their experimental observations. They acknowledged making some oversimplifying assumptions which could explain the large disparity in their theoretical predictions and experimental results. Han and Han [6] studied the polystyrene-toluene system. They modified the CN theory by considering two additional factors that might contribute to the formation of a critical nucleus, change of free energy of the solvent due to the dissolution of macromolecules and free energy of formation of a critical bubble. The value of the pre-exponential factor in the nucleation bubble density equation was determined using experimental nucleation rate data for the polystyrene-toluene system. Goel and Beckman [7] studied the batch microcellular foaming of the poly(methyl methacrylate)-CO_2 system. They found that the agreement between their data and their CN theory model calculations was good at higher saturation pressures (above 15 MPa); however, CN theory under-predicted the nucleation rates at lower pressures (below 10.5 MPa). They attributed the higher experimental nucleation bubble densities to heterogeneous nucleation at lower pressures, triggered by the presence of trace contaminants in the system. Park [8,9], Shafi and Flumerfelt [10], and Sirupurapu et al. [11] have also attempted to study the nucleation mechanism in pressurized systems experimentally and to predict bubble nucleation rates in their experiments using CN theory or modifications thereof. Despite the valuable insights on bubble nucleation offered by past researchers, only a limited number of publications have focused on identifying the nucleation phenomenon in non-pressurized plastic foaming, such as rotational foam molding [12,13].

In this study, the mechanisms involved in the nucleation in such foaming systems have been experimentally investigated which follows our previous work on visualization studies of the foam development process in non-pressurized conditions [13]. It was found that the nucleation process in comprised of two distinct stages: primary and secondary nucleation. Primary nucleation was shown to be the controlling stage in determining the final cellular structure. The majority of the first generation of bubbles endured the entire foaming process, whereas most of the bubbles generated during secondary nucleation

disappeared over time and very few survived to the final bubble population. The rate of nucleation was defined as the number of survived bubbles that could grow larger than a critical nucleus and the number of collapsed bubbles due to their small sizes was not considered to determine the population of the nucleated bubbles. It was observed that bubble coalescence can be considered virtually negligible during the timing of nucleation and the growth of the bubbles during the transition between two stages of nucleation does not interfere with the identified nucleation rate.

According to the definition of the rate of nucleation, rheology of the polymer matrix as a highly viscous system may have substantial influence on the nucleation rate. While the role of rheology has been studied extensively for bubble growth mechanism, the effect of rheological properties of the polymer matrix on the nucleation phenomenon has received little attention [14]. Therefore, the aim of this study is to experimentally elucidate the nucleation phenomenon in a foaming process under non-pressurized conditions and investigate the significance of viscosity constraints on nucleation theoretically and experimentally. The nucleation process will be examined using a hot-stage batch foaming apparatus, with its experimental observations compared to numerically simulated results based on a modified form of the classical nucleation theory.

3.2 Experimental

3.2.1 Materials

Five medium density polyethylenes (PE) supplied by Total Petrochemicals (Feluy, Belgium) were used for this study. These resins were selected to represent a broad range of physical and rheological properties. The powder quality of the resins was quantified by particle size measurements. Sieve analysis was conducted in accordance with ASTM D 1921 using a Rototap sieving machine. A set of sieves ranging in opening size from 35 mesh (500 μm) to 200 mesh (100 μm) was used. The average particle size and particle size distribution of polyethylene materials are presented in Figure 3.1. All resins showed

comparable mean particle size and very similar distributions with the peak value of 300-500 µm. Physical properties of the resins are listed in Table 3.1.

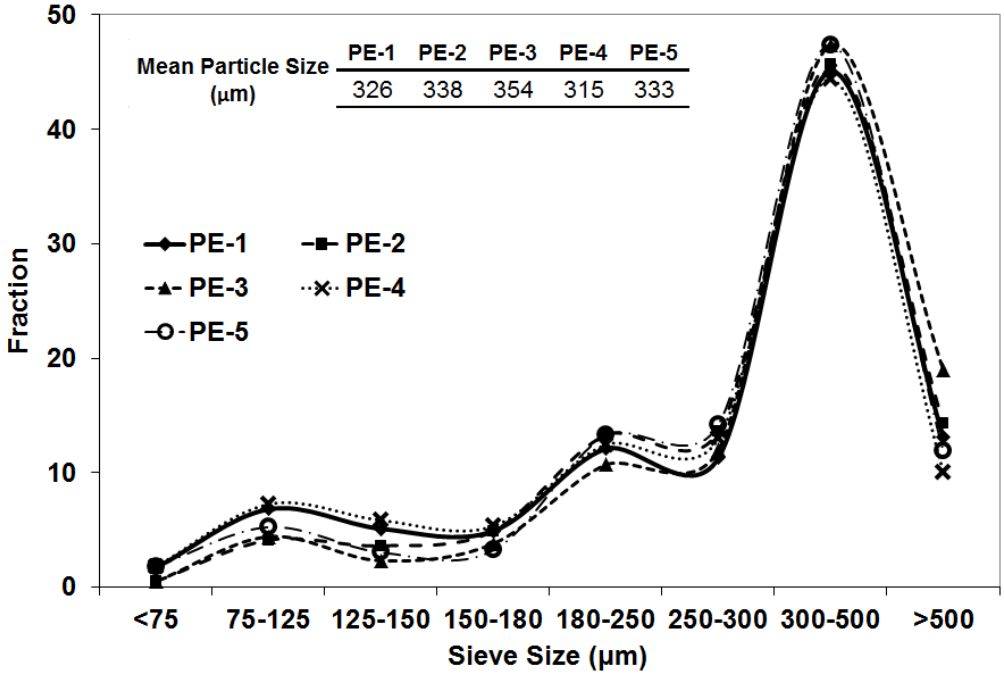

Figure 3-1: Average particle size and particle size distribution of polyethylene materials.

Table 3-1: Physical properties of polymer materials.

Material	MFI (g/10min)[1]	Density (g/cm^3)	Melting Point (°C)[2]
PE-1	8	0.934	122.6
PE-2	4	0.94	126.7
PE-3	3.5	0.941	125.3
PE-4	2.7	0.934	123.4
PE-5	2	0.932	121.7

[1] ASTM D1238, 230˚C/2.16 Kg
[2] By DSC measurements at a heating rate of 10°C/min.

An exothermic chemical blowing agent (CBA), 4,4'-oxy-bis(benzenesulfonylhydrazide), was used for the foaming experiments. According to our previous studies on screening

CBAs for non-pressurized foaming systems [15], it was found that decomposition temperature of the blowing agent should be in a range to maintain a high melt strength of polymer during the foaming process and 4,4'-oxy-bis(benzenesulfonylhydrazide) was shown to provide the most acceptable foaming performance compared to other exothermic and endothermic blowing agents. Particle size measurements by optical microscopy of the CBA powder revealed an average dimension of 6 μm. All the materials were used as-received.

3.2.2 Thermal Characterization

Thermal characteristics of the chemical blowing agent, polyethylenes and mixtures of PE/CBA were evaluated by using a TA Instruments Q200 differential scanning calorimeter (DSC) (New Castle, DE, USA). Samples of 5-10 mg of powder were sealed in an aluminum hermetic pan, and subsequently heated from 20˚C to 200˚C at a rate of 10˚C/min. This temperature range and heating rate appropriately simulated conditions used by the foaming process. The sample was then cooled to 20˚C, and a second heating sequence was performed at the same heating rate in order to characterize the post-processing product, namely the final foamed polyethylene. The degree of crystallinity within the samples was determined by normalizing the observed heat of fusion of the sample to that of a 100 % crystalline polyethylene (293 J/g [16]). A nitrogen atmosphere was used during the measurements. The DSC experiments were replicated five times to determine their reproducibility, showing results with a maximum deviation between the repeated runs of about 2%.

Thermal stability of the blowing agent was studied by thermogravimetric analysis (TGA Netzsch STA 409) under atmospheric air. Testing was done under non-isothermal conditions over a temperature range from room temperature to 200°C, with a heating rate of 10°C/min.

3.2.3 Rheological Characterization

Measurements in dynamic oscillatory mode were performed on a parallel plate TA Instruments ARES rheometer (New Castle, DE, USA) under strain-controlled conditions. The plates' diameter was 25 mm and the gap between plates was set to 1.5 mm. Disc test samples having the same diameter as the rheometer plates were produced by compression molding at 180°C for 6 min. Strain sweeps were performed to ensure the measurements were within the linear viscoelastic regime. The complex viscosity (η^*), elastic modulus (G'), and viscous modulus (G'') were determined as a function of the angular frequency (ω) ranging from 0.01 to 500 rad/s. Zero-shear viscosity values for the resins were extrapolated from the dynamic viscosity data using the Cross Model. Time sweeps confirmed that the samples were sufficiently stabilized and did not degrade during the period of a typical experiment.

3.2.4 Visualization Procedure

A hot stage optical microscopy setup was used to investigate the foaming mechanism. Dry-blending was selected as the method for preparing samples of PE/CBA mixture despite other available methods such as compression molding [17] and melt-blending [18]. Dry-blending replicates the conditions that blowing agents are added into industrial rotational foam molding processes. Compared to compression molding, dry-blending provides a precise technique to control the content of the chemical blowing agent and improves the dispersion and distribution of the components in the sample. Also, because of the heat sensitive nature of exothermic blowing agents, melt blending leads to an unstable mixing system and causes uncontrollable premature decomposition in the compounding process due to high heating rates, high shear forces and the subsequent generated viscous heat. Premature decomposition has detrimental effects on the cellular morphology and final foam properties. In addition, loss of the blowing agent in the melt-blending process makes it difficult to control the amount of CBA used in the process [18].

Dry-blended mixtures of the polyethylene materials and CBA were prepared for the experiments using 0.5% of the blowing agent. Low CBA content was used in this study in order to minimize errors involved with the two-dimensional imaging of bubble morphology, by avoiding excessive bubble overlap during foaming. A sample cup holder, made of glass (D = 2.5cm. H = 1 cm), was loaded with a predetermined amount of the blend and placed in the center of the hot stage. The stage was kept at a constant temperature with the aid of a temperature controller. All of the experiments were done isothermally at 190°C under atmospheric pressure. The temperature of the polymer melt was constantly monitored and recorded by a K-type thermocouple. The initial thickness of the powder bed inside the cup was approximately 2 mm. The process of foam development was observed with an Olympus optical microscope and recorded with a Panasonic BP-310 digital video camera. Image analysis was performed using SigmaScan Pro 5 (SYSTAT Inc., San Jose, CA, USA) in order to quantify the morphology during different stages of foaming. The bubble number density for a unit volume of foam was computed using the following expression [19]:

$$N_f = \left(\frac{nM^2}{A}\right)^{3/2} \qquad \text{Eq. 3-1}$$

where n is the number of bubbles in the micrograph, A is the area of the micrograph (cm^2), M is the magnification factor of the micrograph, and N_f is the number of bubbles per cubic centimeter of the final foam. The foaming experiments were repeated at least five times to determine accuracy and reproducibility of the experimental results and offset the effect of any possible inconsistency in the sample preparation. The observed results in microscopic experiments through the discussed foaming method in this work have shown strong correlations to the foaming performance of the tested materials at higher production scales and under actual processing conditions in our previous research study, conducted in a lab-scale rotational foam molding machine [13].

3.3 Results and Discussion

3.3.1 Thermal Properties of Pure and Foamed PEs

Decomposition behavior of the neat blowing agent was studied by DSC and TGA analysis prior to mixing with polymers. The DSC thermogram of the pure blowing agent showed a sharp exothermic transition with a peak temperature of 166.6˚C (Figure 3.2a). The decomposition of the CBA occurred over a very short period of time. A positive shift in the baseline of the thermogram was observed after termination of the reaction which is believed to be due to the mass reduction and different composition of the residual materials in the pan. TGA analysis results of the pure blowing agent were consistent with the DSC measurements despite being conducted under air rather than nitrogen. Complete liberation of nitrogen and water vapor produced by the CBA occurred at 166^{o}C. The chemical residuals from the reaction demonstrated thermal stability with no further change in masses noted for the blowing agent from 166^{o}C to 200^{o}C.

Decomposition behavior of the blowing agent in the presence of the resin, as well as the effect of its reaction by-products on the thermal properties of the resin were subsequently investigated. Figure 3.2 shows the DSC curves of the PE materials and an example of tested powder mixture comprised of the resin with 0.5% CBA. The DSC thermogram of the mixtures showed an endothermic peak demonstrating PE melting and an exothermic peak corresponding to the CBA decomposition in the first heating cycle for all samples. The onset of the exothermic peak in all cases corresponded to the peak decomposition temperature determined for the pure CBA (166˚C). Compared to the pure state, CBA exhibited a different decomposition behavior in the polymer matrices with its reaction slowed and spanning a broad temperature range of approximately 30˚C (Figure 3.2b). The blowing agent provided a reproducible and predictable decomposition reaction regardless of the type of the resin used in the mixture. Minor differences in the values of enthalpy during decomposition, ranging from 6.757 J/g to 10.88 J/g, can be explained by small variations in the content of the blowing agent during sample preparation. No considerable change was observed on the baseline after decomposition reaction. A consecutive second

heating run yielded a single endothermic peak in all samples with no additional peaks appearing, indicating that the CBA decomposed completely during the first heating run.

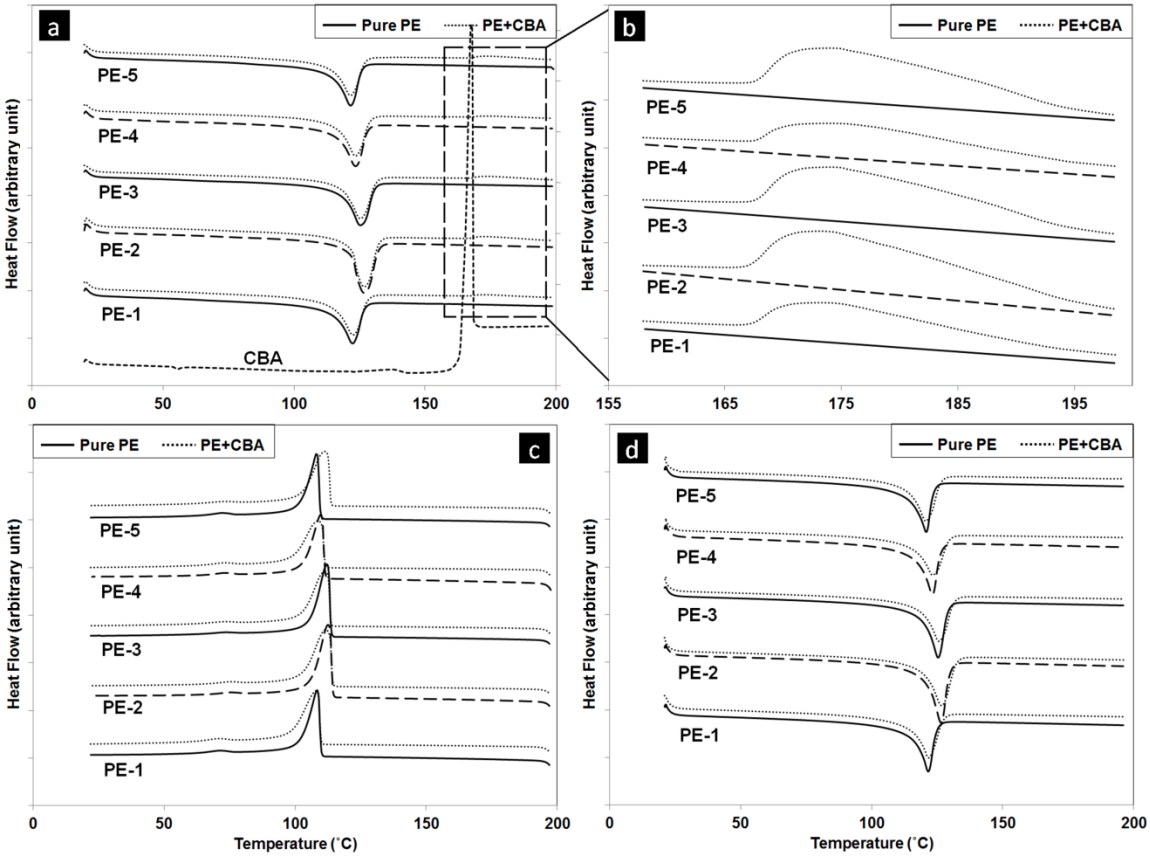

Figure 3-2: Thermal analysis of the resins, blowing agent (CBA), and resin-blowing agent mixture with 0.5% CBA, using DSC. a) First heating cycle, b) Expanded view of decomposition behavior of CBA, c) Cooling cycle, d) Second heating cycle.

Melting and crystallization temperatures of the samples are reported in Table 3.2. It was noted that despite the presence of CBA residuals, the onset and peak temperatures of the endotherms in the second heating cycle of the mixtures remained virtually unchanged and consistent with the first heating run to that of the neat PE resins. In terms of crystallinity, pure PEs showed very comparable level of crystallinity. However, DSC scans revealed that the foaming process accelerated crystallization and foamed samples were more crystalline than pure resins (Figure 3.3). The extensional flow-induced crystallization is well-known to increase the kinetics of crystallization [20,21,22,23]. Extensional flows by

nature are particularly effective at causing alignment and deformation of polymer chains in the flow direction, and therefore, the speed of the crystallization kinetics is greatly enhanced by the application of extensional forces present in the foaming process. The highest increase in the degree of crystallinity was observed with PE-3, with an increase of 13.5% in crystallinity, while this value for the rest of foamed samples was approximately 5.9%. The impact of minor differences in the enthalpy during decomposition due to inconsistent quantities of CBA in the samples on crystallization is negligible as no correlation between the change in the degree of crystallization and value of enthalpies was detected. Differences in the crystallinity of the foamed samples is due to the different foaming behavior of the resins during growth and coalescence mechanisms and nucleation process is not affected by foamed materials' crystallinity values. The information provided by the DSC analysis outlined the thermal transitions involved in the foam formation process to be studied. The data were used to determine appropriate processing conditions.

Table 3-2: Thermal properties of the PE materials and foamed PE, measured by DSC.

Material	Onset Melting Point (°C)	Peak Melting Point (°C)	Onset Crystallization Point (°C)	% of Crystallinity
PE-1	114.3 [1]	122.6 [1]	109.8 [3]	46.61 [1]
Foamed PE-1	115.1 [2]	121.7 [2]	109.7 [3]	49.28 [2]
PE-2	118.9 [1]	126.7 [1]	114.3 [3]	46.32 [1]
Foamed PE-2	118.8 [2]	126.7 [2]	114.2 [3]	49.03 [2]
PE-3	117.9 [1]	125.3 [1]	113.6 [3]	45.94 [1]
Foamed PE-3	118.4 [2]	125.5 [2]	113.5 [3]	52.14 [2]
PE-4	116.1 [1]	123.4 [1]	111.3 [3]	46.12 [1]
Foamed PE-4	115.7 [2]	123.2 [2]	111.3 [3]	49.14 [2]
PE-5	113.9 [1]	121.7 [1]	109.5 [3]	46.27 [1]
Foamed PE-5	113.4 [2]	120.9 [2]	109.5 [3]	48.89 [2]

[1] First heating cycle [2] Second heating cycle [3] Cooling cycle

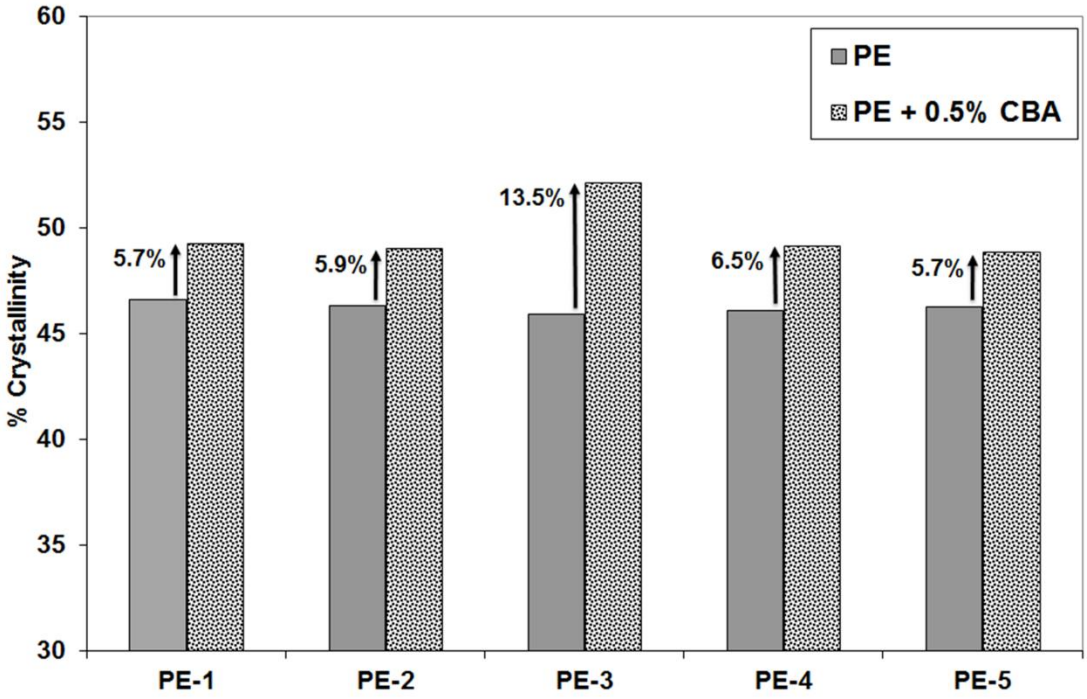

Figure 3-3: Crystallinity of polymer materials and their mixtures with 0.5% CBA.

3.3.2 Shear Rheological Characterization

Zero-shear viscosities of the tested materials are listed in Table 3.3 for 190°C and 140°C, sorted from the lowest to highest values. Figure 3.4 summarizes the complex viscosity (η*), storage modulus (G') and loss modulus (G") of the materials as a function of frequency. With increasing zero-shear viscosity, the polymer materials showed higher values in complex viscosity and PE-1 exhibited considerably lower viscosity than the rest of the resins. The viscosity curve of PE-1 showed a Newtonian plateau at small frequencies less than 1 s^{-1} and exhibited the lowest degree of shear thinning at higher frequencies. The highest shear thinning behavior was observed with PE-5. Storage and loss modulus measurements followed a similar trend to the complex viscosity. PE-5 had the highest zero-shear viscosity and demonstrated the highest storage and loss modulus compared to other samples. The difference was more significant at lower frequencies and it decreased at higher frequencies.

Table 3-3: Zero-shear viscosity of polymer materials.

Material	Zero-Shear Viscosity 190°C (Pa.s)	Zero-Shear Viscosity 140°C (Pa.s)
PE-1	1052	3796
PE-2	2672	9625
PE-3	3199	10526
PE-4	4948	16712
PE-5	7271	33768

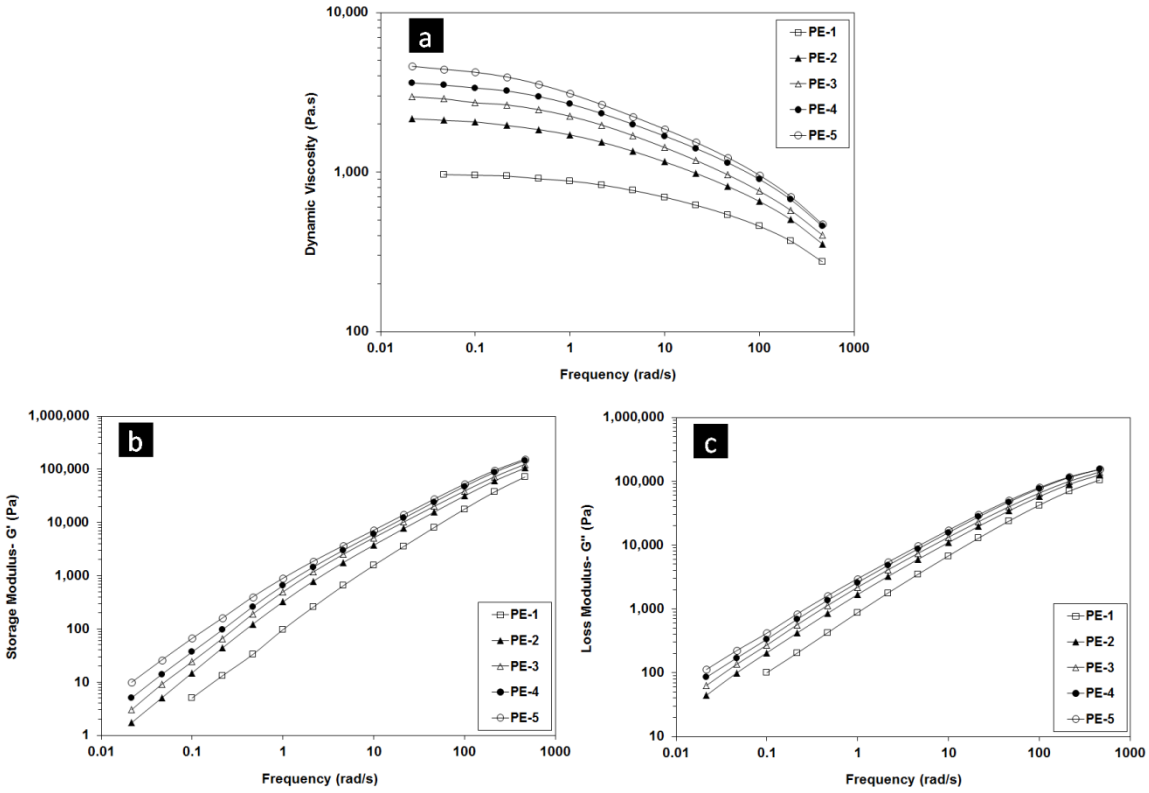

Figure 3-4: Rheological properties of polymer materials as a function of frequency at 190°C. a) Complex viscosity, b) storage modulus, and c) loss modulus.

3.3.3 Visual Experiments of Bubble Nucleation

Figure 3.5 presents a series of micrographs for the foam development process with the five PE samples during the early stages of expansion demonstrating the bubble nucleation mechanism. The term nucleation used in this paper and applied in analysis of the micrographs refers to only the survived bubbles that could grow larger than the critical nucleus and could be observed through the microscopic setup.

At the beginning of the processing cycle, the temperature of the solid powder bed was raised steadily. After having reached their melting temperature, the powder particles in contact with each other sintered and formed a porous network. The sintering process proceeded in two stages, first by developing interfaces and bridges between adjacent particles while the individual particles still remained distinctive in shape. It was followed by densification in which the density of the melt pool increased by decreasing the inter-particle cavities and a coherent network of voids was formed as the interstitial air trapped in the melt decreased in size (Figures 3.5a, 3.5d, 3.5g, 3.5j, 3.5m). Densification of the sintering polymer continued until the onset of decomposition for the blowing agent at 166˚C. A detailed explanation of the sintering stage has been discussed in our previous work [13].

The sintering process is significantly affected by material properties, including powder particle size, thermal transitions and rheology of the polymer matrix [24,25,26]. Polymer powders with smaller particle size tend to melt earlier in the heating cycle and sinter faster. Coarser fractions in the powder result in a slower coalescence rate and the formation of larger interstitial voids in the melt [24]. The comparable average particle size and particle size distribution of the resins eliminated the effect of these parameters on the melt densification. Also, similarity of the melting point and crystallinity of polyethylene resins excluded the influence of the thermal properties during this stage. However, different rheological characteristics of the polymer matrixes resulted in different rates of particle coalescence. Numerical and experimental observations of the

powder particle coalescence have shown that the sintering rate increases as the viscosity of the resin decreases and higher elasticity decelerates the densification process [25,27].

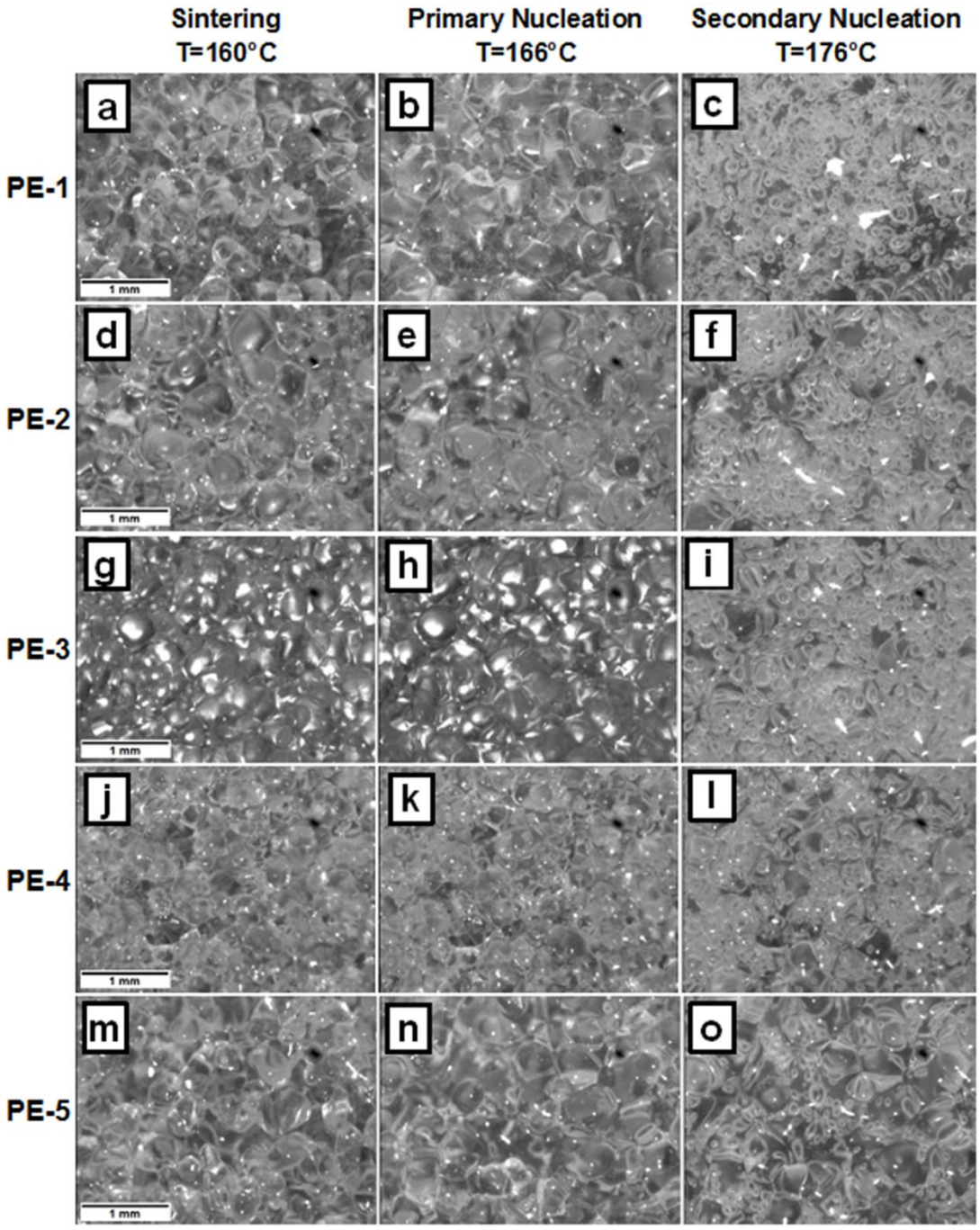

Figure 3-5: Nucleation stage of the foam development process, using 0.5% CBA.

Our visual observations were consistent with the above mentioned influence of rheology. PE-1 and PE-2 with lower viscosity and storage modulus showed an improved sintering behavior which directly affected the rate of removing the interstitial air trapped in the polymer melt (Figures 3.5a, 3.5d). Due to their high melt viscosity/elasticity, there was not enough time for PE-4 and PE-5 to proceed with the densification process before CBA decomposition which resulted in the formation of large voids in the melt pool (Figures 3.5j, 3.5m). The interstitial voids remaining from sintering of the polymer matrix were observed to act as nucleating sites during the nucleation and will be discussed in the next section. The existence of large bubbles prohibited nucleation of a large number of nuclei since the blowing gas molecules prefer to diffuse into the larger bubbles. In order to form a fine-bubble structure, the size of the interstitial voids should be minimized and therefore a high melt viscosity/elasticity may not be desirable at this stage. However, considering other factors involved in the foaming process, including thermo-physical properties of the materials and mechanical properties of the final product, an optimum melt viscosity/elasticity needed to be determined.

By reaching the onset of decomposition of the blowing agent at 166˚C, the sintering process in all samples was followed by two stages of nucleation: primary and secondary nucleation [13]. According to DSC analysis, at this point the crystalline structure for all polyethylene materials was disappeared and a completely amorphous phase was yielded. During the primary nucleation stage, the interstitial regions of the sintered plastic powder as well as the agglomerated blowing agent particles acted as nucleation sites for the diffused gases generated from the decomposing CBA which had a certain size from the beginning (Figures 3.5b, 3.5e, 3.5h, 3.5k, 3.5n). The interstitial voids (7-75μm in size) were observed to start to grow from this point. Also small bubbles, about 30-40μm, were formed at the boundaries of incompletely fused polymer particles, which were believed to match the dimensions of agglomerated CBA particles. Subsequently, the secondary nucleation stage formed a new generation of bubbles within the polymer melt. Secondary nucleation resulted in a cellular structure with smaller bubble size (20-30μm) and greater uniformity compared to the bubbles initiated by the primary nucleation, as shown in

Figures 3.5c, 3.5f, 3.5i, 3.5l, 3.5o. Second series of the bubbles developed in the areas not previously experiencing foaming when the system reached 176^{o}C, and therefore a fully sintered, more homogenous bed of molten polymer was available for nucleation. Secondary nucleation occurred over a short period of time (10s).

Figure 3.6 shows the bubble density profile during the two stages of nucleation. Since it was not possible to determine the onset point of nucleation through the microscopy setup, the number of nucleated bubbles has only been reported from a point in the process that the bubbles could be detected visually. The visual observation of nucleation covered a time span of 60 s on average for all tested materials, starting from the onset decomposition of CBA at 166°C until 176°C which corresponds to the peak point of decomposition according to DSC results (Figure 3.2b). During the stage of primary nucleation, PE-1 with 2.38×10^{9} bubbles/cm^{3} resulted in the highest number of nucleated bubbles, while foamed samples produced by PE-5 which had the highest viscosity/elasticity, showed the lowest number of 1.4×10^{9} bubbles/cm^{3}. A rapid increase in the number of bubbles for all resins was observed as the system transitioned to the second stage of nucleation. The maximum bubble density was observed after passing approximately 60 s from the detection of the primary nucleated bubbles (60 s < t < 120 s) and no further changes in the number of bubbles were identified for the next 90 s (120 s < t < 210 s). All resins followed the similar trend of bubble density increase; however, different rates of change were observed for each foamed sample (Figure 3.6b). The number of nucleated bubbles that were produced through the two stages of nucleation decreased with increasing the viscosity/elasticity of the polymer material. The highest and lowest number of nucleated bubbles present by the end of the secondary nucleation stage corresponded to PE-1 (7.89×10^{9} bubbles/cm^{3}) and PE-5 (4.62×10^{9} bubbles/cm^{3}), respectively. It is believed that low viscosity and low melt elasticity for a gas-laden matrix positively influenced bubble nucleation and allowed a greater number of bubbles to survive and grow larger than the critical nucleus.

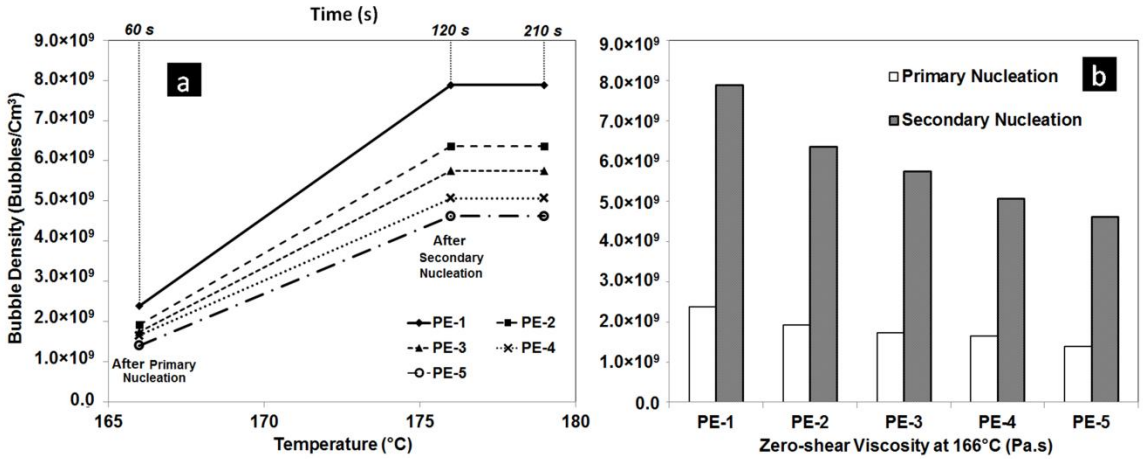

Figure 3-6: Bubble density profile during two stages of nucleation of foaming, using polyethylene and 0.5% CBA.

3.3.4 The Role of Viscosity on Nucleation Rate

Experimental observations during the nucleation process showed that rheology has an impact on the mechanism of bubble generation in non-pressurized foaming systems. In order to evaluate the influence of viscous forces on the rate of nucleation, a modified form of the classical nucleation theory proposed by Kagan [28] was employed. Kagan's model is an extension of Zeldovich's theory of bubble nucleation in liquids which describes the evolution of spontaneously arising bubbles from metastable liquid, considering thermodynamically determined transitions and random effects [29,30]. Kagan's model accounts for viscosity and inertial controls on the rate of bubble nucleation in simple liquids. For a very viscous liquid, inertia can be neglected and a particular equation was obtained by Kagan which expresses the nucleation rate, J, considering the effect of viscosity:

$$J \approx 4N_0 \frac{\sigma}{\gamma\eta}\sqrt{\frac{\sigma}{kT}}\frac{1}{b}\, e^{-\frac{1}{3}K} \qquad \text{Eq. 3-2}$$

and

$$K = \frac{4\pi r_c^2 \sigma}{kT} \quad \text{Eq. 3-3}$$

$$b = \frac{2\sigma}{r_c\, p_c} \quad \text{Eq. 3-4}$$

$$p_c = p_{atm} + \frac{2\sigma}{r_c} \quad \text{Eq. 3-5}$$

where N_0 is the Avogadro number, σ is the interfacial tension, γ is a numerical coefficient that has a value of approximately 4, η is the viscosity of the liquid, k is the Boltzmann constant, T is the temperature, r_c is the radius of the critical nucleus, p_c is the pressure of the critical nucleus, and p_{atm} is the atmospheric pressure.

Considering our system as a viscous liquid, the effect of viscosity on the experimentally observed nucleation rate was examined. In the present experimental work, the rate of nucleation was expressed as the ratio of the maximum number of observed bubbles over the time period of bubble generation. The nucleation temperature was considered 166°C based on thermal analysis of the samples. According to thermodynamics studies and based on the modified classical nucleation theory by Goel [7] and Blander [30], the predicted critical nucleus size for viscous foaming systems is typically on the order of 1 to 45 Å. Ramesh also reported the values of critical nucleation radius of bubble embryo for polystyrene and nitrogen foaming systems to be in the range of 5 to 20 Å [31]. Kim and Park [32] compared the predicted value by classical nucleation theory to self-consistent field theory and reported that for nanoscale bubbles, classical nucleation theory can be more than a third too large in its estimation of the critical radius. The Arrhenius equation was used to describe the temperature dependence of the viscosity of the polymer melts, using a reference temperature of 140°C and activation energy of 20,000 J/mol. The surface tension values for polymer melts were obtained from literature [33,34] and an average value of 0.0255 N/m was used in the simulation process. The variations of surface tension with viscosity were considered negligible in this analysis. According to the studies by Tinson et al. [34,35], the surface tension of polyethylenes used for

rotational molding vary over a small range of 0.0245 to 0.0265 N/m and show very weak dependency on viscosity. Jones also [36] showed that surface tension has little sensitivity on the viscosity for high molecular weight polymers and it can be considered virtually independent for polymers with higher relative molecular mass (M_n) than 10,000 g/mol, while all our samples have a M_n greater than 22,000 g/mol.

The Kagan model has a dependency to the critical nucleus size in the square and exponential manner and exhibited a great degree of sensitivity to its value. The theoretical predictions by Kagan's model for the rate of nucleation for different critical nucleus sizes are demonstrated in Figure 3.7. The model prediction by using a nucleus

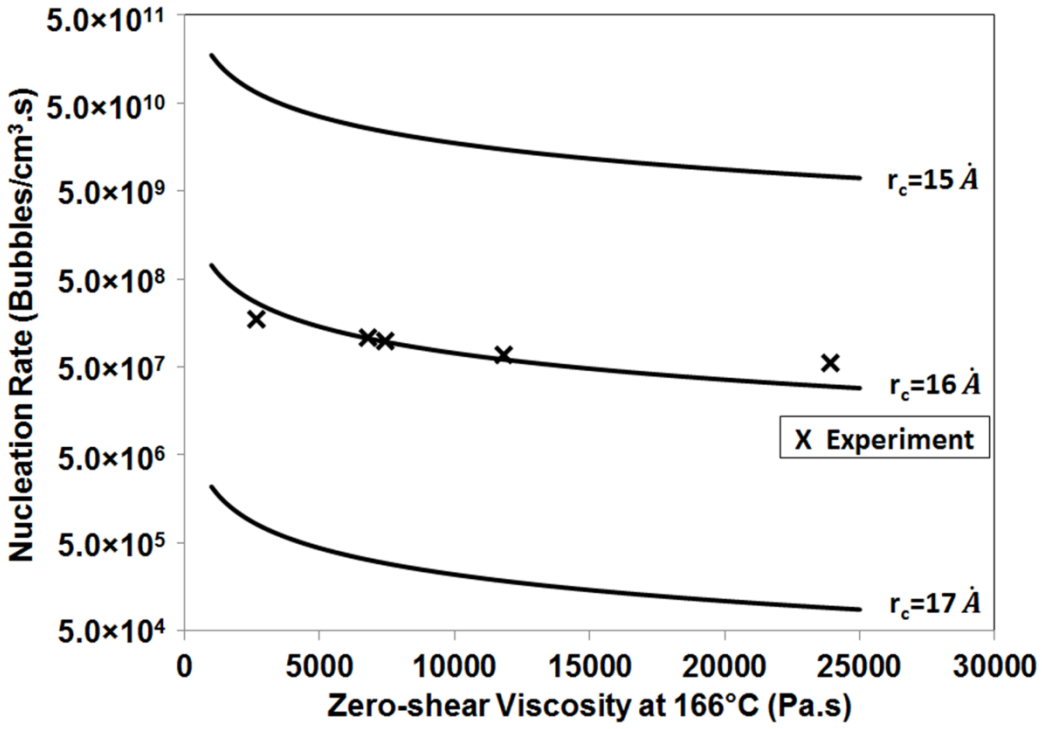

Figure 3-7: Kegan model, theoretical predictions and experimental results for different critical nucleus sizes.

size of 16 Å provided reasonably good agreement with the experimental data and a linear scale of the comparison between numerical and experimental results is shown in Figure 3.8. Due to negligible variations in the values of surface tension for the resins, one value of critical nucleus size was used for all experimental cases. The prediction obtained from

the model can well simulate the trend experimentally observed for the impact of viscous forces on the nucleation rate. The numerical results indicated that higher viscosity can impede the number of nuclei generated in the foaming system. This trend showed to be significant for viscosities lower than 12,000 Pa.s (at 166°C). The presented results in Figure 3.7 showed that the rate of nucleation exhibited less dependency on viscosity for values higher than 12,000 Pa.s (at 166°C). The Kagan model seems to provide an adequate representation of the significance of the viscosity forces. The differences from the experimental data might be related to other effects, such as viscoelastic, which were not considered.

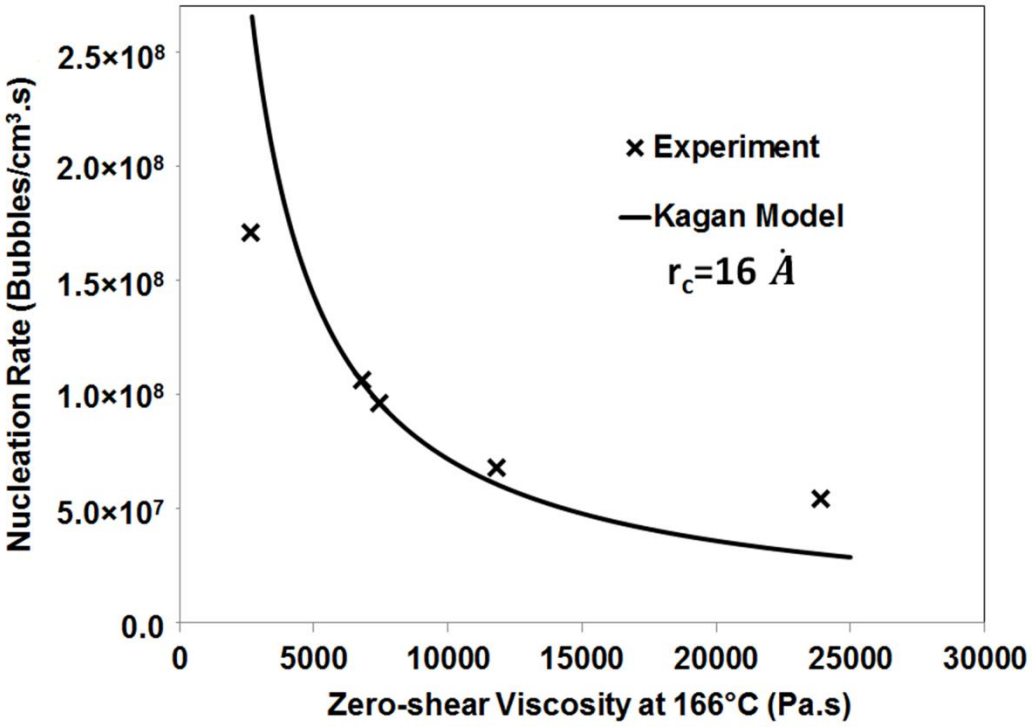

Figure 3-8: Effect of viscosity constraint on the rate of nucleation, theoretical prediction and observed results.

3.4 Conclusions

The mechanism of bubble nucleation in foaming processes under non-pressurized conditions was investigated using a plastic-foaming visualization setup. The microscopic observations of the foaming process indicated that the nucleation phase was comprised of two major stages, primary and secondary nucleation, and it occurred after sintering and partial densification of polymer particles. During sintering stage, adjacent particles developed interfaces and by increasing temperature, started to lose their identity and formed a coherent network of voids. The interstitial voids remaining from the sintering process, as well as agglomerated blowing agent particles acted as nucleation sites during the first stage of nucleation, primary nucleation. It was followed by secondary nucleation which formed a new generation of bubbles within the polymer melt. Experimental and numerical studies of the nucleation process revealed that the rate of nucleation is influenced by the rheology of the polymer materials. The visualization experiments showed that lower viscosity and melt elasticity of the gas-laden matrix allowed a greater number of bubbles to survive and grow larger than the critical nucleus. Furthermore, theoretical predictions obtained from the Kagan model for viscous systems simulated experimentally observed trend for the impact of viscosity on the nucleation rate rather well and suggested that higher viscosity could impede the number of nuclei generated in the foaming system.

3.5 References

[1] J.L. Throne, *Thermoplastic Foams*. Hinckley OH: Sherwood Publishers, 1996.

[2] D. Klempner and K.C. Frisch, *Handbook of Polymeric Foams and Foam Technology*. New York: Oxford University Press, 1991.

[3] J. Colton and N. Suh, "The Nucleation of Microcellular Thermoplastic Foam with Additives: Part I: Theoretical Considerations," *Polym. Eng. Sci.*, 27, 485-492, 1987.

[4] J.W. Gibbs, *The Scientific Papers of J. Willard Gibbs*. Mineola, NY: Dover Publ. Inc., 1961.

[5] J. Colton and N. Suh, "The Nucleation of Microcellular Thermoplastic Foam with Additives: Part II: Experimental Results and Discussion," *Polym. Eng. Sci.*, 27, 493-499, 1987.

[6] J. Han and C. Han, "Bubble Nucleation in Polymeric Liquids. II. Theoretical Considerations," *J. Polym. Sci. B: Polym. Phys.*, 28, 711-741, 1990.

[7] S.K. Goel and E.J. Beckman, "Generation of microcellularpolymeric foams using supercritical carbon dioxide. Part I.Effect of pressure and temperature on nucleation," *Polym. Eng. Sci.*, 34, 1137–1147, 1994.

[8] C.B. Park, D.F. Baldwin, and N.P. Suh, "Effect of the pressure drop rate on cell nucleation in continuous processing of microcellular polymers," *Polym. Eng. Sci.*, 35, 432-440, 1995.

[9] C.B. Park and L.K. Cheunge, "A study of cell nucleation in the extrusion of polypropylene foams," *Polym. Eng. Sci.*, 1-10, 1997.

[10] M. Shafi and R. Flumerfelt, "Initial Bubble Growth in Polymer Foam Processes," *Chem. Eng. Sci.*, 52, 627-633, 1997.

[11] S. Siripurapu, J. Coughlan, R. Spontak, and S. Khan, "Surface- Constrained Foaming of Polymer Thin Films with Supercritical Carbon Dioxide," *Macromolecules*, 37, 9872–9879, 2004.

[12] G. Liu, C.B. Park, and J.A. Lefas, "Production of Low-Density LLDPE Foams in Rotational Molding," *Polym. Eng. Sci.*, 38, 1997- 2009, 1998.

[13] M. Emami, E. Takacs, M.R. Thopmson, J. Vlachopoulos, and E. Maziers, "Visual Studies of Model Foam Development for Rotational Molding Processes," *Adv. Polym. Tech.*, 2012.

[14] S. Shukla and K.W. Koelling, "Classical Nucleation Theory Applied to Homogeneous Bubble Nucleation in the Continuous Microcellular Foaming of the Polystyrene−CO_2 System," *Ind. Eng. Chem. Res.*, 48, 7603-7615, 2009.

[15] M. Emami, E. Takacs, and J. Vlachopoulos, "Rotational Foam Molding of Metallocene Catalyzed Polyethylene: CBA Screening and Process Characteristics," *J. Cell. Plast.*, 46, 333-351, 2010.

[16] R.L. Blaine. Polymer Heats of Fusion, TA Instruments.

[17] R. Pop-Iliev, N. Dong, D. Xu, and C.B. Park, "Visualization of the Foaming Mechanism of Polyethylene Blown by Chemical Blowing Agents Under Ambient Pressure," *Adv. Polym. Tech.*, 26, 213-222, 2007.

[18] F. Liu, *Processing of Polyethylene and Polypropylene Foams in Rotational Molding*.: M.A.Sc. Thesis; University of Toronto, 1998.

[19] V. Kumar and N. Suh, "A process for making microcellular thermoplastic parts," *Polym. Eng. Sci.*, 30, 1323-1329, 1990.

[20] A. McHugh, R. Guy, and D. Tree, "Extensional Flow-Induced Crystallization of a Polyethylene Melt," *Colloid Polym. Sci.*, 271, 629-645, 1993.

[21] C. Hadinata et al., "Elongation-Induced Crystallization of a High Molecular Weight Isotactic Polybutene-1 Melt Compared to Shear-Induced Crystallization," *J. Rheol.*, 51, 195-215, 2007.

[22] M. Sentmanat, O. Delgadillo-Velazquez, and S.G. Hatzikiriakos, "Crystallization of

an Ehtylene-Based Butene Plastomer: The Effect of Unixatial Extension," *Rheol. Acta*, 49, 931-939, 2010.

[23] M. Chellamuthu, D. Arora, H.H. Winter, and J.P. Rothstein, "Extensional Flow-Induced Crystallization of Isotactic Poly-1-butene Using a Filament Stretching Rheometer," *J. Rheol.*, 55, 901-920, 2011.

[24] C.T. Bellehumeur, M.K. Bisaria, and J. Vlachopoulos, "An experimental study and model assessment of polymer sintering," *Polym. Eng. Sci.*, 36, 2198-2207, 1996.

[25] C.T. Bellehumeur, M. Kontopoulou, and J. Vlachopoulos, "The Role of Viscoelasticity in Polymer Sintering," *Rheol. Acta*, 37, 270-272, 1998.

[26] M. Kontopoulou and J. Vlachopoulos, "Bubble Dissolution in Molten Polymers and Its Role in Rotational Molding," *Polym. Eng. Sci.*, 39, 1189-1999, 1999.

[27] B.I. Chaudhary, E. Takacs, and J. Vlachopoulos, "Processing Enhancers for Rotational Molding of Polyethylene," *Polym. Eng. Sci.*, 41, 1731–1742, 2001.

[28] Y. Kagan, "The Kinetics of Boiling of a Pure Liquid," *Russ. J. Phys.Chem.*, 34, 42-46, 1960.

[29] J. Zeldovich, "On the Theory of New Phase Formation: Cavitation," *Acta Physicochem. U.S.S.R.*, 18, 1-22, 1943.

[30] M. Blander, "Bubble Nucleation in Liquids," *Adv. Colloid Interface Sci.*, 10, 1-32, 1979.

[31] N.S. Ramesh, D.H. Rasmussen, and G.A. Campbell, "The Heterogeneous Nucleation of Microcellular Foams Assisted by the Survival of Microvoids in Polymers Containing low Glass Transition Particles. Part I: Mathematical Modeling and Numerical Simulation," *Polym. Eng. Sci.*, 34, 1685- 1697, 1994.

[32] Y. Kim, C.B. Park, P. Chen, and R.B. Thompson, "Origins of the Failure of Classical Nucleation Theory For Nanocellular Polymer Foams," *Soft Matter*, 7, 7351-7358, 2011.

[33] S. Wu, *Polymer Interface and Adhesion*. New York: Marcel Dekker, 1982.

[34] A. Tinson, E. Takacs, and J. Vlachopoulos, "The Role of Surface Tension in Sintering for Rotational Molding," *Rotoworld*, 1, 43-47, 2005.

[35] A. Tinson, *A Study of the Surface Tension of Polymer Melts and Its Role in Particle Coalescence for Rotational Molding*.: M.A.Sc. Thesis, McMaster University, 2004.

[36] R.L. Jones and R.W. Richards, *Polymers at Surface and Interfaces*. Cambridge, U.K.: Cambridge University Press, 1999.

Chapter 4

Experimental and Numerical Studies on Bubble Dynamics in Non-Pressurized Foaming Systems

This chapter has been accepted for publication as:

M. Emami, M. R. Thompson, and J. Vlachopoulos "Experimental and Numerical Studies on Bubble Dynamics in Non-Pressurized Foaming Systems" *Polym. Eng. Sci.*, August 2013. I am the sole contributor to this paper.

Abstract

This work explores the influence of rheological properties on polymer foam development in non-pressurized systems. To understand the complex contributions of rheology on the mechanism of bubble growth during different stages of foam processing, visualization studies were conducted by using a polymer-foaming microscopy setup. The evolving cellular structure during foaming was analyzed for its bubble surface density, bubble size, total bubble projected area, and bubble size distribution. Morphological analysis was used to determine the rheological processing window in terms of shear viscosity, elastic modulus, melt strength and strain-hardening, intended for the production of foams with

greater foam expansion, increased bubble density and reduced bubble size. A bubble growth model and simulation scheme was also developed to describe the bubble growth phenomena that occurred in non-pressurized foaming systems. Using thermophysical and rheological properties of polymer/gas mixtures, the growth profiles for bubbles were predicted and compared to experimentally observed data. It was verified that the viscous bubble growth model was capable of depicting the growth behaviors of bubbles under various processing conditions. Furthermore, the effects of thermophysical and rheological parameters on the bubble growth dynamics were demonstrated by a series of sensitivity studies.

4.1 Introduction

Polymer foaming is a complicated process that involves complex mechanisms and unique morphology transformations. This field of processing combines material principles, engineering design, processing methodologies, and property characterization. Polymeric foams are intended for thermal and electrical insulation, packaging, auto industry, and structural applications. Their unique characters come from their diverse functionalities such as stiffness, strength, impact resistance, dielectric and thermal resistance, and acoustical absorbing properties [1]. These functionalities can be customized to obtain properties beyond the limits of other classes of engineering materials.

Bubble nucleation and subsequent bubble growth are the processing steps governing the final structures and quality of foam products and knowledge about the mechanisms of these phenomena is indispensable for controlling and optimizing the performance of processing technologies utilized in the foaming industry. Various researchers have investigated bubble nucleation and growth in different foaming systems such as batch processes [2,3,4,5,6], extrusion foaming [7,8,9,10], injection molding [11,12], and rotational molding [13,14,15,16]. Experimental studies, in conjunction with the measured thermophysical and rheological properties of the polymer/gas mixtures, have provided a solid information base to develop theoretical models and simulation schemes for bubble

growth behavior [17,18]. The foaming industry will, in turn, be able to draw strategically from the research to determine the optimal processing conditions and critical material compositions for polymer foam manufacturing.

Rheological properties of the polymeric matrix and gas-laden polymer melt in polymer foaming have received great attention by researchers due to the important role of polymer matrix response to the mechanisms involved in the foaming process. Bradley and Phillips [19] stressed the importance of extensional viscosity and strain-hardening in the foaming process in their production of low density foams using high-melt-strength polypropylene. Park and Cheung [9] and Naguib [20] used a long-chain-branching polypropylene, which exhibits significant strain-hardening under extension, and demonstrated much higher bubble density and expansion ratio during foam extrusion compared to linear polypropylene. Similar conclusions were obtained by Yamaguchi et al. [21], who blended a cLLDPE (linear low-density polyethylene with some crosslinks) with an LLDPE to enhance the strain-hardening behavior. Enhanced strain-hardening favored uniform deformation during foaming, and resulted in foams with a uniform bubble size distribution. Recently, Spitael and Macosko [22] and Stange and Münstedt [23] characterized the uniaxial extensional viscosities for a series of linear polypropylenes, long chain branched (LCB)-polypropylenes, and their blends at conditions relevant to foaming, and then attempted to relate those rheological properties to bubble morphology in foamed samples. Besides showing that long chain branching suppresses bubble coalescence, they found that a small amount of LCB- polypropylene (e.g., 10% by weight) in the blend could improve the expansion and reduce the occurrence of bubble opening with linear polypropylenes. Stange and Münstedt attributed the higher volume expansion of LCB- polypropylenes and the blends to their higher strains at rupture and their more uniform deformation during extension compared to linear polypropylenes. Spitael and Macosko did not find any direct correlation between strain-hardening and bubble density or expansion ratio.

While the role of rheology has been studied broadly for pressurized foaming processes, limited work has been carried out on the foaming process in non-pressurized systems such as rotational molding. Due to the pressure-free nature of such systems and abrupt temperature changes during the foam molding, the foam development process is less controllable and one hypothesis is that rheological properties play a significant role in controlling the foaming process. Therefore, a thorough investigation on the influence of rheology on molded foamed structures is essential. The aim of this work is to understand the effects which rheology of a polymer matrix has on bubble dynamics during different stages of non-pressurized foaming and the resultant foam structure at a microscopic level. A systematic experimental examination is attempted to correlate foamability of polymer materials with their off-line rheological properties. This paper reports also on a mathematical model which was implemented in a simulation scheme based on the well-known cell model to predict the bubble growth phenomena. A series of sensitivity studies were performed to demonstrate the effects of different physical parameters on bubble growth dynamics.

4.2 Experimental

4.2.1 Materials

Five medium density polyethylenes (PE) supplied by Total Petrochemicals (Feluy, Belgium) were used for this study. These resins were selected to represent a broad range of physical and rheological properties. Thermal characteristics of the PEs were evaluated by using a TA Instruments Q200 differential scanning calorimeter (DSC) (New Castle, DE, USA). DSC studies were carried out between 20°C and 200°C heating/cooling/heating cycle at a rate of 10°C/min under a nitrogen gas flow. The degree of crystallinity within the samples was determined by normalizing the observed heat of fusion of the sample to that of a 100% crystalline polyethylene (293J/g [24]). Thermal and physical properties of the resins are listed in Table 4.1. The powder quality of the resins was quantified by particle size measurements. Sieve analysis was conducted in

accordance with ASTM D 1921 using a Rototap sieving machine. A set of sieves ranging in opening size from 35 mesh (500 μm) to 200 mesh (100 μm) was used. All resins showed comparable mean particle size of 310μm and very similar distributions with the peak value of 300-500 μm.

Table 4-1: Physical properties of polymer materials.

Material	MFI (g/10min)[1]	Density (g/cm^3)	Melting Point (°C)[2]	Crystallinity (%)[2]
PE-1	8	0.934	122.6	46.6
PE-2	4	0.940	126.7	46.3
PE-3	3.5	0.941	125.3	45.9
PE-4	2.7	0.934	123.4	46.1
PE-5	2	0.932	121.7	46.3

[1] ASTM D1238, 230˚C/2.16 kg
[2] DSC measurements at a heating rate of 10°C/min.

An exothermic chemical blowing agent (CBA), 4,4'-oxy-bis(benzenesulfonylhydrazide), was used for the foaming experiments. The decomposition behavior of the blowing agent was studied by thermogravimetric analysis (TGA, Netzsch STA409) and the measurements are presented in Figure 4.1. The blowing agent showed a rapid decrease in sample weight over a very narrow range of temperatures during heating, with both onset and peak weight loss corresponding to 166.7°C. Complete liberation of nitrogen and water vapor occurred at this temperature. The chemical residuals from the reaction demonstrated thermal stability with no further change in masses noted for the blowing agent from 166.7^{o}C to 200^{o}C. Particle size measurements by optical microscopy of the CBA powder revealed an average dimension of 6 μm. All the materials were used as-received.

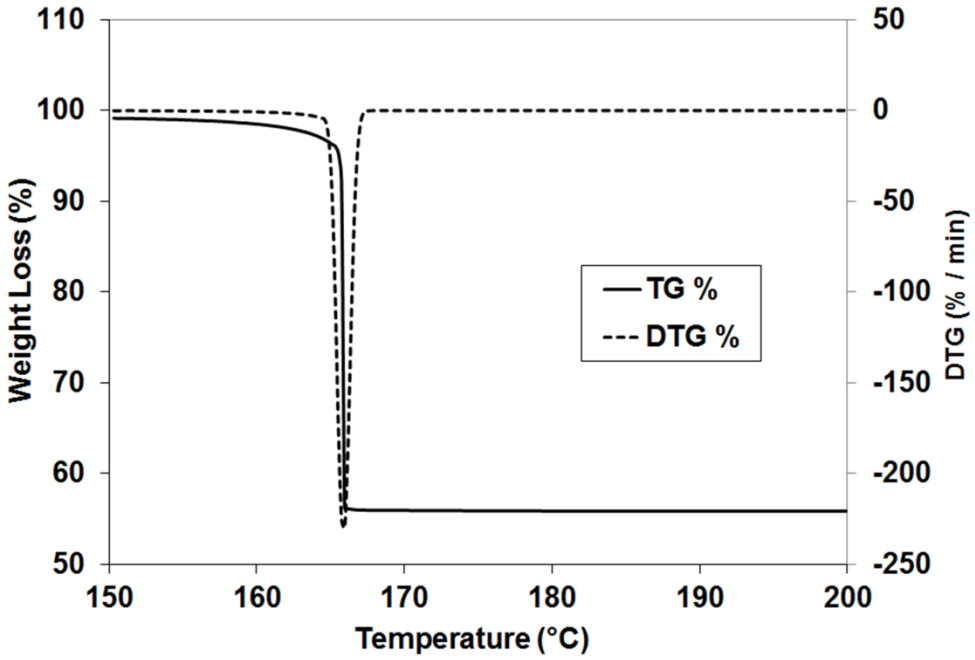

Figure 4-1: Thermal analysis of the pure blowing agent, using TGA technique.

4.2.2 Rheological Characterization

Measurements in dynamic oscillatory mode were performed on a parallel plate TA Instruments ARES rheometer (New Castle, DE, USA) under strain-controlled conditions. The plates' diameter were 25 mm and the gap between plates was set to 1.5 mm. Disc test samples having the same diameter as the rheometer plates were produced by compression molding at 180°C for 6 min. Strain sweeps were performed to ensure the measurements were within the linear viscoelastic regime. The complex viscosity (η*), elastic modulus (G´), and viscous modulus (G˝) were determined as a function of the angular frequency (ω) ranging from 0.01 to 500 rad/s. Zero-shear viscosity values for the resins were extrapolated from the dynamic viscosity data using the Cross Model. The dynamic temperature ramp tests were also conducted within the linear viscoelastic region, i.e. at 10 rad/s with stain at 5%, and the temperature was increased from 140°C to 190°C followed by a decrease to 140°C at a rate of 10°C/min. Time sweeps confirmed that the samples

were sufficiently stabilized and did not degrade during the duration of a typical experiment.

Resins were also rheologically characterized for their uniaxial extensional properties using an SER Universal Testing Platform from Xpansion Instruments [25]. The SER unit is a dual windup extensional rheometer that has been specifically designed for use as a detachable fixture on rotational rheometer host platforms. Specimens were prepared by compression molding of the polymer samples to a thickness of approximately 1mm using a hydraulic press. Individual polymer specimens were then cut to a width of 6-8 mm. Measurements were conducted at 140ºC, slightly above the melting point of the polymers, to ensure that the viscosities of the samples were high enough to prevent sagging.

4.2.3 Visualization Procedure

A hot stage optical microscopy setup was used to investigate the foaming mechanism. Dry-blended mixtures of the polyethylene materials and CBA were prepared for the experiments using 0.5% of the blowing agent. Low CBA content was used in this study in order to minimize errors involved with the two-dimensional imaging of bubble morphology by avoiding excessive bubble overlap during foaming. A sample cup holder, made of glass (D = 2.5cm. H = 1 cm), was loaded with a predetermined amount of the blend and placed in the center of the hot stage. The stage was kept at a constant temperature with the aid of a temperature controller. The temperature of the polymer melt was constantly monitored and recorded by a K-type thermocouple. The initial thickness of the powder bed inside the cup was approximately 2 mm. The process of foam development was observed with an Olympus optical microscope and recorded with a Panasonic BP-310 digital video camera. Image analysis was performed using SigmaScan Pro 5 (SYSTAT Inc., San Jose, CA, USA) in order to quantify the morphology during different stages of foaming. All of the experiments were done isothermally at 190°C under atmospheric pressure for a duration of 30 min.

4.3 Results and Discussion

4.3.1 Shear Rheological Characterization

Zero-shear viscosities of the tested materials are listed in Tables 4.2 and 4.3 for 190°C and 140°C, sorted from the lowest to highest values. Figure 4.2 summarizes the complex viscosity (η*), storage modulus (G') and viscous modulus (G") of the materials as a function of frequency. With increasing zero-shear viscosity, polymer materials showed higher values in complex viscosity, with PE-1 exhibiting considerably lower viscosity than other resins. The viscosity curve of PE-1 showed a Newtonian plateau at small frequencies less than 1 s^{-1} and exhibited the lowest degree of shear thinning at higher frequencies. The highest shear thinning behavior was observed with PE-5. The difference in the values of the shear viscosity of samples was more significant at lower frequencies and it decreased at higher frequencies. Storage modulus which represents the elasticity of the polymer melt and loss modulus which is a measure of material's viscous flow behavior followed a similar trend to the complex viscosity. PE-1 had the lowest storage and loss modulus compared to other samples.

Similar rheological characteristics were detected among the tested polyethylenes for the dynamic temperature ramp test which simulates the operating conditions that resins experience during the foaming process and analyzes the behavior of samples as a function of temperature to ensure no unexpected changes of rheology happen during the process (Figure 4.3). All resins showed a similar temperature dependency with the expected difference in terms of magnitude. The elastic modulus gradually decreased without abrupt changes as temperature increased. Similar trend was observed for the loss modulus. A hysteresis was displayed by all samples, with the temperature-specific modulus value being higher as the test scanned from low to high temperatures versus from high to low temperatures. This is consistent with the assumption that the entanglement among the polymer chains is facilitated when they are exposed to a high temperature for long time.

Table 4-2: Zero-shear viscosity of polymer materials at 190°C (Cross Model).

Material	Power Law Index (n)	Time Constant (λ)	Zero-Shear Viscosity at 190°C (Pa.s)
PE-1	0.53	0.015	996
PE-2	0.56	0.089	2296
PE-3	0.56	0.153	3199
PE-4	0.56	0.179	3934
PE-5	0.57	0.358	5164

Table 4-3: Zero-shear viscosity of polymer materials at 140°C (Cross Model).

Material	Power Law Index (n)	Time Constant (λ)	Zero-Shear Viscosity at 140°C (Pa.s)
PE-1	0.63	0.063	3796
PE-2	0.65	0.85	9625
PE-3	0.64	0.91	10526
PE-4	0.66	2.82	16712
PE-5	0.70	34.79	33768

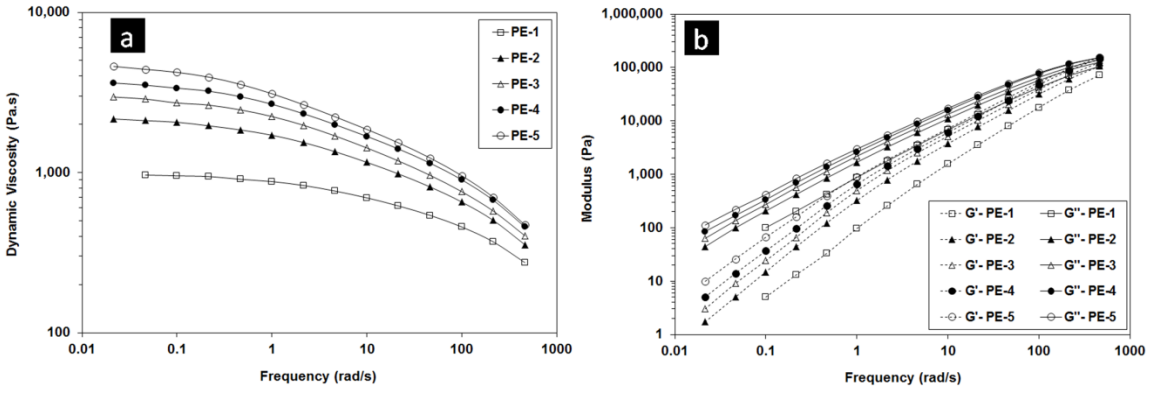

Figure 4-2: Rheological properties of polymer materials as a function of frequency at 190°C. a) Complex viscosity, b) Storage and Loss modulus.

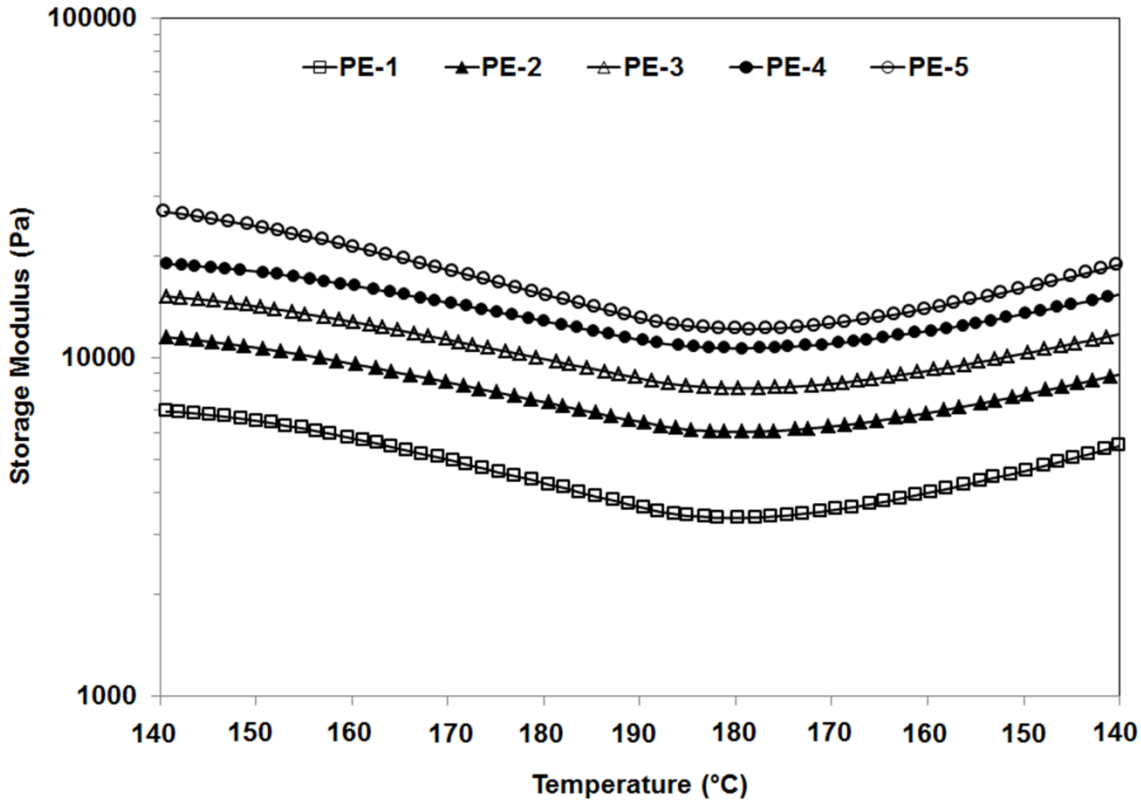

Figure 4-3: Dynamic temperature ramp of storage modulus- frequency of 10 rad/s, strain of 5%, heating rate of 10°C/min.

4.3.2 Extensional Rheological Characterization

Measurements of the tensile stress growth coefficients versus time, shown in Figure 4.4, provided a characterization of the extensional melt flow behavior of the polymer materials. Due to low zero-shear viscosity and sagging issues, the measurements could not be performed with PE-1. For all other resins, five different extensional rates were used, 0.05, 0.1, 0.5, 1, 5 and 10 s^{-1}. These tested resins displayed strain-hardening, manifested as a deviation from the linear viscoelastic stress growth behavior. The most significant strain-hardening was observed for PE-3 as the extensional viscosity increased considerably above the dynamic viscosity for all strain rates. This behavior became more pronounced as the strain rate was increased. It was noted that the onset of strain-

hardening at a given rate occurred at approximately the same strain rate for all tested resins, independent of the molecular structure of the polymer materials.

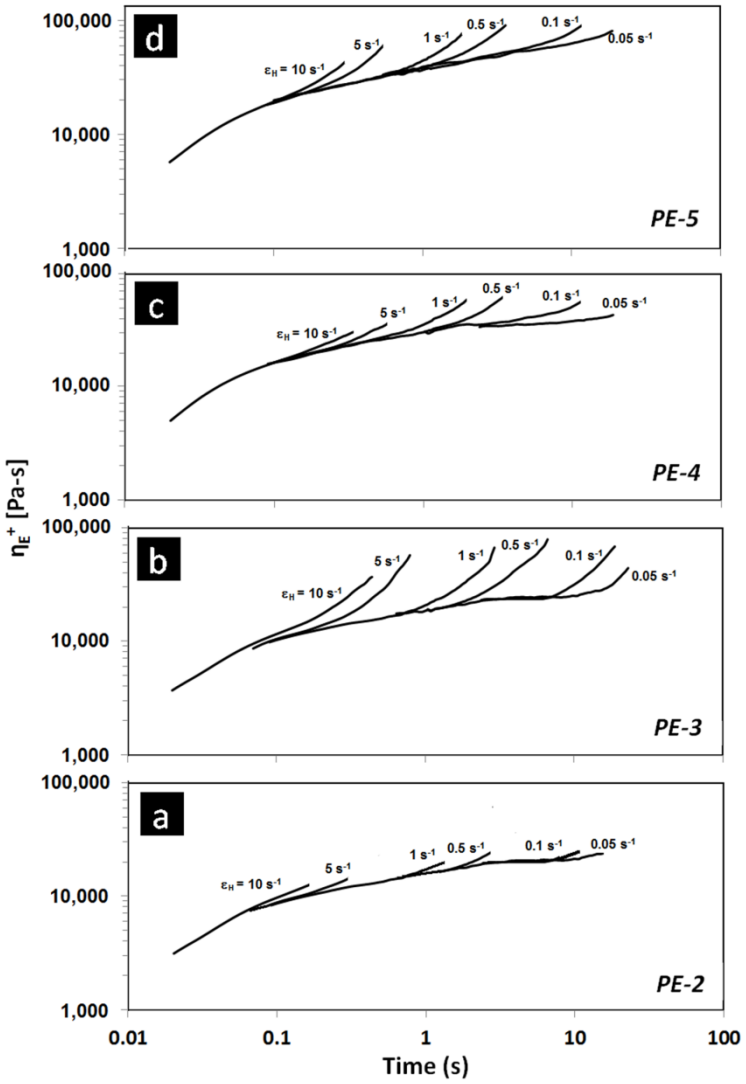

Figure 4-4: Extensional stress growth coefficient rate at various strain rates at 140ºC for a) PE-2, b) PE-3, c) PE-4, and d) PE-5.

4.3.3 Visualization Experiments of Foaming

Figure 4.5 presents a series of micrographs for the foaming process to demonstrate the dynamic behavior of bubbles during sintering, primary and secondary nucleation [16],

and bubble growth. It was observed that all foamed samples resulted in a closed structure. An irregular shaped cellular structure was formed initially (1 min< t < 2 min). However, bubbles became more spherical as time passed, to reach a more energetically stable state by reducing the air-polymer interfacial area. The foamed structure exhibited fully spherical-shape bubbles during the bubble growth stage (t > 3.5 min). The evolving cellular structure during different stages of the foaming process was analyzed for its bubble surface density, bubble diameter, total bubble projected area [16], and bubble size distribution, as shown in Figures 4.6-4.9.

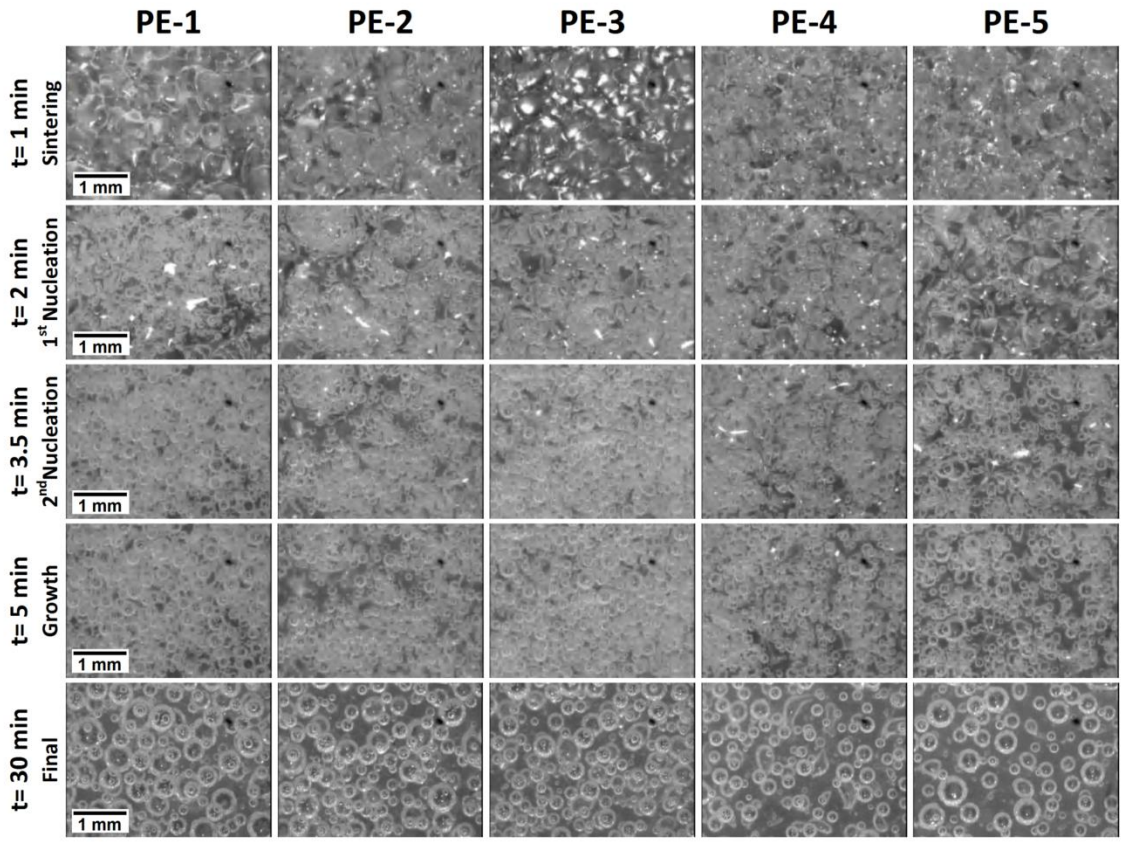

Figure 4-5: Dynamic behavior of bubbles during different stages of the foaming process.

The profile for bubble surface density generally consisted of two characteristic stages (Figure 4.6). Initially, a rapid increase in the number of bubbles was observed as the system transitioned between two stages of nucleation (1 min < t < 2 min). This was

followed by a significant reduction in bubble density due to early stages of coalescence and gas re-dissolution, and the steepness of this decline corresponded to the level of activity of bubble coalescence. This rapid decline started immediately after secondary nucleation, though bubble density continued to decline up to the end of the foaming process at a progressively slower rate. All resins followed similar trends of bubble density reduction, however, different rates of change were observed for each foamed sample (as seen by the included table in Figure 4.6). The number of nucleated bubbles that were generated and survived through the two stages of nucleation decreased with increasing viscosity/elasticity for the polymer matrix. The highest and lowest number of nucleated bubbles present by the end of the secondary nucleation stage corresponded to the resins PE-1 (63.4 bubbles/mm^2) and PE-5 (44.4 bubbles/mm^2), respectively. It was observed that low viscosity and melt elasticity for a gas-laden matrix allowed a larger number of bubbles to survive and grow larger than the critical nucleus. A detailed explanation of the effect of rheology on the nucleation behavior of polyethylene materials has been discussed in our previous work [26]. The trend of decline in bubble density after nucleation was notably similar for all resins, however, resins with higher melt viscosity/elasticity resulted in lower rate of bubble density reduction. This behavior indicates that higher melt viscosity/elasticity of the polymer matrix effectively restricted the mechanism of bubble coalescence. Similar observations were reported for the foaming in pressurized systems using polypropylene [9,27]. The total number of the surviving bubbles to the end of the full foaming process seen in Figure 4.6 was lower with resins of higher melt viscosity/elasticity, due to the considerably lower number of survived bubbles during the nucleation stage (PE-1: 17.2 bubbles /mm^2, PE-5: 11.6 bubbles /mm^2). An exception to this trend was found with PE-3 which followed a different path of changes in the bubble density. PE-3 exhibited a lower rate of bubble number reduction than all of the other resins towards the end of the process ($t > 5$ min) and demonstrated a completely stable cell structure with no changes in bubble number by the final stages of foaming ($20 \text{ min} < t < 30 \text{ min}$). PE-3 showed the highest value for the

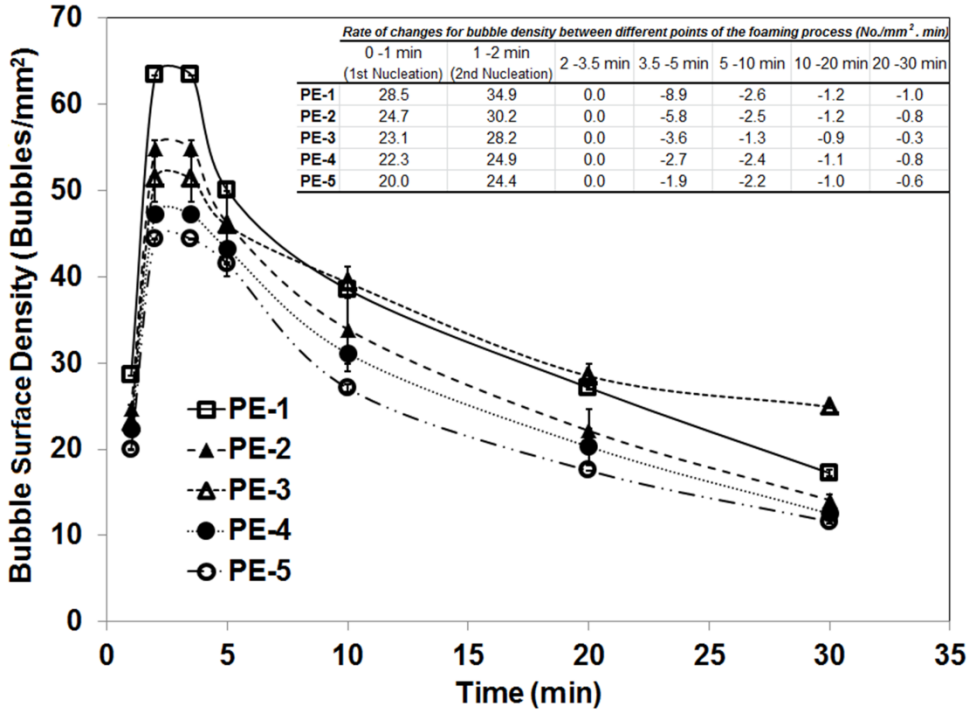

Rate of changes for bubble density between different points of the foaming process (No./mm² . min)

	0 -1 min (1st Nucleation)	1 -2 min (2nd Nucleation)	2 -3.5 min	3.5 -5 min	5 -10 min	10 -20 min	20 -30 min
PE-1	28.5	34.9	0.0	-8.9	-2.6	-1.2	-1.0
PE-2	24.7	30.2	0.0	-5.8	-2.5	-1.2	-0.8
PE-3	23.1	28.2	0.0	-3.6	-1.3	-0.9	-0.3
PE-4	22.3	24.9	0.0	-2.7	-2.4	-1.1	-0.8
PE-5	20.0	24.4	0.0	-1.9	-2.2	-1.0	-0.6

Figure 4-6: Bubble density of developing polyethylene foams during the foaming process, using 0.5% CBA and under isothermal conditions.

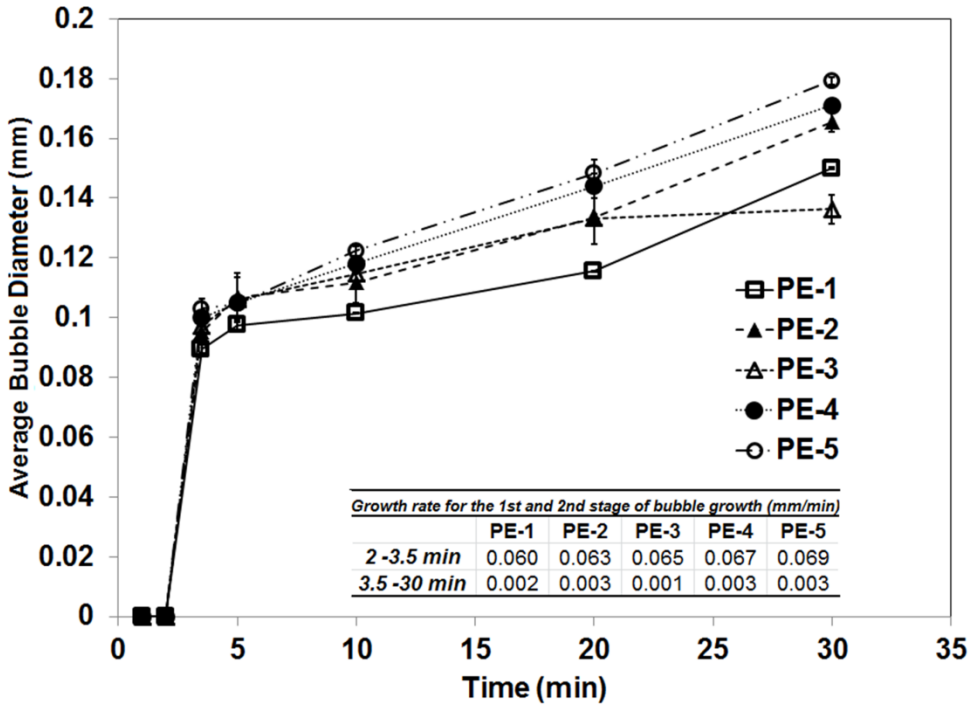

Growth rate for the 1st and 2nd stage of bubble growth (mm/min)

	PE-1	PE-2	PE-3	PE-4	PE-5
2 -3.5 min	0.060	0.063	0.065	0.067	0.069
3.5 -30 min	0.002	0.003	0.001	0.003	0.003

Figure 4-7: Average bubble size of developing polyethylene foams during the foaming process, using 0.5% CBA and under isothermal conditions.

final number of surviving bubbles in the foamed sample (24.9 bubbles/mm^2). This observation will be discussed later.

As illustrated by the plotted progression of average bubble diameter in Figure 4.7, the results showed two distinct stages of bubble growth: an initial rapid expansion in which the bubble volume increased rapidly (2 min < t < 3.5 min), and a slower second phase of bubble growth (t > 3.5 min). The rapid expansion in bubble sizes during the first phase demonstrates the bubble growth mechanism at its highest level of activity in the foaming process. Beyond this time, the bubbles continued to grow at a considerably slower rate. Having exhausted most of the dissolved gas in the melt, bubbles gained little volume from this point onwards. Generally, the resins with higher melt viscosity/elasticity resulted in larger average bubble diameter during all stages of the foaming process. This can be explained by the concentration of the available foaming gas in the polymer matrix. As it was discussed earlier, higher melt viscosity/elasticity yielded a lower bubble density at the early stage of growth. With the smaller number of formed bubbles, the amount of gas consumed for creating the bubbles became lower and hence, the concentration of remaining gas in the polymer matrix increased. Consequently, the rate of mass transfer for dissolved gas from the matrix polymer to bubbles increased, which led to the greater bubble sizes and higher rate of bubble growth. As shown in the table included within 4.7, PE-5 with the highest melt viscosity exhibited the highest rate of expansion during the first and second stages of bubble growth (0.0687 mm/min and 0.0029 mm/min, respectively), and PE-1 showed the lowest growth rates (0.0597 mm/min and 0.0023 mm/min, respectively).There was an exception for PE-3 which followed the same profile but with a considerably lower growth rate displayed during the second phase of the bubble expansion compared to the other resins. The average bubble diameter within PE-3 remained practically unchanged towards the end of the process (20 min < t < 30 min), and it exhibited the lowest final average bubble size among all the other foamed samples (130 μm).

In order to determine the combined effect of the bubble growth and coalescence/dissolution, the calculated total bubble projected area, which represents the two-dimensional foam thickness variation in actual foam molding, was included in the analysis of foaming (Figure 4.8). The total projected area is the cumulative two-dimensional area measurement of the three-dimensional foamed particle, by projecting the bubble shapes onto a plane parallel to the foam wall. More details of the definition of this parameter have been discussed elsewhere [16]. The parameter showed a rapid increasing trend immediately after nucleation (t > 2 min) and up to t= 5 min, at which time a reduction in the total area of bubbles was observed. The rising and declining trends seen with this parameter are associated with the dominant mechanisms of bubble growth and bubble coalescence/dissolution, respectively. The declining trend depicts through-plane shrinkage of the developing foam, similar to the reported trend in our

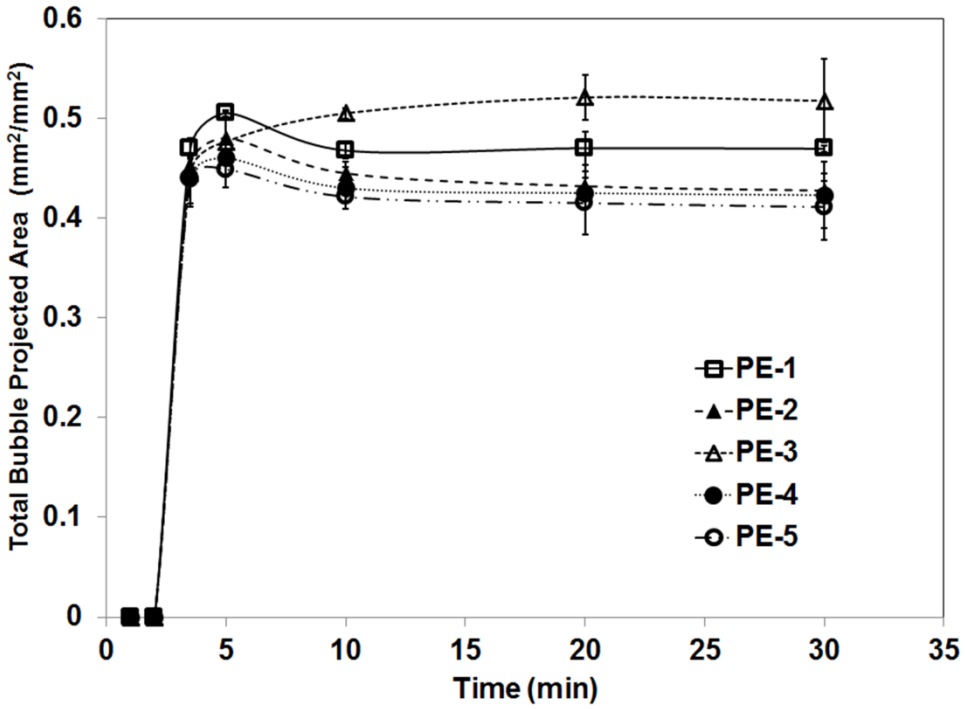

Figure 4-8: Total bubble projected area of developing polyethylene foams during the foaming process, using 0.5% CBA and under isothermal conditions.

previous study [16]. Once again, an exception in the trend of this parameter was noted for PE-3. Interestingly, PE-3 did not show the shrinkage behavior. In the last stages of foaming (t > 15 min), the foam essentially stopped expanding and the total area of bubbles showed a plateau reflecting a balance between the two competing mechanisms. Despite the balance achieved in the total projected area in final stages of foaming with PE-3, continuous changes in the bubble density and bubble size showed that the foam morphology had not stabilized since the matrix continued to be heated.

Figure 4.9 shows the bubble size distribution at different stages of foam development. Measurements of the size distributions further confirmed the dynamic changes in the morphological structure of the developing foam observed by the discussed parameters. During the early stages of bubble growth (3.5 min< t <5 min), all samples showed a unimodal distribution of bubbles in the size range of 0.04-0.12 mm. Commencement of bubble growth and coalescence mechanisms led to a polydispersed and less uniform size distribution. Variance in the bubble size was reported in the table included in Figure 4.9. Initially, foaming with PE-1 yielded the narrowest distribution among all resins with a variance of 0.179 mm^2 and smallest peak value of 0.04-0.08 mm, however, the significant reduction in the bubble density in later stages led to the least uniform distribution in terms of bubble size in the final structure (variance of 1.415 mm^2). The cellular structure of the foams obtained from PE-4 and PE-5 exhibited the lowest level of uniformity after the nucleation, while the variances in the bubble size distribution at the final stage were comparable with PE-1. PE-3 foam showed approximately the same uniformity of bubble size distribution in PE-1 foam during early stages, whereas the final cellular structure yielded the most uniform size structure compared to other samples (variance of 0.797 mm^2).

PE-3 has already been noted to exhibit a different foaming behavior compared to the other resins. The results showed that by controlling the bubble growth mechanism and suppressing bubble coalescence/dissolution, PE-3 produced a cellular structure with the

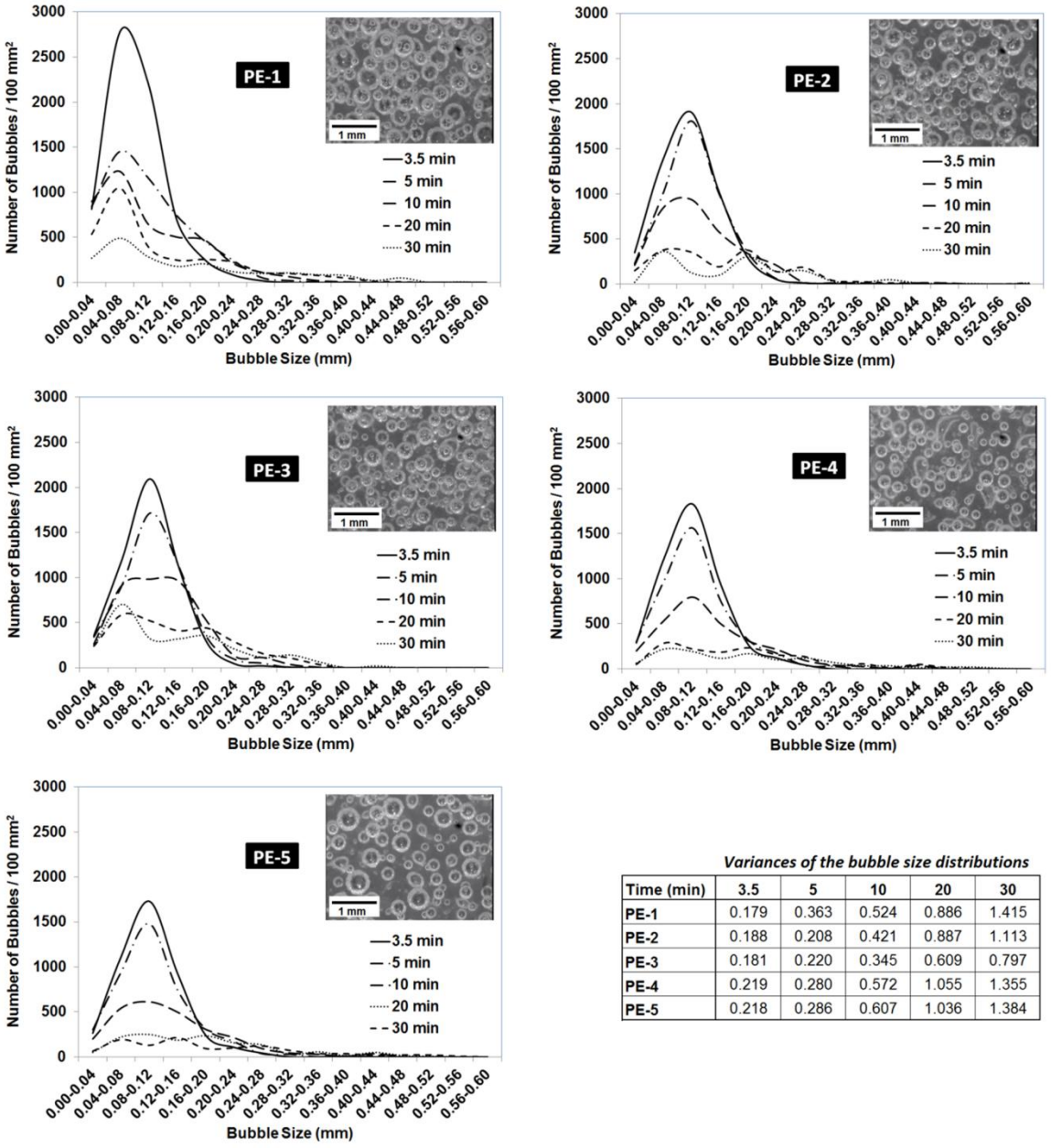

Variances of the bubble size distributions

Time (min)	3.5	5	10	20	30
PE-1	0.179	0.363	0.524	0.886	1.415
PE-2	0.188	0.208	0.421	0.887	1.113
PE-3	0.181	0.220	0.345	0.609	0.797
PE-4	0.219	0.280	0.572	1.055	1.355
PE-5	0.218	0.286	0.607	1.036	1.384

Figure 4-9: Bubble size distribution of developing polyethylene foams during the foaming process, and images of the final cellular structures, using 0.5% CBA and under isothermal conditions.

highest bubble density, smallest bubble size, the most uniform bubble size distribution, and greatest foam expansion. These observations can be explained by the differences in the rheology of the resins. The improved bubble stability in terms of density and size for

the foamed PE-3 can be attributed to the increased melt strength and higher degree of strain-induced hardening. This melt strength provides a resistance to deformation and facilitates the stabilization of the bubble [22,23]. It helps to stabilize the foam structure through a mechanism that leads to increasing extensional viscosity as the level of strain is increased. Therefore, the growing bubbles stay intact longer as the increased viscosity prevents excessive bubble growth and bubble coalescence. PE-3 with higher melt strength and strain-hardening behavior showed more capacity to withstand the stretching forces during the stage of bubble growth.

Considering the effect of melt viscosity/elasticity during the bubble nucleation and contribution of melt strength to the stabilization of the cellular structure in the bubble growth stage, nucleation, growth and bubble coalescence must be considered simultaneously to arrive at a satisfactory conclusion. Results indicate that low shear viscosity accelerates the rate of removing the interstitial voids during polymer melt sintering and allows a greater number of bubbles to survive and grow at the nucleation stage [26], while high elasticity hinders bubble formation and strain-hardening reduces the bubble coalescence and stabilizes the growing bubble. On the other hand, very low shear viscosity may not be desirable for the foaming process because of the associated reduction in melt strength. Therefore, a balance in rheology can lead to a high nucleation rate combined with bubble stabilizing effect, which results in higher bubble density, smaller bubble size, and greater foam expansion.

4.3.4 Bubble Growth Model for a Purely Viscous Fluid

The next part of the work reports on the development of a bubble growth model and simulation scheme to describe the non-isothermal bubble growth phenomena that occur in non-pressurized foaming systems. A bubble expansion model based on the well-known cell model [17,18] was tested to determine if viscous forces adequately matched the experimental data, this model was modified for the present study to be used for non-isothermal processes. The cell model approximates the diffusion-induced growth of a gas

bubble surrounded by a thin film of Newtonian liquid to simulate cases where a large number of bubbles grow in close proximity during foaming. A schematic diagram of the cell model is illustrated in Figure 4.10. To implement the cell model in the simulation algorithm of the CBA-based bubble growth, the following assumptions were made:

1. After heating the system to a certain set point temperature, the bubble growth is isothermal.
2. The bubble is spherically symmetric throughout the bubble growth process.
3. The polymer melt is Newtonian and incompressible.
4. The inertial forces and gravity are negligible.
5. The gas inside the bubble obeys Henry's law.
6. The accumulation of adsorbed gas molecules on the bubble surface is negligible.
7. The initial accumulated stress around the growing bubble is zero.

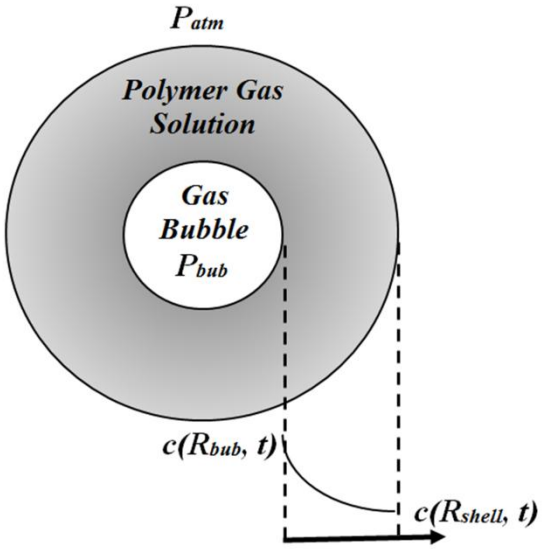

Figure 4-10: Schematic of the bubble growth model.

Mathematical Formulations and Numerical Simulation Algorithm

The bubble expansion mechanisms can be described by a standard group of governing equations including momentum equation, mass balance equation over the bubble, and gas

diffusion equation in the surrounding polymer melt. The dynamics of the foaming system are governed by the conservation of momentum in the radial direction. With the assumption of negligible inertia and gravitational forces (assumption 4) and considering the surrounding pressure to be atmospheric (P_{atm}), the corresponding momentum equation can be written as [18]:

$$P_{bub} - P_{atm} - \frac{2\sigma}{R_{bub}} + 2\int_{R_{bub}}^{R_{shell}} \frac{\tau_{rr} - \tau_{\theta\theta}}{r} = 0 \qquad \text{Eq. 4-1}$$

where P_{atm} is the atmospheric pressure, P_{bub} is the bubble pressure at time t, R_{bub} is the bubble radius at time t, R_{shell} is the radius of the corresponding polymer/gas solution shell, σ is the surface tension, and τ_{rr} and $\tau_{\theta\theta}$ are the stress components in the r and θ directions.

The normal stresses in the conservation of momentum equation, τ_{rr} and $\tau_{\theta\theta}$, can be calculated by combining the generalized Newtonian constitutive equation, Eq. 4-2, and the rate of deformation components for a symmetrical bubble, Eq. 4-3 and Eq. 4-4 [28]:

$$\tau_{ij} = \eta\Delta_{ij} \qquad \text{Eq. 4-2}$$

$$\Delta_{rr} = -4\frac{\dot{R}_{bub}R_{bub}^2}{r^3} \qquad \text{Eq. 4-3}$$

$$\Delta_{\theta\theta} = \Delta_{\varphi\varphi} = 2\frac{\dot{R}_{bub}R_{bub}^2}{r^3} \qquad \text{Eq. 4-4}$$

$$\tau_{rr} = -4\eta\left(\frac{\dot{R}_{bub}R_{bub}^2}{r^3}\right) \qquad \text{Eq. 4-5}$$

$$\tau_{\theta\theta} = 2\eta\left(\frac{\dot{R}_{bub}R_{bub}^2}{r^3}\right) \qquad \text{Eq. 4-6}$$

where Δ is the rate of deformation tensor along the diagonal (Δ_{rr}, $\Delta_{\theta\theta}$ and $\Delta_{\varphi\varphi}$), η is the melt viscosity, and $\dot{R}$ is the rate of bubble growth. Inserting Eq. 4-5 and Eq. 4-6 into the

conservation of momentum equation and integrating the fourth term from $r = R_{bub}$ to $r = R_{shell}$ gives:

$$\frac{dR}{dt} = R\left(\frac{P_{bub} - P_{atm} - 2\sigma/R_{bub}}{4\eta}\right)\left(\frac{R_{shell}^3}{R_{shell}^3 - R_{bub}^3}\right) = 0 \qquad \text{Eq. 4-7}$$

The law of conservation of mass requires that the rate of change of the mass in the gas bubble must be balanced by the mass of gas diffusing into the bubble through its surface. Assuming that the gas inside the bubble is ideal, the mass conservation equation can be expressed as:

$$\frac{d}{dt}\left(\frac{P_{bub}}{R_g T}\,\frac{4}{3}\pi R_{bub}^3\right) = 4\pi R_{bub}^2\, D\,\frac{\partial c}{\partial r}\bigg|_{r=R_{bub}} \qquad \text{Eq. 4-8}$$

where R_g is the universal gas constant, D is the gas diffusivity in the polymer, and c is the dissolved gas concentration in the shell. With the knowledge of the concentration gradient at the bubble surface, Eq. 4-8 can be solved with Eq. 4-7 to obtain R_{bub} and P_{bub} at a particular instant. Therefore, it is necessary to determine the concentration profile surrounding the gas bubble. The diffusion equation for spherical coordinates can be written as follows:

$$\frac{\partial c}{\partial t} + \frac{R_{bub}^2 \dot{R}_{bub}}{r^2}\frac{\partial c}{\partial r} = \frac{D}{r^2}\frac{\partial c}{\partial r}\left(r^2\frac{\partial c}{\partial r}\right) \quad \text{for } r \geq R_{bub} \qquad \text{Eq. 4-9}$$

and Eq. 4-9 can be solved subject to the following boundary and initial conditions:

$$c(r, 0) = x\, K_H P_{atm} \quad \text{for } r \geq R_{bub} \qquad \text{Eq. 4-10}$$

$$c(R_{bub}, t) = K_H P_{bub} \quad \text{for } t \geq 0 \qquad \text{Eq. 4-11}$$

$$c(R_{shell}, t) = x\, K_H P_{atm} \quad \text{for } t \geq 0 \qquad \text{Eq. 4-12}$$

where x is the degree of gas saturation in the polymer melt and K_H is Henry's law constant. Eq. 4-7 to Eq. 4-12 constitute a complete set of equations that describes bubble growth process during polymeric foaming.

Due to the nonlinearity and coupling of the governing equations, a numerical simulation algorithm which integrates the explicit finite difference scheme and the fourth order Runge–Kutta method was used in MATLAB to solve the equations and simulate the expanding phenomenon of the formed bubble. In order to eliminate the convective term in Eq. 4-9 and immobilize free-moving boundaries for the governing equations, we followed Arefmanesh [18] and used the Lagrangian coordinate transformation. Bubble nucleation in non-pressurized polymer foaming is initiated by heating the system to a temperature that is higher than the CBA's decomposition temperature. Therefore, the simulation program was modified to consider the heating process in the experiment's initial phase and the changes in the thermo-physical properties of the polymer/gas system caused by the temperature increase.

Comparison of Model Predictions to Experiments

The simulated results by the bubble growth model were compared with the experimental data observed using the visualization setup. Table 4.4 provides a summary of the physical and processing parameters employed in this research. Physical properties were estimated based on the system of PE/Nitrogen, since the majority of the gas released by the decomposition of CBA is nitrogen. The diffusivity and Henry's law constant were estimated by using data and charts published by Lee [29]. According to Sato [30] and Lee [29], diffusivity and Henry's law constant are virtually independent from temperature variations at atmospheric pressure and these two parameters were considered constant during the bubble expansion process. The surface tension values for polymer melts were obtained from literature [31,32]. The viscosity of the polymer at the processing temperature was calculated using the Arrhenius temperature dependence, with the reference temperature of 140°C.

Table 4-4: Numerical values of physical and processing properties.

Parameter	Value
Atmospheric Pressure (Pa)	101325
Diffusion Coefficient (m^2/s)	6.04×10^{-9}
Henry Constant ($mol/m^3.Pa$)	3.71×10^{-5}
Surface Tension (N/m)	0.026
Initial Temperature (°C)	166
Max. Temperature (°C)	190
Activation Energy (J/mol)	20,000
Heating Rate (°C/min)	10
Degree of Saturation	95%
Initial Bubble Radius (m)	3.00×10^{-6}
Initial Shell Radius (m)	5.00×10^{-4}

Computer-simulated predictions of the bubble growth behavior for five foamed polyethylene samples were compared with the experimental results and are shown in Figure 4.11. The theoretical calculations at t=0 s were matched with the experiment at t=2 min, where the bubbles could be detected visually in the process. The predicted bubble growth profiles reasonably followed the experimentally observed trend during the first stage of rapid bubble expansion. The slower bubble growth rate at the very beginning of the process is due to the retarding forces contributed by the surface tension which is very large for small bubbles and it is continuously reduced as the bubbles grow and the bubble growth rate increases accordingly. The first stage of bubble growth continues until t=144 s at which the foaming system moves into the isothermal conditions (Figure 4.11f). Beyond this point, the model exhibits a plateau behavior for the bubble expansion, while experimental foaming process showed the bubbles continued to grow at a slow rate. This can be explained by the significant bubble-to-bubble interaction at this stage as it was discussed in the visualization experiments. This effect has not been reflected in the model. Therefore, the developed bubble growth model accounts for most of the underlying physics that describes the growth dynamics of the nucleated bubbles and can

predict the bubble growth behavior before the interactions among bubbles become significant.

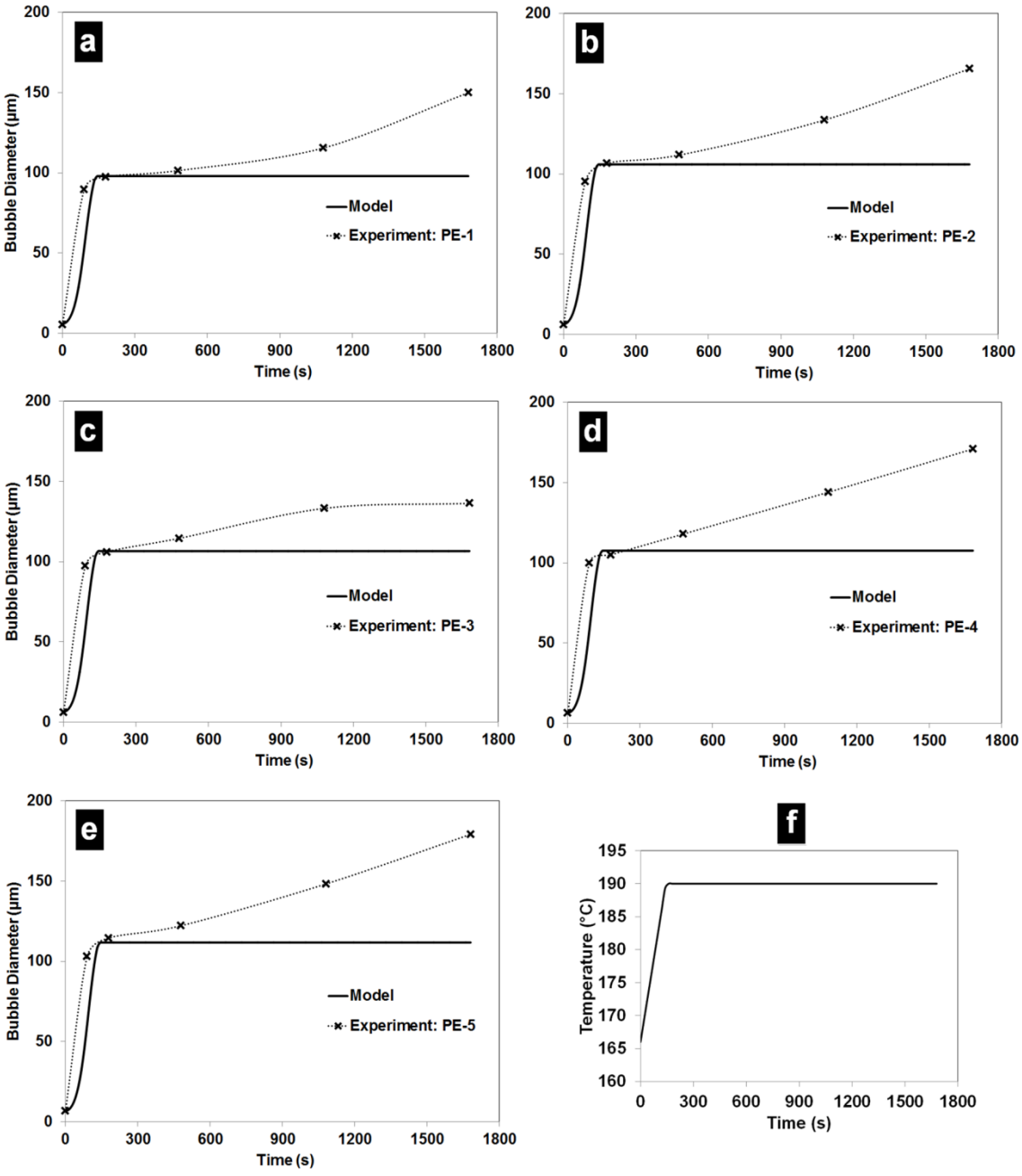

Figure 4-11: Comparison of the simulation results and experimental observations, a) PE-1, b) PE-2, c) PE-3, d) PE-4, e) PE-5, and f) Temperature profile. Theoretical calculations at t=0 s were matched with the experiment at t=2 min.

4.3.5 Sensitivity Analysis

A series of sensitivity analyses was performed to study the effects of various simulation variables as well as thermophysical and rheological parameters on the bubble growth phenomena. PE-2 was used as the reference sample for analyses.

Effect of Initial Bubble Size: Simulated bubble growth profiles using different initial bubble diameters are demonstrated in Figure 4.12a. The initial bubble size greatly affected the final bubble size and larger initial bubble size led to significantly higher growth rate in early stages. The simulation results suggest that nucleation of small size bubbles is an important factor to minimize the formation of coarse bubbles and has a remarkable influence on the average bubble size in the final cellular structure.

Effect of Heating Rate: The effect of different heating rates on the bubble growth behavior is shown in Figure 4.12b, in which the rate of heating varied from 8°C/min to 16°C/min. The rate of heating had negligible effects on the early stages of bubble growth and all curves were overlapping at this stage. However, the final bubble size at lower heating rate was considerably greater than that at a higher rate of heating. This behavior can be explained by the changing properties of the polymer matrix over a longer period of time by using a lower heating rate.

Effect of Diffusivity: The effect of diffusivity on the bubble-growth profiles was studied by varying its value over a range of 0.01×10^{-9} to 15×10^{-9} m^2/s and the simulation results are shown in Figure 4.12c. An increase in the diffusion coefficient led to a faster diffusion rate of gas molecules into the nucleated bubbles and therefore increased the bubble growth rate in its initial phase. At the final stages of the growth, bubbles reached similar bubble sizes. This is due to availability of a certain amount of gas for the whole process in each case and indicates diffusion is matter of time. Long processing time can virtually offset the effect of diffusivity on final cellular structure.

Effect of Henry's Law Constant: The influence of Henry's constant on the bubble growth is shown in Figure 4.12d. An increase in Henry's constant from 0.01×10^{-5} up to

10×10^{-5} mol/m^3.Pa showed negligible effects on the rate of growth. A further increase to 100×10^{-5} mol/m^3.Pa led to a smaller final bubble size. This is conceivable as larger amount of gas is retained in the polymer-gas solution due to the higher gas solubility, and therefore the amount of gas available for bubble growth is reduced. The higher gas concentration in the polymer-gas solution shell and in particular at the gas bubble interface also results in a reduced concentration gradient and slower mass transfer into the bubble. Consequently the rate of bubble growth is lower.

Effect of Viscosity: The effect of zero shear viscosity on the bubble growth was simulated and the results are shown in Figure 4.12e. Simulation results suggested that the effect of zero-shear viscosity on the bubble growth was negligible within the range of 500 to 40000 Pa.s (at 140°C) and bubble growth profiles appeared totally independent of viscosity when using similar initial bubble size. However, lower melt viscosity than 500 Pa.s resulted in significantly larger bubble size at the final stages. These simulated results are contradictory to our experimental observations in which increasing melt viscosity led to a higher final bubble size. The difference between numerical and experimental results can be explained by the effect of viscosity during the nucleation stage. Our previous experimental and theoretical studies showed that higher viscosity could impede the number of nuclei survived during the nucleation stage in the foaming system [26]. Due to lower nucleated bubble density and higher availability of foaming gas in the polymer matrix, foams produced by resins with higher viscosity showed in larger average bubble size during all stages of the foaming process. The initial size of the bubble is very critical in determining the final bubble size, as it was discussed previously. It can be concluded that the pronounced effect of the shear viscosity observed experimentally on the final cellular structure arises from its influence on the nucleation stage.

Effect of Surface Tension: Figure 4.12f illustrates the effect of interfacial tension on bubble growth by varying surface tension values from 0.0014 to 0.038 N/m. The bubble growth profile showed almost no sensitivity to the changes in surface tension. This might

result from the fact that in our simulation the rheology and gas transport properties of the materials dominate and the role of surface tension is negligible.

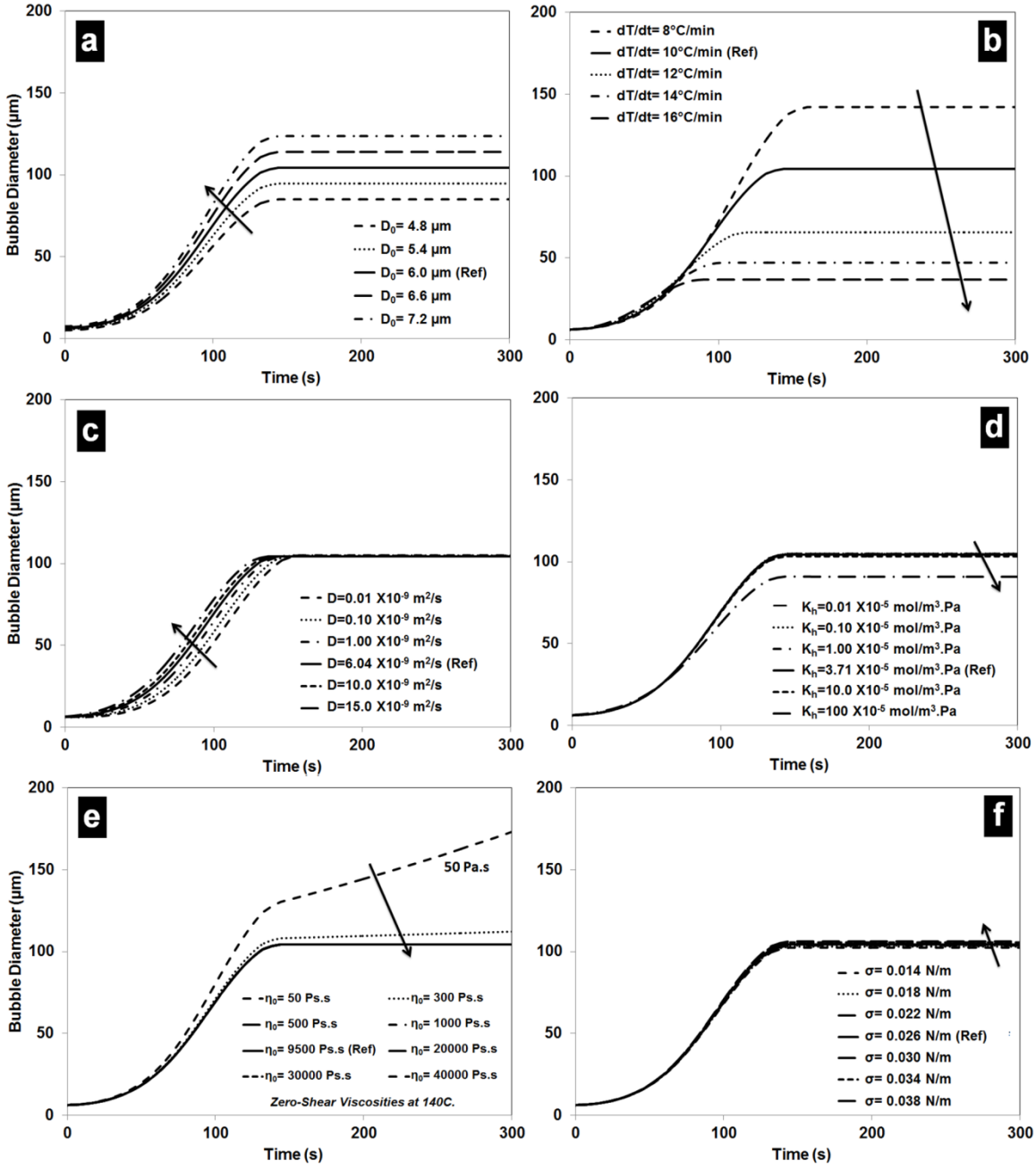

Figure 4-12: Effects of simulation variables, thermophysical and rheological parameters on the bubble growth, a) initial bubble size, b) heating rate, c) diffusivity, d) Henry's law constant, e) zero-shear viscosity, and f) surface tension.

4.4 Conclusions

Microscopic studies on the foaming performance of several polyethylene polymers under non-pressurized conditions revealed that the developed cellular structure and final foam properties are profoundly influenced by the rheological properties of the polymer materials. It was found that lower melt viscosity/elasticity of the polymer matrix allowed a greater number of bubbles to grow larger than the critical nucleus and resulted in a higher total number of the survived bubbles to the end of the foaming process. Due to lower bubble density and higher availability of foaming gas in the polymer matrix, foams produced by highly viscous polymer materials showed larger average bubble size during all stages of the foaming process. The experimental results revealed that increased melt strength and higher degree of strain-hardening improved bubble structure stability by controlling the bubble growth mechanism and suppressing bubble coalescence/dissolution and resulted in greater foam expansion and effectively expanded the foam processing window. Strain-hardening led to stabilization of growing bubbles and prevented bubble coalescence under extreme processing conditions. Considering the effects of melt viscosity and elasticity in determining the foam processing window and contribution of melt strength to the stabilization of the growing bubbles, it was concluded that a balance in rheology is essential to attain an improved foamed structure with higher bubble density, smaller bubble size, and more uniform bubble size distribution. Among five tested resins in this work, the rheological behavior of PE-3 provided the most stable cellular structure and promising foaming performance.

Visualization data was then compared to the predictions of a mathematical model and simulation algorithm based on the well-known cell model which describes bubble growth dynamics in a purely viscous fluid. It was shown that the simulated growth profiles for bubbles can predict the observed bubble growth behaviors for different processing conditions during the initial stages of foaming and it can serve as a tool for predicting bubble growth behavior during the polymer foaming process. A series of sensitivity

analyses was performed to investigate the effect of thermophysical, rheological, processing, and simulation parameters on bubble growth simulation.

4.5 References

[1] J.L. Throne, *Thermoplastic Foams*. Hinckley OH: Sherwood Publishers, 1996.

[2] V. Kumar and J. Weller, "Production of microcellular polycarbonate using carbon dioxide for bubble nucleation," *J.Eng. Ind. Trans. ASME*, 116, 413-420, 1994.

[3] Y.P. Handa et al., "Some thermodynamic and kinetic properties of the system PETG-CO_2 and morphological characteristics of the CO_2-blown PETG foams," *Polym. Eng. Sci.*, 39, 55-61, 1999.

[4] N.S. Ramesh, D.H. Rasmussen, and G.A. Campbell, "Numerical and experimental studies of bubble growthduring the microcellular foaming process," *Polym. Eng. Sci.*, 31, 1657–1664, 1991.

[5] S.K. Goel and E.J. Beckman, "Generation of microcellularpolymeric foams using supercritical carbon dioxide. Part I.Effect of pressure and temperature on nucleation," *Polym. Eng. Sci.*, 34, 1137–1147, 1994.

[6] K. Song and R.E. Apfel, "Foaming of Low-Density Polyethylene in a Dynamic Decompression and Cooling Process," *Polym. Eng. Sci.*, 41, 735-742, 2001.

[7] C.B. Park, D.F. Baldwin, and N.P. Suh, "Effect of the pressure drop rate on cell nucleation in continuous processing of microcellular polymers," *Polym. Eng. Sci.*, 35, 432-440, 1995.

[8] C.B. Park and N.P. Suh, "Filamentary extrusion of microcellular polymers using a rapid decompressive element," *Polym. Eng. Sci.*, 36, 34- 48, 1996.

[9] C.B. Park and L.K. Cheung, "A study of cell nucleation in the extrusion of polypropylene foams," *Polym. Eng. Sci.*, 37, 1-10, 1997.

[10] S.T. Lee and K. Lee, "Surrounding temperature effects on extruded polyethylene foam structure," *Adv. Polym. Tech.*, 19, 87- 96, 2000.

[11] L.S. Turng and H. Kharbas, "Effect of Process Conditions on the Weld-line Strength and Microstructure of Microcellular Injection Molded Parts," *Polym. Eng. Sci.*, 43, 157-168, 2003.

[12] X. Qin, M.R. Thompson, and A.N. Hrymak, "Rheology studies of foam flow during injection mold filling," *Polym. Eng.Sci.*, 47, 522-529, 2007.

[13] G. Liu, C.B. Park, and J.A. Lefas, "Production of Low-Density LLDPE Foams in Rotational Molding," *Polym. Eng. Sci.*, 38, 1997- 2009, 1998.

[14] S.J. Liu and C.H. Yamg, "Rotational Molding of Two- Layered Polyethylene Foams," *Adv. Polym. Tech.*, 20, 108- 155, 2001.

[15] E. Archer, E. Harkin-Jones, and M.P. Kearns, "Processing Characteristics and Mechanical Properties of Metallocene Catalyzed Linear Low-Density Polyethylene Foams for Rotational Molding," *Polym. Eng. Sci.*, 44, 638- 647, 2004.

[16] M. Emami, E. Takacs, M. R. Thompson, J. Vlachopoulos, and Eric Maziers, "Visual Studies of Model Foam Development for Rotational Molding Processes," *Advances in Polymer Technology*, 2012.

[17] M. Amon and C.D. Denson, "A Study of the Dynamics of Foam Growth: Simplified Analysis and Experimental Results for Bulk Density in Structural Foam Molding," *Polym. Eng. Sci.*, 26, 255-267, 1986.

[18] A. Arefmanesh and S.G. Advani, "Diffusion-Induced Growth of a Gas Bubble in a Viscoelastic Fluid," *Rheol Acta*, 30, 274-283, 1991.

[19] M.B. Bradley and E.M. Phillips, "Novel polypropylenes for foaming on conventional equipment," *Plast. Eng.*, 47, 82-84, 1991.

[20] H.E. Naguib, C.B. Park, U. Panzer, and N. Reichelt, "Strategies for achieving ultra-low density PP foams," *Polym. Eng. Sci.*, 42, 1481-1492, 2002.

[21] M. Yamaguchi and K I. Suzuki, "Rheological properties and foam processability for blends of linear and crosslinked polyethylenes," *J. Polym. Sci. Part B. Pol.Phys.*, 39, 2159- 2167, 2001.

[22] P. Spitael and C.W. Macosko, "Strain hardening in polypropylenes and its role in extrusion foaming," *Polym. Eng. Sci.*, 44, 2090-2100, 2004.

[23] J. Stange and H. Münstedt, "Rheological properties and foaming behavior of polypropylenes with different molecular structures," *J. Rheol.*, 50, 907-923, 2006.

[24] R L. Blaine. TA Instruments.

[25] M. L. Sentmanat, "Miniature Universal Testing Platform: From Extensional Melt Rheology to Solid-State Deformation Behavior," *Rheol. Acta*, 43, 657- 669, 2004.

[26] M. Emami, M.R. Thompson, and J. Vlachopoulos, "Bubble Nucleation in Non-Pressurized Polymer Foaming Systems," 2013.

[27] K. Taki, K. Tabata, S. Kihara, and M. Ohshima, "Bubble Coalescence in Foaming Process of Polymers," *Polym. Eng. Sci.*, 46, 680-690, 2006.

[28] R. Elshereef, J. Vlachopoulos, and A. Elkamel, "Comparison and Analysis of Bubble Growth and Foam Formation Models," *Eng. Computations*, 27, 387- 408, 2010.

[29] J.G. Lee and R.W. Flumerfelt, "Nitrogen solubilities in low-density polyethylene at high temperatures and high pressures," *J. Appl. Polym. Sci.*, 58, 2213-2219, 1995.

[30] Y. Sato et al., "Solubilities and diffusion coefficients of carbon dioxide and nitrogen in polypropylene, high-density polyethylene, and polystyrene under high pressures and temperatures," *Fluid Phase Equilibr.*, 162, 261-276, 1999.

[31] S. Wu, *Polymer Interface and Adhesion*. New York: Marcel Dekker, 1982.

[32] A. Tinson, E. Takacs, and J. Vlachopoulos, "The Role of Surface Tension in Sintering for Rotational Molding," *Rotoworld*, 1, 43-47, 2005.

Chapter 5

Examining the Influence of Production Scale on the Volume Expansion Behavior of Polyethylene Foams in Rotational Foam Molding

This chapter will be submitted for publication as:

M. Emami, J. Vlachopoulos, M. R. Thompson, and E. Maziers "Examining the Influence of Production Scale on the Volume Expansion Behavior of Polyethylene Foams in Rotational Foam Molding" *Adv. Polym. Tech.* I am the sole contributor to this paper.

Abstract

In the present study, an evaluation of the effect of scale of production on rotational foam molding process with respect to rheological impact was conducted and experimental observations from microscopic, lab- and pilot-scale foam systems were used for investigation. A systematic comparison of the influence of the rheological properties of the polymer matrix on the expansion behavior of polyethylene foams indicated that the

size of the foam system does not affect the principles of the foaming process and the effects of system size of foam technique could be suppressed by tailoring the processing conditions. It was demonstrated that the observed trend of the impact of rheology in microscopic studies can be practically extended to higher scales foaming systems and it can provide guidelines for the selection of the polymer materials for customized foam applications.

5.1 Introduction

Over the past few decades much research has been undertaken in the area of polymer foam products. Substantial needs for polymer foams with improved cushioning, dielectric and thermal insulating, energy absorbing, structural performances, and other distinctive characteristics have made the plastic foaming to be one of the most promising industries. Continuous advancements of foaming technology have greatly encouraged commercial applications of plastic foams [1]. This trend has had a strong impact on the rotational molding industry, where the production of foamed polymers has become a progressively important process [2].

The production of foams by rotational molding is conditioned by the special nature of this molding process. [3,4,5,6,7,8]. To develop a foam structure in rotational molding, the polymer matrix has to form a continuous melton bed brfore decomposition of the blowing agent. Sintering and densification of polymer particles should be completed and the chemical blowing agent should be uniformly dispersed and wet by the molten polymer. By increasing the processing temperature, the blowing agent decomposes where bubble nucleation begins at initiation sites within the polymer melt that has been supersaturated with the foaming gas. The nucleated bubbles contiue to grow and the rate of bubble growth is limited by the available blowing gas, the rate of gas diffusion within the polymer matrix, and the rheological properties of the polymer melt. As the bubbles grow, adjacent bubbles eventually come into contact with each other. These bubbles tend to coalesce as the thickness and strength of the bubble wall decreases. Bubble coalescence

generally results in a coarse cellular structure and a reduction in the bubble population density, both of which could have detrimental effects on the mechanical and thermal properties of molded foams [3,6,8]. Low pressure and abrupt temperature changes during rotational foam molding makes the foam development process less controllable than other foaming applications such as extrusion or injection molding. Theoretical and experimental studies at microscopic level has shown that rheological properties play a significant role in controlling different stages of non-pressurized foaming and the resultant foam structure [3,9,10]. Foam processing window was found to be determined by melt viscosity and melt elasticity. Melt strength and strain-hardening can substantially improve bubble structure stability and polymeric matrix with higher melt strength exhibit more capacity to withstand the stretching forces during the stage of bubble growth.

Experiments and development work are normally performed at the laboratory scale due to cost concerns regarding materials and lost productivity with plant equipment. In engineering applications, experimental observations from small-scale trials are used to provide quantitative proof that a technique or processing strategy has potential to succeed at the larger manufacturing scale. Similar results are expected theoretically for identical production systems, even though the feasibility of extending small scale experimental observations to larger production scales must be verified, since theories are invariably based on assumptions that may not be completely satisfied in real systems. The aim of this research study is to conduct a systematic investigation of the influence of different scales of production on rotational foam molding technology from microscopic to lab- and pilot-scale systems to evaluate of the impact of rheology on the final properties of the foamed material and identify the effect of equipment size on expansion behavior of polymer foams.

5.2 Experimental

5.2.1 Materials

Five medium density polyethylenes (PE) supplied by Total Petrochemicals (Fluey, Belgium) were used for this study. These resins were selected to represent a broad range of physical and rheological properties. The polyethylene materials had an average particle size of 310μm and very similar distributions with the peak value of 300-500 μm according to ASTM D1921. Physical properties of the resins are listed in Table 5.1.

An exothermic chemical blowing agent (CBA), 4,4'-oxy-bis(benzenesulfonylhydrazide), was used for the foaming experiments. The decomposition behavior of the blowing agent was studied by thermogravimetric analysis (TGA, Netzsch STA409). The blowing agent showed a rapid decrease in sample weight over a very narrow range of temperatures during heating, with both onset and peak weight loss corresponding to 166.7^{o}C. Complete liberation of nitrogen and water vapor occurred at this temperature. The chemical residuals from the reaction demonstrated thermal stability with no further change in masses noted for the blowing agent from 166.7^{o}C to 200^{o}C. Particle size measurements by optical microscopy of the CBA powder revealed an average dimension of 6 μm. The foamability of this CBA with these PE resins has been well studied by microscopy in previous papers [8,9,10].

Table 5-1: Physical properties of polymer materials.

Material	MFI (g/10min)[a]	Density (g/cm^3)	Melting Point (°C)[b]
PE-1	8	0.934	122.6
PE-2	4	0.94	126.7
PE-3	3.5	0.941	125.3
PE-4	2.7	0.934	123.4
PE-5	2	0.932	121.7

[a] ASTM D1238, 230˚C/2.16 Kg

[b] By DSC measurements at a heating rate of 10°C/min.

5.2.2 Rheological Characterization

Measurements in dynamic oscillatory mode were performed on a parallel plate TA Instruments ARES rheometer (New Castle, DE, USA) under strain-controlled conditions. The plate diameters were 25 mm while the gap between the two plates was set to 1.5 mm. Disc shaped samples (1.5 mm thick) having the same diameter as the rheometer plates were produced by compression molding at 180°C for 6 min. Strain sweeps were performed to ensure the measurements were within the linear viscoelastic regime. The complex viscosity (η^*), elastic modulus (G'), viscous modulus (G'') were determined as a function of the angular frequency (ω) ranging from 0.01 to 500 rad/s. Zero-shear viscosity values for the resins were extrapolated from the dynamic viscosity data using the Cross Model. Time sweeps confirmed that the samples were sufficiently stabilized and did not degrade for the duration of a typical analysis.

The resins were also rheologically characterized for their simple extensional properties using an SER Universal Testing Platform from Xpansion Instruments [11]. The SER unit is a dual windup extensional rheometer that has been specifically designed for use as a detachable fixture on rotational rheometer host platforms. Specimens were prepared by compression molding the polymer samples to a thickness of approximately 1mm using a hydraulic press. Individual polymer specimens were then cut to a width of 6-8 mm. Measurements were conducted at 140ºC, slightly above the melting point of the polymers, to ensure that the viscosities of the samples were high enough to prevent sagging.

5.2.3 Visualization Procedure

Micro-scale foaming experiments were conducted by using a hot stage optical microscopy setup to observe and investigate the foaming process. The stage was kept at a constant temperature with the aid of a temperature controller. The temperature of the polymer melt was constantly monitored and recorded by a K-type thermocouple. Dry-blended mixtures of the polyethylene materials and CBA were prepared for the

experiments. A sample cup holder, made of glass (D = 2.5cm. H = 1 cm), was loaded with a predetermined amount of the blend and placed in the center of the hot stage. In order to obtain as uniform powder particle size as possible, the powders were sieved and the fraction with diameter between 300 and 500 microns was retained. The initial thickness of the powder bed inside the cup was approximately 2 mm. Foaming experiments were performed isothermally at 190°C and under atmospheric pressure to evaluate the density variations of the foamed samples as a function of heating time and to visualize the cellular structure throughout the foaming process. The maximum duration of the experiments was 30 min. After passing certain amounts of time, the cup holder containing the melt was removed and quenched into cold water to freeze the structure of the foamed sample. For density measurements, segments of dimensions 1cm ×1cm were cut around the center of the solidified samples to eliminate end effects. The foaming experiments were repeated three times to determine accuracy and reproducibility of the experimental results and offset the effect of any possible inconsistency in the sample preparation. The error in the measurements ranged from 0.2% to 5.4%.

5.2.4 Rotational Foam Molding Procedure

Rotational molding experiments of foams with a monolayer wall structure were performed in a laboratory scale uniaxial rotomolding machine. The machine consisted of an electrically heated oven surrounding a square-shaped Teflon-coated steel mold. The mold was approximately 9.5cm × 9.5cm × 10cm cube shaped, and the front of the mold was covered with Pyrex glass to allow visual observation of the process. A shot weight of l00g was used in each experiment which was known to produce a molding of 3mm wall thickness when no blowing agent was added to the polyethylene. The mold rotation speed was set at 4 RPM. A thermocouple inserted into the center of the mold through a rotating hollow shaft was used to measure and record the in-mold temperature changes during processing.

Rotational molding experiments of skin-foam runs were conducted using a two shot molding procedure in a pilot-scale Caccia AR 1400 shuttle type machine (Varese, Italy),

with an oven temperature of 300°C. Moldings were produced in a 30cm × 30cm × 30cm steel cube mold. Varied amount of shot weights with a mold rotation ratio of 4:1 were used in each trial. A Datapaq temperature-measuring device (Cambridge, UK) was used to record inside mold air temperature and oven temperature.

5.2.5 Foam Characterization

The foam samples were analyzed for foam density, thickness and volume expansion ratio. The density of the foamed samples was determined using a Mirage MD-200S electronic densimeter. Specimens with dimensions of 1cm × 1cm were cut from the center of the molded parts. This instrument operates using the Archimedes principle. The determination of the density value is based on the density of water at 4°C (1g/cm^3). The measurements were repeated three times in order to determine their reproducibility and the average values have been reported. The wall thickness of the foamed rotomolded parts was measured by using a Mitutoyo horseshoe-shaped digital micrometer. Mean wall thickness was determined by taking measurements at twenty positions on the same side of the molded wall of each sample.

The volume expansion ratio (VER) of the foams was computed as the ratio between the expanded volume of the foam (V_{foam}) and the initial volume of the solid unfoamed plastic material (V_{polym}), also it can be calculated as the ratio of the bulk density of pure material (ρ_{polym}) to the bulk density of the foam sample (ρ_{foam}) as follows:

$$VER = \frac{V_{foam}}{V_{polym}} \approx \frac{\rho_{polym}}{\rho_{foam}} \qquad \text{Eq. 5-1}$$

5.3 Results and Discussions

5.3.1 Rheological Characterization

Figure 5.1 presents the zero-shear viscosities of the tested materials at 190°C and 140°C, as well as the fitting parameters of the Cross model. With increasing MFI, the polymer melt showed higher values of zero-shear viscosity and increased relaxation time, with PE-1 exhibiting considerably lower viscosity than the rest of the resins. Figures 5.2 and 5.3 summarize the complex viscosity (η^*) and elastic modulus (G') of the materials as a function of frequency. The same trend of dependency on MFI for zero-shear viscosity was observed with complex viscosity. The onset of shear thinning behavior was observed to be influenced by MFI of the resin and it moved to smaller values of frequency by increasing MFI. The viscosity curve of PE-1 showed a transition to non-Newtonian flow behavior at the frequency of 0.2 s^{-1} and exhibited the lowest degree of shear thinning at higher frequencies. The degree of shear thinning was most pronounced in PE-5 with a 94% reduction in shear viscosity over the five decades of frequency investigated. The difference in the values of the shear viscosity of samples was more significant at lower frequencies and it decreased at higher frequencies. Dynamic modulus exhibited a general trend of a monotonic growth with frequency and showed similar sensitivity to the changes of MFI as complex viscosity. PE-5 with the highest MFI was observed to possess the highest values of storage modulus over the range of tested frequency. Further details on shear rheological characterizations of polymer materials can be found elsewhere [9,10].

The extensional stress growth coefficient measurements at 140°C are shown in Figure 5.4 which provides a characterization of the extensional melt flow behavior of the polymer materials. Due to low zero-shear viscosity and sagging issues, the measurements could not be performed with PE-1. PE-2 exhibited slight strain-hardening behavior, evidenced by the deviation from the linear viscoelastic stress growth behavior. At lower elongation rates, the stress growth coefficient curve superposed on the linear viscoelastic shear curve. PE-3, PE-4 and PE-5 all exhibited strain-hardening character at all elongation rates

studied. However, PE-3 appeared to possess the most significant strain-hardening character for all elongation rates. This behavior became more pronounced as the strain rate was increased. It was noted that the onset of strain-hardening at a given rate occurred at approximately the same strain rate for all tested resins, independent of the molecular weight of the polymer materials. More detailed descriptions of the extensional rheological characterization of polyethylene materials have been discussed in our previous work [10].

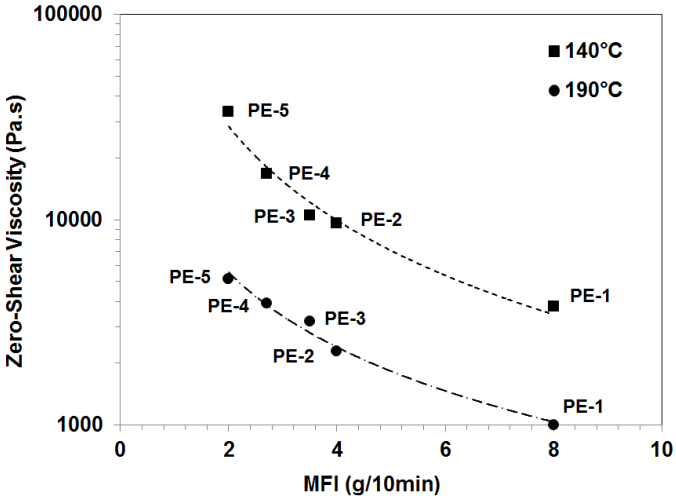

140°C	PE-1	PE-2	PE-3	PE-4	PE-5
Time Constant (λ)	0.063	0.853	0.913	2.817	34.793
Power Law Index (n)	0.63	0.65	0.64	0.66	0.70

190°C	PE-1	PE-2	PE-3	PE-4	PE-5
Time Constant (λ)	0.015	0.089	0.153	0.179	0.358
Power Law Index (n)	0.53	0.56	0.56	0.56	0.57

Figure 5-1: Zero-shear viscosity of polymer materials (Cross Model).

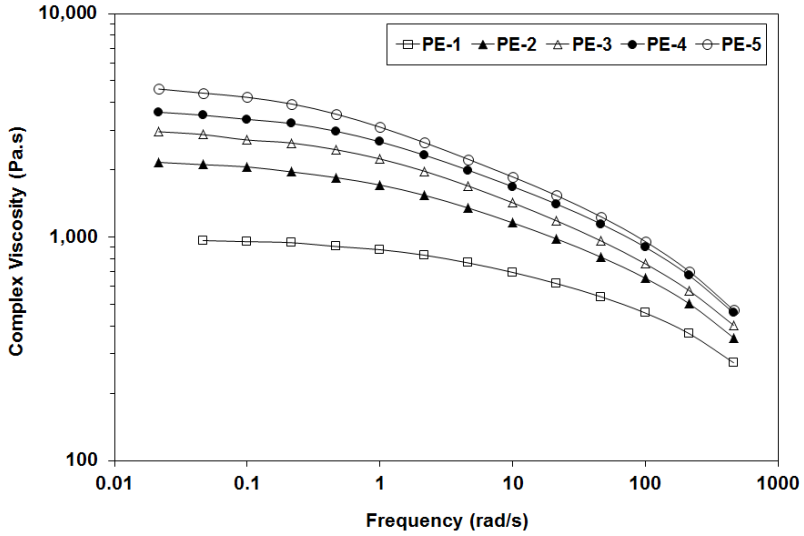

Figure 5-2: Complex viscosity of polymer materials as a function of frequency at 190°C.

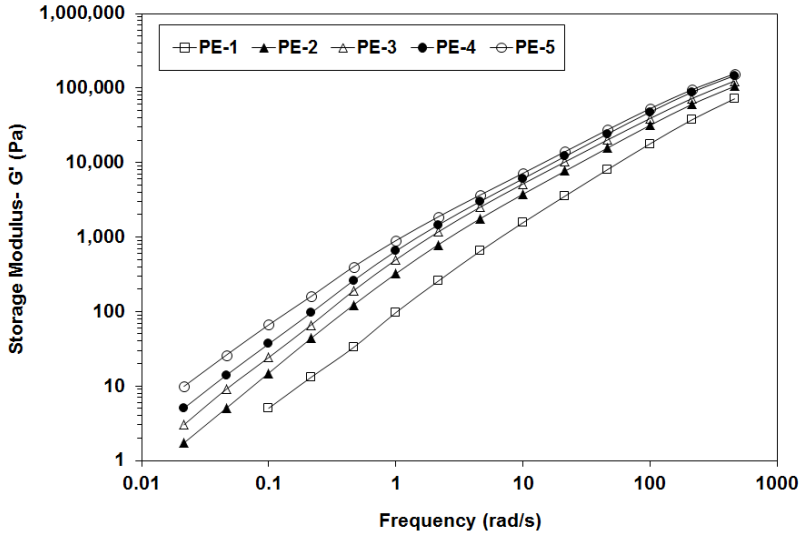

Figure 5-3: Storage modulus of polymer materials as a function of frequency at 190°C.

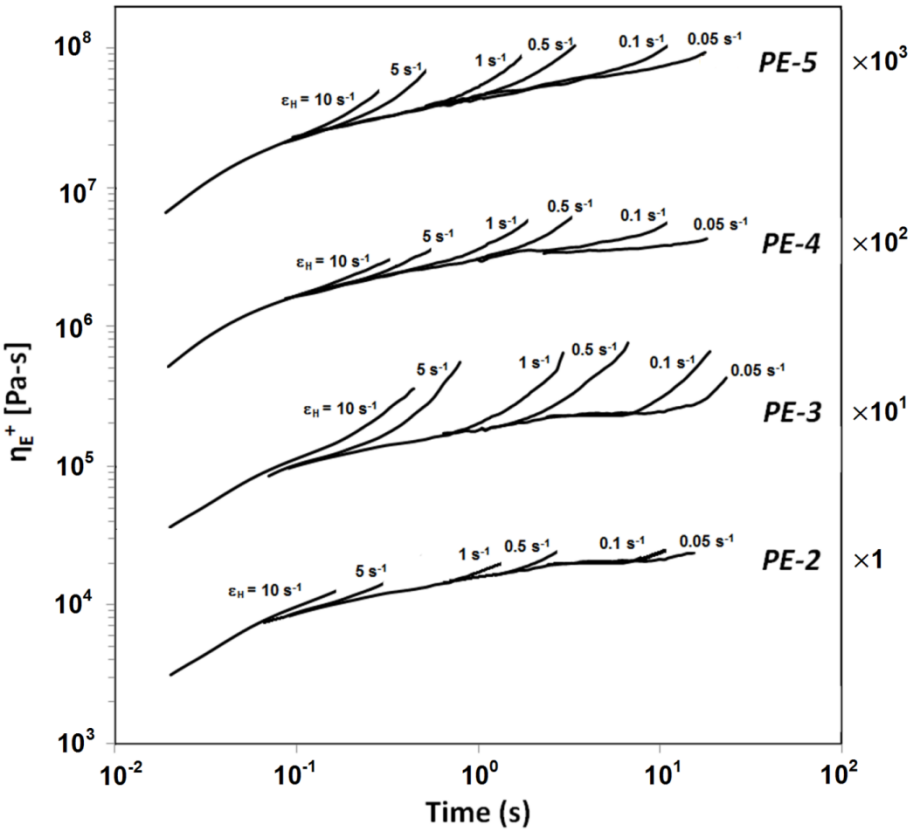

Figure 5-4: Extensional stress growth coefficient rate at various strain rates at 140ºC.

5.3.2 Foam Expansion Analysis

In order to analyze the influence of scale on the foaming process, volume expansion ratio has been chosen as the target variable to describe the processing-to-structure relationships to compare the foam expansion behavior of resins at different scales of production. Using volume expansion ratio as a dimensionless value will exclude the effect of geometrical dissimilarity of molds in terms of shape and dimensions, as well as different material amount used in the study. Except for cycle duration and content of the blowing agent, other processing variables affecting the foaming system were kept identical to facilitate the comparison of different systems. In all cases, polymer matrix experienced similar maximum temperature during the foaming process. The effect of scale on pressure and shear were considered to be negligible.

Visualization Studies- Microscopic Experiments

Figure 5.5 presents volume expansion ratios obtained using micro-scale set up using 0.5% blowing agent with respect to cycle time. Generally, the resins with lower melt viscosity/elasticity resulted in greater volume expansion during all stages of the foaming process. The experimental results showed an increasing trend up to t= 5 min, at which time a reduction in the volume expansion ratio was observed. Beyond t=10 min, the foam essentially stopped expanding and exhibited a plateau behavior reflecting foam stability, a steady state condition between the competing mechanisms involved in the foaming process. The declining trend depicts through-plane shrinkage of the developing foam, similar to the reported trend in our previous study [8]. An exception to this trend was found with PE-3 which did not show the shrinkage behavior and resulted in the greatest foam expansion. We have shown in our detailed studies that these observations can be explained by the differences in the rheology of the resins [9,10]. The increased melt strength and higher degree of strain-hardening of PE-3 improved bubble structure stability by controlling the bubble growth mechanism and suppressing bubble coalescence/dissolution and effectively expanded the foam processing window.

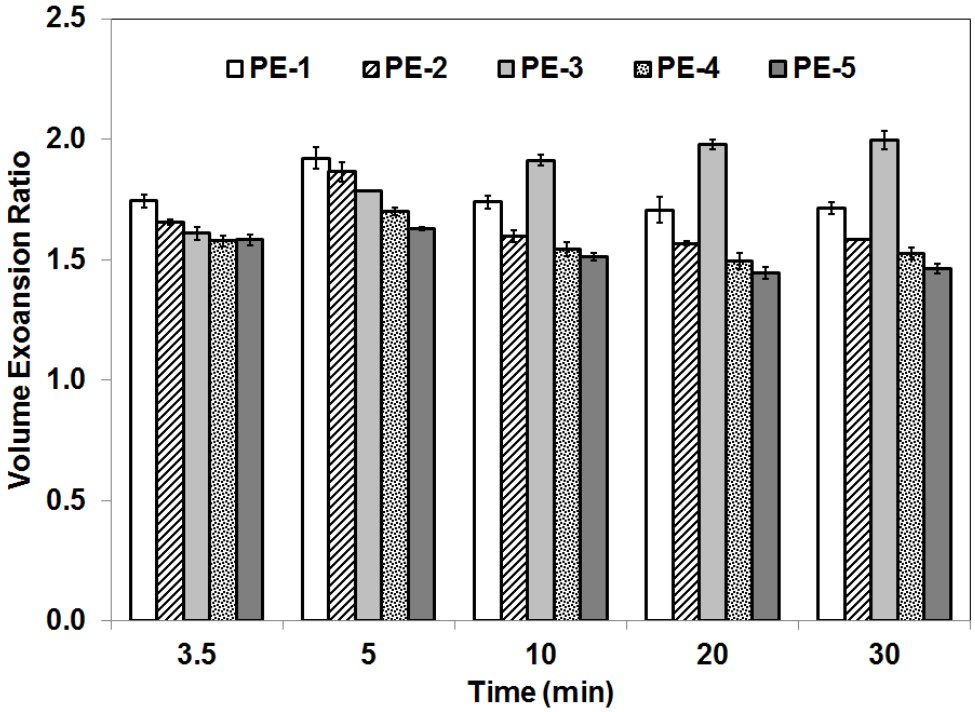

Figure 5-5: Volume expansion ratios of microscopic experiments containing 0.5% CBA.

Exposing the polymer matrix to 30 min of heating and foaming condition can be considered as extreme processing circumstances in actual rotational foam molding process and according to the visualization experiments, processing time longer than 5 min highlights the effect of melt strength in the foaming performance.

Monolayer Foam Moldings- Lab-scale Experiments

In order to validate the foaming performance of tested polymer materials under actual processing conditions and investigate the effect of their rheological properties at higher production scales, monolayer foam moldings experiments were performed using a lab-scale rotational molding machine. The foaming experiments were conducted by using 0.5, 1.5 and 2.5% of the chemical blowing agent. Comparisons of the inside air temperature profiles of rotomolding cycles are illustrated in Figure 5.6. The heating cycle was interrupted when the inside air temperature in the mold reached 180°C.

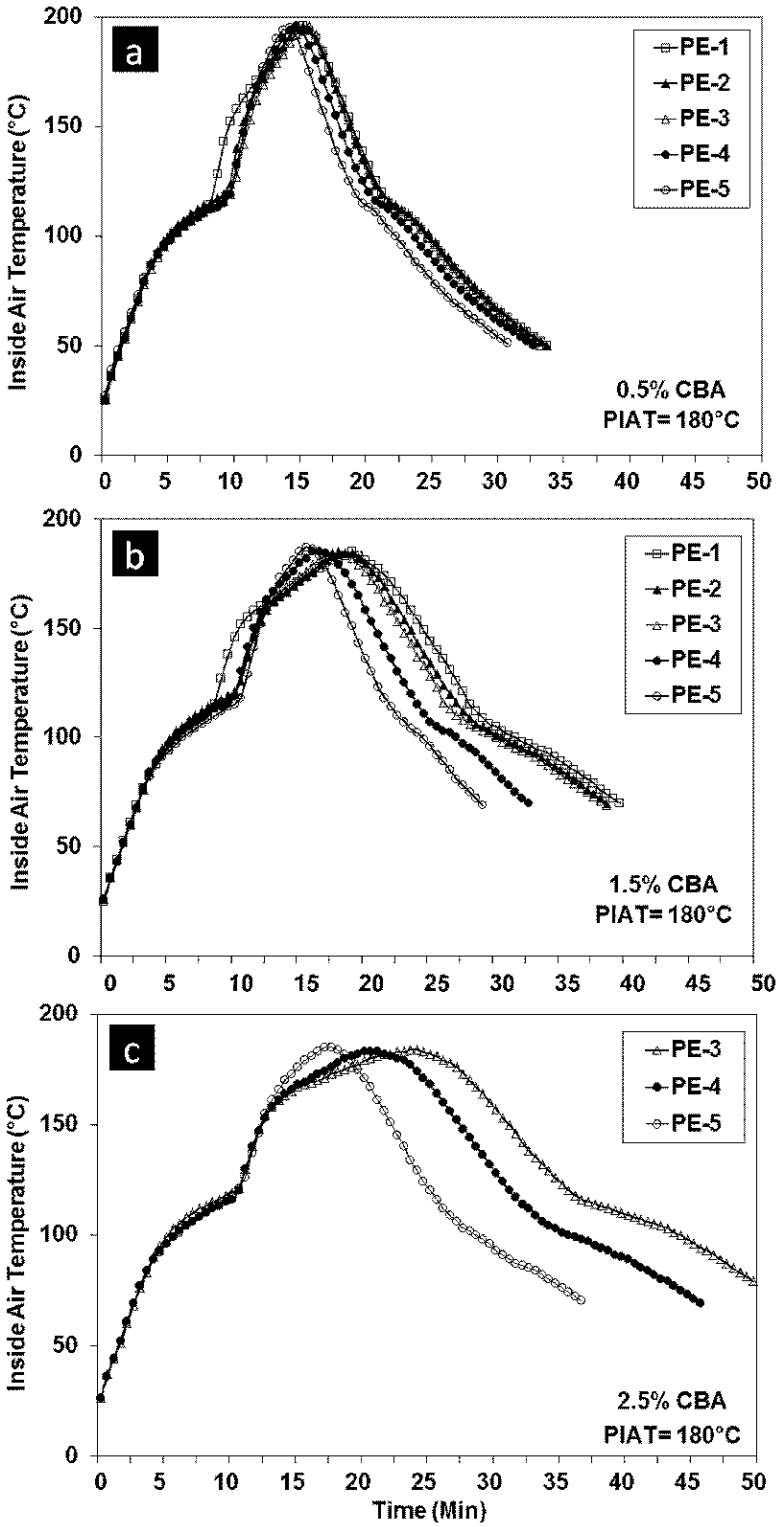

Figure 5-6: Temperature profiles of lab-scale rotational foam molding experiments (monolayer), PIAT = 180°C, a) PE+0.5% CBA, b) PE+1.5% CBA, c) PE+0.5% CBA.

The temperature profiles reflect different melting and foaming behavior of the polymer materials. For all contents of CBA, polymer materials followed similar trends during the stages of the foaming process. However, by increasing zero-shear viscosity significant reduction in the processing time was observed and the rate of foaming and densification was considerably increased. Shorter processing time was required due to the different thermal insulating properties of the foams; resins with lower zero-shear viscosity produced higher thickness foams which provided more thermal insulation to the heat flow during heating and cooling cycles. Because of thermal insulating properties of the foam, the inside air temperature overshot the removal temperature by up to 10°C. Polymer materials with high zero-shear viscosity and melt elasticity produced foams with bumpy surfaces. It was observed that powder particles tend to keep their identities and similar observations have been made for all contents of the blowing agent. With addition of 2.5% CBA, PE-1 and PE-2 showed poor foaming performances and produced foams with very large voids and severe deformations (Figure 5.7). This was attributed to the low zero-shear viscosity and low melt strength of PE-1 and PE-2 which could not provide enough resistance during the bubble growth for the extension forces caused by 2.5% of the blowing agent.

Figure 5-7: PE-1 + 2.5% CBA- Monolayer foam with extensive structural failure.

Volume expansion ratios of monolayer foams subjected to different contents of the blowing agent are presented in Figure 5.8. Similar to microscopic studies, there is a general downward trend in foam expansion by increasing the melt viscosity/elasticity. The highest volume expansion attained using PE-1 with the lowest melt viscosity/elasticity, while higher melt elasticity of PE-4 and PE-5 caused considerable hindrance to foam expansion and resulted in rough surfaces. PE-3 foams followed the general trend and did not show a different foam expansion behavior. This can be explained by the shorter heating cycle in the lab-scale trials compared to the microscopic experiments. The reduced heating time terminated the expansion process at an earlier point in the process and compared to the microscopic results presented in Figure 5.5, the observations in lab-scale experiments matches the trend noted in visualization experiments for t <10 min.

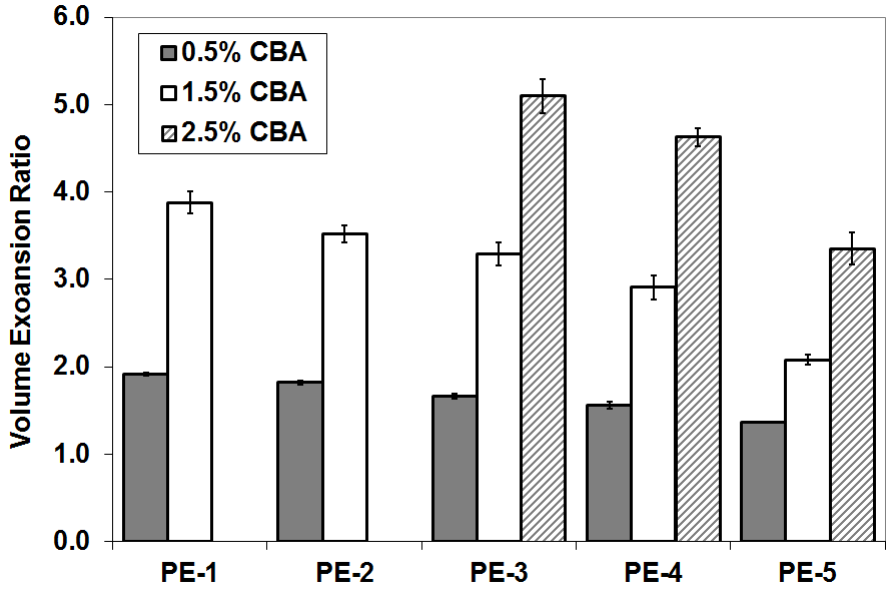

Figure 5-8: Volume expansion ratios of monolayer foam moldings containing different contents of CBA, lab-scale experiments.

The same trend of dependency of the foam expansion on rheology was recognized for all contents of the blowing agent. By increasing the blowing agent from 0.5% to 1.5%, foams experienced a significant volume expansion of approximately 55%. Further

increase of the blowing agent to 2.5% resulted in approximately 65% more foam expansion compared to the 0.5% blowing agent.

Skin-Foam Molding- Pilot-scale Experiments

The foaming behaviors of polyethylene materials were also examined at pilot manufacturing scales and under industrial operating conditions. Skin-foam moldings were conducted using 2.5% and 3.5% of the blowing agent and in a pilot scale, biaxial rotational molding machine. The inside air temperature profiles of rotomolding cycles are presented in Figure 5.9. Similar observations to monolayer experiments in terms of dependency of the processing time to the rheology were made in skin-foam molding trials. In monolayer experiments, addition of 2.5% of blowing agent led to poor foaming performance. However, because of the higher surface area for heating/cooling in the biaxial machine, it was possible to use higher contents of the blowing agent successfully. Due to the high melt elasticity of PE-4 and PE-5 and unacceptable volume expansion, these two resins were eliminated from the pilot-scale examinations.

The first set of experiments was performed to study the effect of cycle time on the molded foams, using different amount of polymer materials for the foam layer (900 g and 1800 g shot weight) and 2.5% blowing agent, as shown in Figure 5.9a and 5.9b. Shot weights of 900 g and 1800 g produce unfoamed parts with a wall thickness of 3 mm and 6.5 mm, respectively. Using 900 g shot weight, all moldings exhibited fair foaming performances and produced foams with uniform and smooth surface finish. Figure 5.10 presents the volume expansion ratio measurements of the molded foams. Similar to observations in microscopic and lab-scale experiments, the greatest foam expansion was obtained using PE-1, followed by PE-2 and PE-3. In the experiments using 1800 g shot weight, PE-1 produced foam with severe deformations and extensive structural failure. The inner surface of the molded foam was extremely bumpy and exhibited very large voids in the skin-foam boundary. Low melt strength of PE-1 was not able to stabilize the growth of large bubbles. PE-2 and PE-3 performed well; however, early evidence of

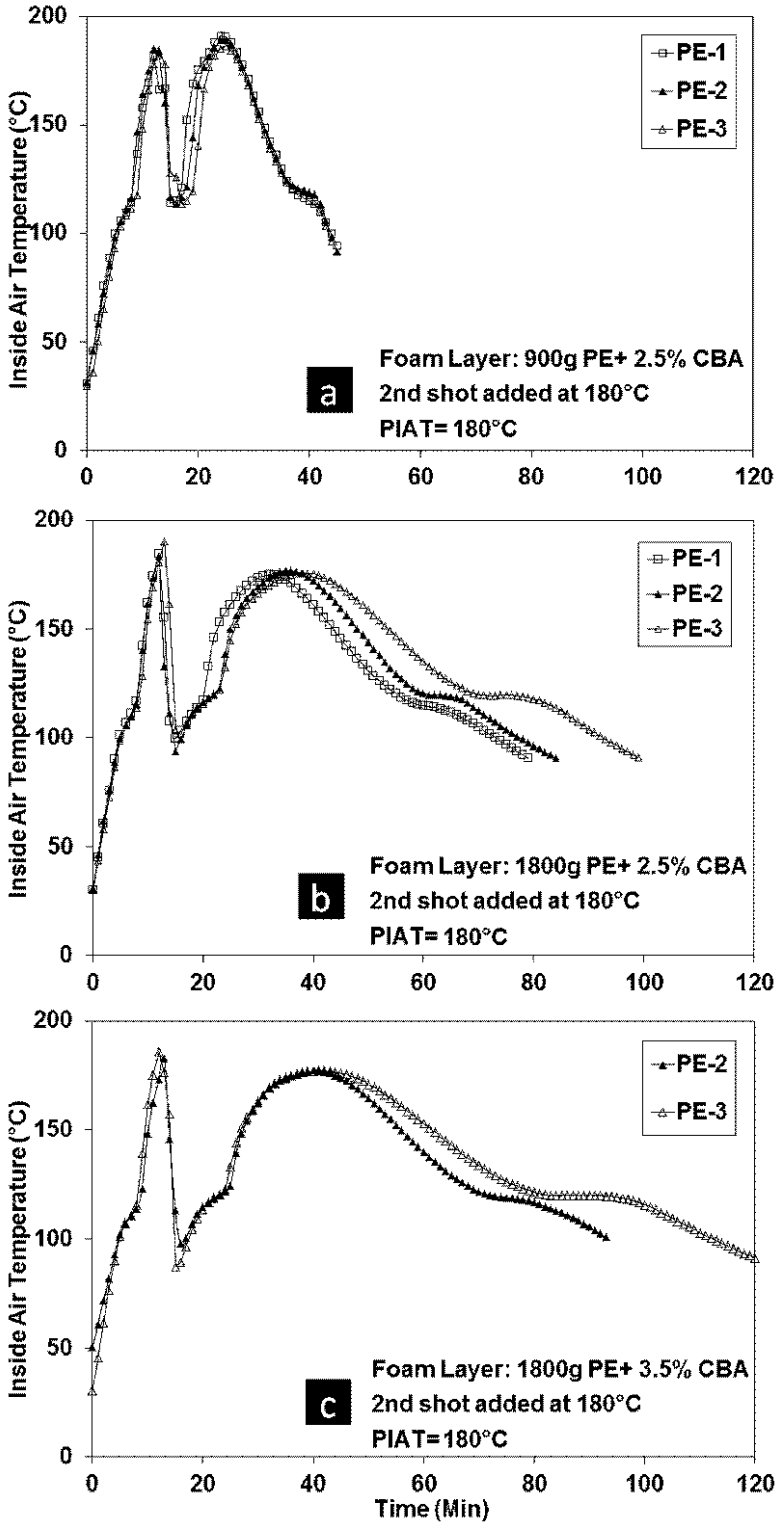

Figure 5-9: Temperature profiles of pilot-scale rotational foam molding experiments (skin-foam), a) 900g PE+2.5% CBA, b) 1800g PE+2.5% CBA, c) 1800g PE+3.5% CBA.

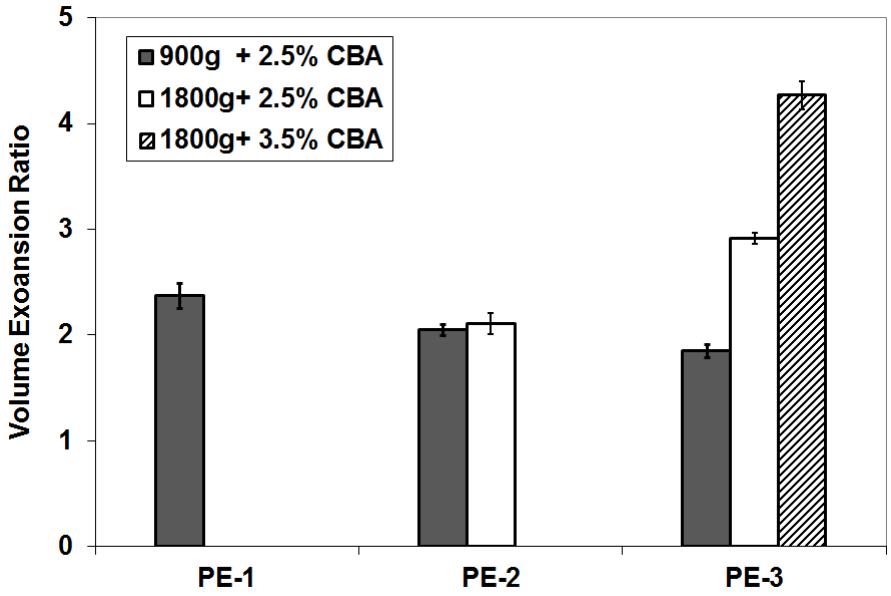

Figure 5-10: Volume expansion ratios of the skin-foam moldings containing different contents of CBA, pilot-scale experiments

separation at the interface of the foam layer and skin layer for PE-2 was noted. Examples of the cross-sectional and inner surface are shown in Figure 5.11. PE-3 showed a much higher volume expansion than PE-2, 2.1 and 2.9 folds, respectively (Figure 5.10). The

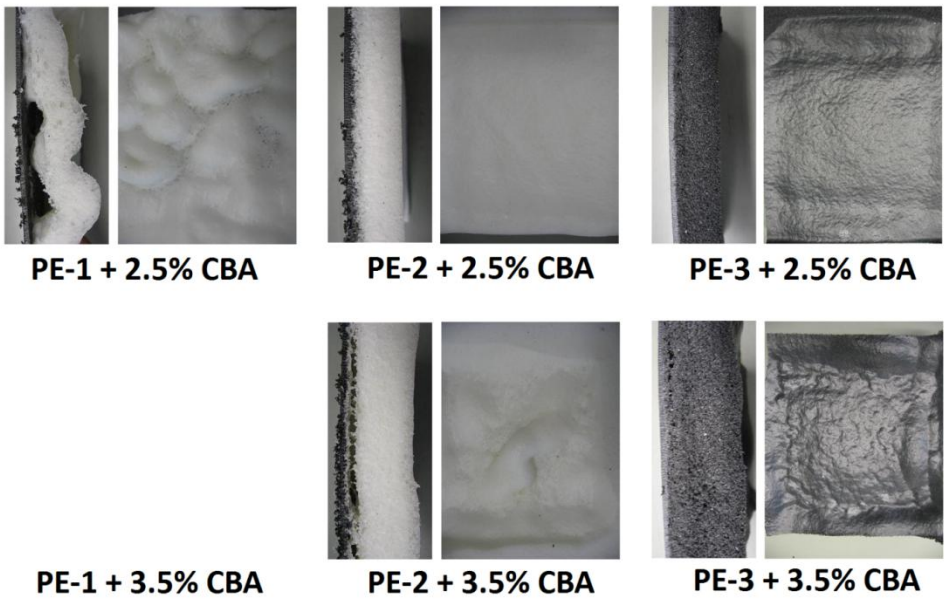

Figure 5-11: Cross-sectional and inner surface images of the skin-foam moldings, pilot-scale experiments.

higher foam expansion of PE-3 well confirmed the behavior observed during the microscopic studies. By passing the point in the process when it simulates the applied conditions in the visualization experiments for t >10 min, the different foaming performance of PE-3 was prominent. The superior behavior of PE-3 was further supported by the next set of skin-foam trials. .

The second set of experiments examined the use of higher content of blowing agent to reduce the density of the foam to a possible minimum value to exemplify extreme processing conditions. Foam moldings were performed using 1800 g shot weight of polymer materials with 3.5% CBA. PE-1 was eliminated from evaluation due to the poor performance. PE-2 resulted in a very deformed cellular structure with long cracks along the interface of the foam layer and skin (Figure 5.11). PE-3 exhibited excellent foaming performance with almost 4.3 folds volume expansion. The pilot-scale experiments provided excellent support for the findings of the microscopic studies. PE-3 showed a promising foaming performance which highlights the significant contribution of strain hardening in rotational foam molding. Considering the comparable rheology of PE-2, PE-3 and PE-4, it was shown than the higher melt strength of PE-3 effectively broadens the processing window by establishing an enhanced stability in developing cellular structure. Figure 5.12 qualitatively illustrates the conclusion.

5.4 Conclusions

An experimental study was carried out to investigate the effect of equipment size on the rotational foam molding process from experimental observations on microscopic level to lab and pilot-scale productions and evaluate the impact of rheology on the foam expansion behavior. The principles of the foaming process were not affected by the scale of the foam system. Experimental observations on the effect of rheological properties of polymer matrix in microscopic foaming studies were shown to be reasonably extended to the higher levels of manufacturing. The foaming processing window was found to be

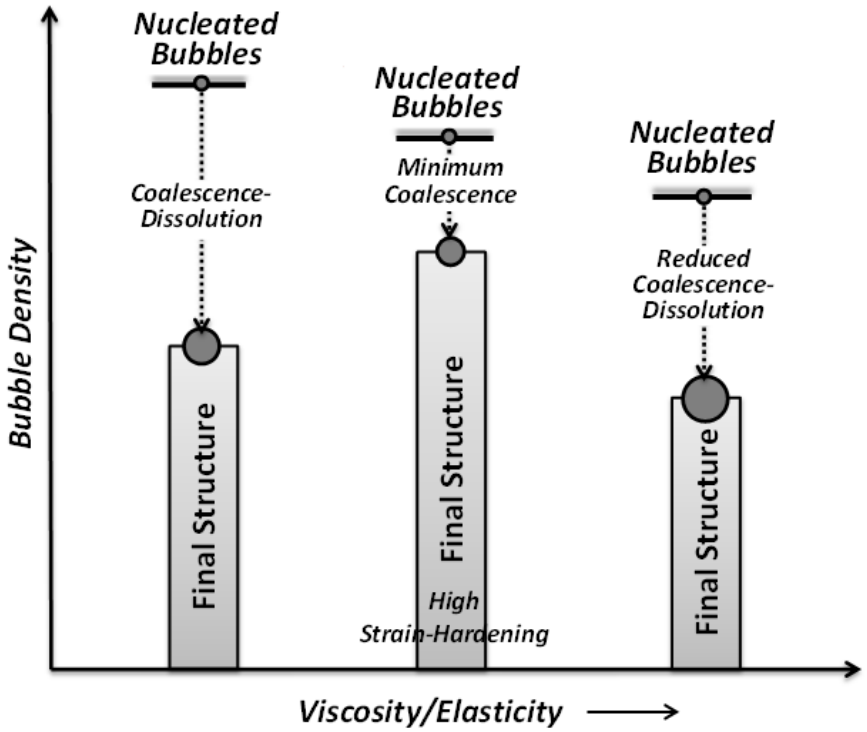

Figure 5-12: Summary of effect of rheology on the foam bubble structure. Controlled bubble growth and reduced coalescence/dissolution lead to higher bubble density and smaller bubble size.

determined by the shear viscosity and elasticity of the resin in all equipment sizes. Strain-hardening was observed to significantly affect the foaming performance. The experimental results at lab and pilot-scale confirmed that increased melt strength and higher degree of strain-hardening improved bubble structure stability and resulted in greater foam expansion and effectively expanded the foam processing window under extreme processing conditions.

5.5 References

[1] J.L. Throne, *Thermoplastic Foams*. Hinckley OH: Sherwood Publishers, 1996.

[2] R.J. Crawford and J.L. Throne, *Rotational Molding Technology*. Norwich, NewYork: William Andrew Publishing, 2002.

[3] G. Liu, C. B. Park, and J. A. Lefas, "Production of Low-Density LLDPE Foams in Rotational Molding," *Polym. Eng. Sci.*, 38, 1997- 2009, 1998.

[4] E. Archer, E. Harkin-Jones, and M. P. Kearns, "Processing Characteristics and

Mechanical Properties of Metallocene Catalyzed Linear Low-Density Polyethylene Foams for Rotational Molding," *Polym. Eng. Sci.*, 44, 638- 647, 2004.

[5] D. Xu, R. Pop-Iliev, C.B. Park, and R.G. Fenton, "Fundamental Study of CBA-blown Bubble Growth and Collapse Under Atmospheric Pressure," *J. Cell. Plast.*, 41, 519-538, 2005.

[6] R. Pop-Iliev, N. Dong, D. Xu, and C.B. Park, "Visualization of the Foaming Mechanism of Polyethylene Blown by Chemical Blowing Agents Under Ambient Pressure," *Adv. Polym. Tech.*, 26, 213-222, 2007.

[7] S.N. Leung, A. Wong, Q. Guo, C.B. Park, and J.H. Zong, "Change in the Critical Nucleation Radius and Its Impact on Cell Stability During Polymeric Foaming Processes," *Chem. Eng. Sci.*, 64, 4899-4907, 2009.

[8] M. Emami, E. Takacs, M. R. Thompson, J. Vlachopoulos, and Eric Maziers, "Visual Studies of Model Foam Development for Rotational Molding Processes," *Advances in Polymer Technology*, 2012.

[9] M. Emami, M.R. Thompson, and J. Vlachopoulos, "Bubble Nucleation in Non-Pressurized Polymer Foaming Systems," *Polym. Eng. Sci.*, 2013.

[10] M. Emami, M.R. Thompson, and J. Vlachopoulos, "Experimental and Numerical Studies on Bubble Dynamics in Non-Pressurized Foaming Systems," *Polym. Eng. Sci.*, 2013.

[11] M. L. Sentmanat, "Miniature Universal Testing Platform: From Extensional Melt Rheology to Solid-State Deformation Behavior," *Rheol. Acta*, 43, 657- 669, 2004.

Chapter 6

Conclusions and Recommendations

6.1 Conclusions

The work presented in this thesis contributes to the fundamental mechanisms involved in non-pressurized foaming system such as rotational foam molding and advances our understanding of the role rheology on different stages of the foaming process as well as the resultant foam structure. Polymer materials and experimental techniques have been chosen so that the physical processes of interest become dominant and can be investigated quantitatively. Among the major accomplishments of this thesis are:

- Experimental evidence through visualization studies revealed that the nucleation mechanism in non-pressurized foaming process is comprised of two different stages: primary and secondary nucleation. During the primary nucleation stage, the interstitial regions of the sintered plastic powder as well as the agglomerated blowing agent particles acted as nucleation sites for the blowing gas. Subsequently, secondary nucleation formed a new generation of bubbles within the polymer melt. Morphological analysis of the

developing cellular structure distinctly indicated that primary nucleation was the controlling stage in determining the final cellular structure.

- The significance of the effect of rheology of the polymer matrix on the rate of nucleation in non-pressurized foaming systems was investigated experimentally and theoretically. Experimental observations at microscopic levels revealed that higher viscosity impeded the number of bubbles generated in the foaming system and allowed a lower number of nuclei to grow larger than the critical nucleus. The theoretical predictions of a modified model of the classical nucleation theory (Kagan Model) were also simulated the experimentally observed trend of the impact of rheology for purely viscous systems. The results of this study suggest that the bubble nucleation density computation for polymer foaming systems have to explicitly account for the importance of the viscosity forces on the rate of nucleation to be of real predictive value.

- A detailed study of the role of the rheology on the bubble growth mechanism clearly demonstrated that the developing foam structure and final foam properties are significantly influenced by the rheological properties of the polymer material. Morphological analysis was used to determine the processing window in terms of shear viscosity, elastic modulus, melt strength and strain-hardening, intended for the production of foams with greater foam expansion, increased bubble density and reduced bubble size. It was shown that the operating window is bounded by the melt viscosity/elasticity. Lower shear viscosity and elasticity accelerated the sintering rate and resulted in a higher total number of the survived bubbles to the end of the foaming process. However, very low shear viscosity was not suitable for the foaming process because of the associated reduction in melt strength. The experimental results indicated that increased melt strength and higher degree of strain-hardening can effectively expand the processing window and improve the foaming performance by controlling the bubble growth and retarding the bubble coalescence mechanism.

- Using the established mathematical model for the bubble growth phenomena, a series of sensitivity analyses were performed to investigate the effect of various thermophysical,

rheological, processing, and simulation parameters on the bubble growth behavior. It was shown that initial bubble size and heating rate are two of the most important factors that govern bubble growth dynamics in non-pressurized foaming process. Although the expansion behaviors of bubbles also depends on blowing gas diffusivity and solubility and viscosity of the polymer matrix, the effects are less prominent than those of initial bubble size and heating rate under the processing range being considered.

- A systematic comparison of the influence of the rheological properties of the polymer matrix on the expansion behavior of polyethylene foams indicated that the size of the foam system does not affect the principles of the foaming process and the observed trend of the impact of rheology in microscopic studies can be practically extended to higher scales foaming systems. The foaming processing window was found to be determined by the shear viscosity and elasticity of the resin in all equipment sizes. The experimental results at lab- and pilot-scale confirmed that increased melt strength and higher degree of strain-hardening resulted in greater foam expansion and effectively expanded the foam processing window under extreme processing conditions.

6.2 Recommendations for Future Work

The results from this research could be extended in the future into the following areas:

- Developing of a foaming visualization system utilizing a high resolution microscopy such as transmission electron microscopy (TEM). One limiting factor in analyzing the bubble nucleation phenomena regarding the effects of processing parameters, material parameters and processing strategies is the difficulty in capturing the nucleation event. Due to the small size scale and extremely high speed involved in bubble nucleation, it is very challenging to elucidate the process. Arresting the nucleation at early stages could significantly advance the scientific understanding in this research field.

- Studying the pre-existing nucleating sites and gas cavities in the polymer/gas mixture. Developing of measuring techniques for evaluating the sizes and quantities of the

nucleating sites and investigating of the effects of processing parameters (e.g. processing temperature and heating rate, blowing agent content) and material properties would also be beneficial to understand the bubble nucleation phenomena and the end results of these investigations would increase the flexibility to control and tailor the cellular structures and final foam properties.

- Incorporating the nonlinear viscoelastic characteristics and stain-hardening behavior of the polymer matrix in the nucleation and bubble growth model. Such models would provide more insights on the significance of different rheological aspects of polymer matrix in the foaming process and the results could be utilized to develop guidelines for the selection of the polymer materials for customized foam applications.

- Studying the impact of crystallinity and morphology of the polymer matrix on the foam processing and the structure of the resulting foams. The mechanism and kinetics of crystallization of semi-crystalline polymers are influenced by many parameters such as the rate of cooling and the presence of impurities. By tailor-making the crystalline structure of polymer through processing conditions, or using some additives, it would be possible to control the structure of foamed semi-crystalline polymers.

Appendix

7.1 Nucleation Model

Experimental observations during the nucleation process showed that rheology has an impact on the mechanism of bubble generation in non-pressurized foaming systems. In order to evaluate the influence that viscous forces were having on the rate of nucleation, a modified form of the classical nucleation theory proposed by Kagan [1] was employed.

According to Gibbs [2] the critical nucleus would correspond to an aggregate of the new phase of a size for which the energy of formation is a maximum. An increase in the size of such an aggregate or nucleus will lead to its further growth, while a decrease in the size of the nucleus will lead to its annihilation. Zeldovich [3], in his work on phase transitions, described the evolution of spontaneously arising bubbles from a metastable liquid, considering explicitly both thermodynamically determined transitions and random effects. Kagan [1] extended Zeldovich's theory of bubble nucleation in simple liquids to account for viscosity and inertial constraints on the rate of bubble nucleation in simple liquids.

Kagan cast the equation of growth for a nucleating bubble in the following dimensionless form:

$$\omega' z^3 + \frac{8}{9}\,\omega\left(1 + \frac{27\omega'}{64\,\omega}\right) z^2 + \frac{2}{3}\left(\omega + \frac{3-b}{b}\right) z - \frac{1}{2} = 0 \qquad \text{Eq. 7-1}$$

The dimensionless quantities in Eq. 7-1 are defined as

$$z = \left(\frac{d\dot{r}}{dr}\right)_{r_c} \frac{r_c}{\beta\,\nu_t} \qquad \text{Eq. 7-2}$$

$$\omega = \frac{3}{8}\frac{\beta \nu_t \gamma \eta}{\sigma} \qquad \text{Eq. 7-3}$$

$$\omega' = \frac{2}{3}\frac{\beta^2 {\nu_t}^2 \rho r_c}{\sigma} \qquad \text{Eq. 7-4}$$

$$b = \frac{2\sigma}{r_c\,p_c} \qquad \text{Eq. 7-5}$$

$$\upsilon_t = \sqrt{\frac{8\,kT}{\pi m}} \qquad \text{Eq. 7-6}$$

where r is the radius of the nucleating bubble, r_c is the radius of the critical nucleus, β is the condensation coefficient and for these calculations its value was taken to be 1 [4], ρ is the density of the liquid, η is the viscosity of the liquid, γ is a numerical coefficient that has a value of approximately 4, σ is the interfacial tension, υ_t denotes the average thermal velocity of the gas molecules impinging on the nucleus, *k* is the Boltzmann constant, *T* is the temperature, and *m* is the mass of a gas molecule. The dot over a quantity denotes its derivative with respect to time.

In the majority of situations under which Eq. 7-1 has been applied, inertia is not important [5]. The criterion justifying neglect of the inertia terms has been reported as $\frac{\omega'}{\omega^2} \ll 1$ in the literature [1]. For the case of very viscose liquids when their viscosity is the limiting parameter on the rate of growth and collapse of the bubble (where $\omega \gg 1$ and

$3/b\omega \ll 1$), a particular solution of Eq. 7-1 was obtained by Kagan, and the expression for the nucleation rate, J, for the viscosity-limiting case can be expressed as

$$J \approx 4N_0 \frac{\sigma}{\gamma\eta}\sqrt{\frac{\sigma}{kT}}\frac{1}{b}\, e^{-1/3K} \qquad \text{Eq. 7-7}$$

where

$$K = \frac{4\pi r_c^2 \sigma}{kT} \qquad \text{Eq. 7-8}$$

and N_0 is the Avogadro number.

The criteria for vindication of neglecting the inertia terms and justification of the viscosity-limiting case for our foaming system were evaluated. The nucleation temperature was considered 166°C based on thermal analysis of the samples and the Arrhenius equation was used to describe the temperature dependence of the viscosity of the polymer melts, using a reference temperature of 140°C and activation energy of 20,000 J/mol. The surface tension value for polymer melts were obtained from literature (0.0255 N/m) [6,7]. The melt density of the molten polymer was measured according to ASTM D1238 by using a melt flow indexer, with the average value of 733 kg/m^3. The mass of one molecule of nitrogen was calculated to be 4.65173×10^{-23} g. The model prediction by using a nucleus size of 16 Å provided good agreement with the experimental data and the pressure inside the critical nucleus was calculated by

$$P_c = P_{atm} + \frac{2\,\sigma}{r_c} \qquad \text{Eq. 7-9}$$

The values obtained for b, υ_t, ω and ω' were 0.9967, 576.02, 2.526×108 and 10.09, respectively, which satisfy the criteria at which Eq. 7-7 can be applied for viscous liquids. The comparison of the theoretical predictions obtained from the model with the experimentally observed trend for the impact of viscosity on the nucleation rate is discussed in Chapter 3.

7.2 Bubble Growth Model for a Purely Viscous Fluid

In Chapter 4, a bubble growth model and simulation scheme was developed to describe the bubble growth phenomena that occurred in CBA-based, non-pressurized foaming systems. The theoretical framework of the model will be discussed in this section.

Simulating and modeling the bubble-growth phenomena in polymer foaming require consideration of a large number of bubbles growing in close proximity to each other in the polymer/gas solution. The well-known cell model [8,9] was recognized as an appropriate model to describe such a situation and the model was modified for the present study to be used for non-isothermal processes. To implement the cell model in the simulation algorithm, the following assumptions were made:

8. After heating the system to a certain set point temperature, the bubble growth is isothermal.
9. The bubble is spherically symmetric throughout the bubble growth process.
10. The polymer melt is Newtonian and incompressible.
11. The inertial forces and gravity are negligible.
12. The gas inside the bubble obeys Henry's law.
13. The accumulation of adsorbed gas molecules on the bubble surface is negligible.
14. The initial accumulated stress around the growing bubble is zero.

The bubble growth is described by coupled mass and momentum conservation equations.

The continuity equation in spherical coordinates for fluid flow around the spherical bubble yields the velocity distribution in the fluid [10]:

$$\frac{\partial \rho}{\partial t} + \frac{1}{r^2}\frac{\partial}{\partial r}(\rho r^2 V_r) + \frac{1}{r \sin\theta}\frac{\partial}{\partial \theta}(\rho V_\theta \, sin\, \theta) + \frac{1}{r \sin\theta}\frac{\partial}{\partial \phi}\left(\rho V_\phi\right) = 0 \qquad \text{Eq. 7-10}$$

where ρ is the polymer melt density and V is the fluid velocity. For uni-directional flow in the r direction ($V_\theta = V_\phi = 0$) and incompressible fluid ($\frac{\partial \rho}{\partial t} = 0$) and using the

boundary condition that the bubble wall velocity at $r = R_{bub}$ is $V_r = \frac{dR_{bub}}{dt}$, Eq. 7-10 is simplified to:

$$V_r = \frac{\dot{R}_{bub} R_{bub}^2}{r^2} \qquad \text{Eq. 7-11}$$

where $\dot{R}$ is the rate of bubble growth and R is the bubble radius. The dynamics of the system are governed by the conservation of momentum in the radial direction [10]:

$$\rho\left(\frac{\partial V_r}{\partial t} + V_r\frac{\partial V_r}{\partial r}\right) = -\frac{\partial P}{\partial r} + \frac{1}{r^2}\frac{\partial}{\partial r}(r^2\tau_{rr}) - \frac{\tau_{\theta\theta} + \tau_{\phi\phi}}{r} \qquad \text{Eq. 7-12}$$

where P is the pressure as a function of the radial position in the polymer envelope and τ represents different components of stress tensor. In the case of a highly viscous fluid, the inertia term in the left-hand side can be neglected, leading to the following equation:

$$-\frac{\partial P}{\partial r} + \frac{1}{r^2}\frac{\partial}{\partial r}(r^2\tau_{rr}) - \frac{\tau_{\theta\theta} + \tau_{\phi\phi}}{r} = 0 \qquad \text{Eq. 7-13}$$

Considering the spherical symmetry ($\tau_{\theta\theta} = \tau_{\phi\phi}$), an integration from the bubble wall, R_{bub}, to the outer boundary, R_{shell}, allows to relate the stresses within the fluid to the gas pressure inside the bubble and the ambient pressure:

$$P_{bub} - P_{shell} + \tau_{rr}|_{R_{shell}} - \tau_{rr}|_{R_{bub}} + 2\int_{R_{bub}}^{R_{shell}} \frac{\tau_{rr} - \tau_{\theta\theta}}{r} = 0 \qquad \text{Eq. 7-14}$$

The condition of stress continuity at the outer boundary of the shell is assumed to be equal to the applied (ambient) pressure [8]:

$$-P_{shell} + \tau_{rr}|_{R_{shell}} = -P_{atm} \qquad \text{Eq. 7-15}$$

where P_{atm} is the ambient pressure.

Similarly, the condition of stress continuity at the gas-liquid interface is [8]:

$$-P_{bub} + \tau_{rr}|_{R_{bub}} = -P_{bub} + \frac{2\sigma}{R_{bub}} \quad \text{Eq. 7-16}$$

Substituting Eq. 7-15 and Eq. 7-16 into Eq. 7-14, the final integral form of the momentum equation for the bubble growth becomes:

$$P_{bub} - P_{atm} - \frac{2\sigma}{R_{bub}} + 2\int_{R_{bub}}^{R_{shell}} \frac{\tau_{rr} - \tau_{\theta\theta}}{r} = 0 \quad \text{Eq. 7-17}$$

The normal stresses in the conservation of momentum equation, τ_{rr} and $\tau_{\theta\theta}$, can be calculated by combining the generalized Newtonian constitutive equation, Eq. 7-18, and the rate of deformation components for a symmetrical bubble, Eq. 7-19 and Eq. 7-20 [8]:

$$\tau_{rr} = \eta\Delta_{ij} \quad \text{Eq. 7-18}$$

$$\Delta_{rr} = -4\frac{\dot{R}_{bub}R_{bub}^2}{r^3} \quad \text{Eq. 7-19}$$

$$\Delta_{\theta\theta} = \Delta_{\varphi\varphi} = 2\frac{\dot{R}_{bub}R_{bub}^2}{r^3} \quad \text{Eq. 7-20}$$

$$\tau_{rr} = -4\eta(\frac{\dot{R}_{bub}R_{bub}^2}{r^3}) \quad \text{Eq. 7-21}$$

$$\tau_{\theta\theta} = 2\eta(\frac{\dot{R}_{bub}R_{bub}^2}{r^3}) \quad \text{Eq. 7-22}$$

where Δ is the rate of deformation tensor along the diagonal (Δ_{rr}, $\Delta_{\theta\theta}$ and $\Delta_{\varphi\varphi}$) and η is the melt viscosity. Inserting Eq. 7-21 and Eq. 7-22 into the conservation of momentum equation and integrating the fourth term from $r = R_{bub}$ to $r = R_{shell}$ gives:

$$\frac{dR_{bub}}{dt} = R_{bub}\left(\frac{P_{bub} - P_{atm} - 2\sigma/R_{bub}}{4\eta}\right)\left(\frac{R_{shell}^3}{R_{shell}^3 - R_{bub}^3}\right) = 0 \quad \text{Eq. 7-23}$$

To describe the motion of the gas-liquid interface, the conservation of momentum equation must be coupled with the mass diffusion equation. When the principle of conservation of mass is applied to the gas inside the bubble, it results in the following equation [9], assuming the gas inside the bubble is ideal:

$$\frac{d}{dt}\left(\frac{P_{bub}}{R_g T}\,\frac{4}{3}\pi R_{bub}^3\right) = 4\pi R_{bub}^2\, D\,\frac{\partial c}{\partial r}\bigg|_{r=R_{bub}} \qquad \text{Eq. 7-24}$$

where R_g is the universal gas constant, $T$is the melt temperature, D is the gas diffusivity in the polymer, and c is the dissolved gas concentration in the shell. The pressure inside the gas bubble can be also related to the gas concentration at the bubble-liquid interface through Henry's law:

$$c_w = K_H P_{bub} \qquad \text{Eq. 7-25}$$

where c_w is the gas concentration at the interface and K_H is Henry's law constant.

Eq. 7-24 indicates that the gas inside the bubble accumulates at a rate equal to the rate of its diffusion from the polymer melt into the bubble [9] (i.e. across the gas-liquid interface). The diffusion equation for spherical coordinates can be written as follows:

$$\frac{\partial c}{\partial t} + \frac{R_{bub}^2 \dot{R}_{bub}}{r^2}\frac{\partial c}{\partial r} = \frac{D}{r^2}\frac{\partial c}{\partial r}\left(r^2\frac{\partial c}{\partial r}\right) \qquad \text{Eq. 7-26}$$

Eq. 7-26 can be solved subject to the following initial and boundary conditions:

$$c(r, t=0) = x\, K_H P_{atm} \quad \text{for } r \geq R_{bub} \qquad \text{Eq. 7-27}$$

$$c(r = R_{bub}, t) = K_H P_{bub} \quad \text{for } t \geq 0 \qquad \text{Eq. 7-28}$$

$$c(r = R_{shell}, t) = x\, K_H P_{atm} \quad \text{for } t \geq 0 \qquad \text{Eq. 7-29}$$

where x is the degree of gas saturation in the polymer melt and K_H is Henry's law constant. To solve for the concentration profile, Eq. 7-26 is transferred to the Lagrangian coordinate to eliminate the convection term, given as

$$y = r^3 - R_{bub}^3 \quad \text{Eq. 7-30}$$

and define the concentration function as:

$$c' = c - c_0 \quad \text{Eq. 7-31}$$

The diffusion equation in the new coordinate system is:

$$\frac{\partial c'}{\partial t} = 9D \frac{\partial}{\partial y}\left((y + R_{bub}^3)^{4/3} \frac{\partial c'}{\partial y}\right) \quad \text{Eq. 7-32}$$

with the following initial and boundary conditions:

$$c'(y, t = 0) = 0 \quad \text{Eq. 7-33}$$

$$c'(y = 0, t) = K_H P_{bub} - c_0 \quad \text{Eq. 7-34}$$

$$\frac{\partial c'}{\partial y}(y = R_{shell}^3 - R_{bub}^3, t) = 0 \quad \text{Eq. 7-35}$$

At the early stage of growth and near the interface, the concentration gradient in the liquid is large, which makes it difficult to obtain an accurate numerical solution of Eq. 7-32. To avoid this difficulty, we followed Arefmanesh [9] by defining the concentration function Φ as:

$$\frac{\partial \Phi}{\partial y} = c' = c - c_0 \quad \text{Eq. 7-36}$$

The diffusion equation, initial and boundary conditions in terms of new variable can be rewritten as:

$$\frac{\partial \Phi}{\partial t} = 9D(y + R_{bub}^3)^{4/3}\left(\frac{\partial^2 \Phi}{\partial y^2}\right) \quad \text{Eq. 7-37}$$

$$\Phi(y, t = 0) = 0 \quad \text{Eq. 7-38}$$

$$\frac{\partial \Phi}{\partial t}(y = 0, t) = K_H P_{bub} - c_0 \quad \text{Eq. 7-39}$$

$$\frac{\partial^2 \Phi}{\partial y^2}(y = R_{shell}^3 - R_{bub}^3, t) = 0 \quad \text{Eq. 7-40}$$

According to the cell model, the polymer envelope surrounding the gas bubble expands together with the bubble and becomes thinner with time. Therefore, the outer shell radius is treated as a moving outer boundary that has to be determined at each time step during the simulation. The volume of the envelope, V, is described as:

$$V_{shell}(t) = \frac{4\pi}{3}(R_{shell}(t)^3 - R_{bub}(t)^3) \quad \text{Eq. 7-41}$$

By assuming that the polymer volume within the shell is constant, R_{shell}, can be expressed as a function of time and can be used to calculate the outer shell radius at each time step:

$$R_{shell}(t) = (R_{shell}(t-1)^3 + R_{bub}(t)^3 - R_{bub}(t-1)^3))^{1/3} \quad \text{Eq. 7-42}$$

Numerical Simulation Algorithm and Model Implementation

Due to the nonlinearity and coupling of the governing equations, an analytical solution was not possible. Therefore, a numerical simulation algorithm which integrates the explicit finite difference scheme and the fourth order Runge–Kutta method was employed

in MATLAB to solve Eq. 7-23, and Eq. 7-24 and Eq. 7-37 simulate the expanding phenomenon of the formed bubble, following the steps shown below:

- The calculation starts by selecting an appropriate initial bubble radius which must be larger than that of the critical bubble. Given the initial bubble pressure which is assumed to be equal to the saturation pressure, the initial gas concentration can be calculated using Henry law.

- Using the initial and boundary conditions, the diffusion equation, Eq. 7-37, is discretized by the finite differences method. The basic idea of the finite differences scheme is to replace spatial and time derivatives by suitable approximations, then to numerically solve the resulting difference equations for every time step. After approximating the concentration profile using discretization, the concentration gradient of the dissolved gas at the gas-liquid interface can be computed and substituted in Eq. 7-24.

- With the fourth-order Runge-Kutta method, Eq. 7-23 and Eq. 7-24 are then solved simultaneously to calculate the new values of pressure inside the bubble and bubble radius at the end of the first time increment. Using the most recent values of bubble pressure and radius, the new values of gas concentration at the gas-liquid interface can be calculated.

- This procedure is repeated until 30 min or when the dissolved gas concentration falls to zero and consequently the bubble radius becomes constant with time.

The physical and processing parameters used in the simulation, as well as model predictions and sensitivity analyses are reported in Chapter 4.

7.3 References

[1] Y. Kagan, "The Kinetics of Boiling of a Pure Liquid," *Russ. J. Phys.Chem.*, 42-46, 1960.

[2] J.W. Gibbs, *The Scientific Papers of J. Willard Gibbs*. Mineola, NY: Dover Publ.

Inc., 1961.

[3] J. Zeldovich, "On the Theory of New Phase Formation: Cavitation," *Acta Physicochem. U.S.S.R.*, 1-22, 1943.

[4] V. Skripov, *Metastable Liquids*. New York: John Wiley and Sons, 1974.

[5] M. Blander, "Bubble Nucleation in Liquids," *Adv. Colloid Interface Sci.*, 10, 1-32, 1979.

[6] S. Wu, *Polymer Interface and Adhesion*. New York: Marcel Dekker, 1982.

[7] A. Tinson, E. Takacs, and J. Vlachopoulos, "The Role of Surface Tension in Sintering for Rotational Molding," *Rotoworld*, 1, 43-47, 2005.

[8] M. Amon and C.D. Denson, "A Study of the Dynamics of Foam Growth: Analysis of the Growth of Closely Spaced Spherical Bubbles," *Polym. Eng. SCi.*, 24, 1026-1034, 1984.

[9] A. Arefmanesh and S.G. Advani, "Diffusion-Induced Growth of a Gas Bubble in a Viscoelastic Fluid," *Rheol Acta*, 30, 274-283, 1991.

[10] J. Vlachopoulos, *Fundamentals of Fluid Mechanics*.: McMaster University, 2006.